Abstract

Abstract

Aims: Increased ANKRD1 levels linked to gain of function mutations have been associated to total anomalous pulmonary venous return and adult cardiomyopathy occurrence in humans. The link between increased ANKRD1 level and cardiac structural and functional disease is not understood. To get insight into this problem, we have generated a gain of function ANKRD1 mouse model by overexpressing ANKRD1 in the myocardium.

Methods and Results: Ankrd1 is expressed non homogeneously in the embryonic myocardium, with a dynamic nucleo-sarcomeric localization in developing cardiomyocytes. ANKRD1 transgenic mice present sinus venosus defect, which originates during development by impaired remodeling of early embryonic heart. Adult transgenic hearts develop diastolic dysfunction with preserved ejection fraction, which progressively evolves into heart failure, as shown histologically and hemodynamically. Transgenic cardiomyocyte structure, sarcomeric assembly and stability are progressively impaired from embryonic to adult life. Postanatal transgenic myofibrils also present characteristic functional alterations: impaired compliance at neonatal stage and impaired lusitropism in adult hearts. Altogether, our combined analyses suggest that impaired embryonic remodeling and adult heart dysfunction in ANKRD1 transgenic mice present a common ground of initial cardiomyocyte defects, which are exacerbated postnatally. Molecular analysis showed transient activation of *GATA4-Nkx2.5* transcription in early transgenic embryos and subsequent dynamic transcriptional modulation within titin gene.

Conclusions: ANKRD1 is a fine mediator of cardiomyocyte response to hemodynamic load in the developing and adult heart. Increased ANKRD1 levels are sufficient to initiate an altered cellular phenotype, which is progressively exacerbated into a pathological organ response by the high ventricular workload during postnatal life. Our study defines for the first time a unifying picture for ANKRD1 role in heart development and disease and provides the first mechanistic link between ANKRD1 overexpression and cardiac disease onset.

Translational perspective

Increased ANKRD1 levels linked to gain of function mutations have been correlated to total anomalous pulmonary venous return (TAPVR) and adult cardiomyopathy in humans. Myocardial-overexpressing ANKRD1 mouse lines are born with congenital sinus venosus (SV) defect and progressively develop diastolic dysfunction with preserved ejection fraction, which evolves into heart failure. Our data indicate that impaired embryonic remodeling and adult heart dysfunction stem from a common ground of initial cardiomyocyte defects, which are exacerbated postnatally.

Our results open the perspective that gain of function mutations of *ANKRD1* gene could be a prognostic early genetic marker for adult cardiomyopathy, in addition to selective congenital malformations such as SV defects and TAPVR.

Dear Editors,

please find enclosed the second revised version of our manuscript CVR-2019-0215 entitled: "**Myocardial overexpression of ANKRD1 causes sinus venosus defects and progressive diastolic dysfunction".**

As requested by Reviewer 1, we have added a new panel in Figure 8 representing the proposed role of Ankrd1 in wt hearts.

I declare that 1) this manuscript is not submitted elsewhere or under consideration for publication; 2)all Authors have read and agreed with the submission of the manuscript.

In detail, Authors contribution to this work has been the following:

Nicoletta Piroddi, Beatrice Scellini: performed experiments on isolated myofibrils and analyzed data; Paola Pesce: performed *in vivo* ecocardiographic analysis and analyzed data; Giulia S. Ganzetti, Stefano Manzini, Giulia Chiesa, Marco Busnelli, Federica Dellera, Daniele Bruno: mouse breeding and genotyping, sample preparations, histological analysis; Ileana Badi, Raffaella Cinquetti: cloned and validated transgenic constructs, generated transgenic lines; Laura Monti and Michela Menegollo: performed real–time PCR experiment and analyzed data; Virginia Cora, Simone Tiso: performed 3D-Amira reconstructions; Federico Caicci: performed TEM analysis; Lucia Manni: teached Amira-3D and supervised 3D reconstructions; Steven B. Bleyl, Annalisa Grimaldi, Roberto Taramelli, David Sacerdoti, Chiara Tesi, Corrado Poggesi: supervised experiments and analyzed data; Simonetta Ausoni: designed research, performed and supervised experiments, analyzed data; manuscript writing and editing; Francesco Acquati : designed research, supervised experiments, analyzed data; manuscript editing; Marina Campione: global project supervision; performed experiments, analyzed data, drafting, review and final editing of the manuscript.

We hope that you will find our contribution of broad interest for the readers of *Cardiovascular Research.* Thank you in advance for your consideration.

Best regards,

Marina Campione

Reply to reviewers

Reviewer #1: The authors have extensively revised their manuscript in the light of the earlier comments by adding new data, including analysis of heart failure markers and additional in situ and quantative RT-PCR expression analysis. The study represents much work and is now significantly improved, highlighting the complexity and potential of this new mouse model, despite the difficulty of distinguishing direct form indirect effects and of identifying elusive mechanisms of transcriptional changes on Ankrd1 overexpression.

I have one additional point: Figure 8 should be modified to indicate the normal fucntions of Ankrd1 for comparison with the effects of overexpression.

As requested, we have edited Figure 8 by adding an additional panel describing the proposed role of Ankrd1 in normal heart development. Figure 8 legend has been modified accordingly.

CVR-2019-0215

Myocardial overexpression of ANKRD1 causes sinus venosus defects and progressive diastolic dysfunction

Nicoletta Piroddi[1], Paola Pesce[2], Beatrice Scellini[1], Stefano Manzini[3], Giulia S. Ganzetti[3], Ileana Badi[4,5], Michela Menegollo[6], Virginia Cora[6], Simone Tiso[6], Raffaella Cinquetti[4], Laura Monti[4] , Giulia Chiesa[3], Steven B. Bleyl[7], Marco Busnelli[3], Federica Dellera[3], Daniele Bruno[4], Federico Caicci[8], Annalisa Grimaldi[4], Roberto Taramelli[4], Lucia Manni[8], David Sacerdoti[2], Chiara Tesi[1], Corrado Poggesi[1], Simonetta Ausoni[6*], Francesco Acquati[4*], Marina Campione[6,9*].

[1]Department of Experimental and Clinical Medicine, University of Florence, 50134 Florence, Italy; [2]Department of Medicine, University of Padua, 35121 Padua, Italy; [3]Dept. of Pharmacological and Biomolecular Sciences, University of Milan, 20133 Milan, Italy; [4]Dept. of Biotechnology and Life Sciences, University of Insubria, 21100 Varese, Italy; [6]Dept. of Biomedical Sciences, University of Padua, 35121 Padua, Italy; [7] Dept. of Pediatrics, University of Utah, Salt Lake City, 84132 Utah, USA; [8]Dep. of Biology, University of Padua, 35121 Padua, Italy; [9]CNR-Neuroscience Institute, 35121 Padua, Italy.

[5]**Present address:** Division of Cardiovascular Medicine, Radcliffe Department of Medicine, University of Oxford, John Radcliffe Hospital, Oxford OX3 9DU, UK.

***: corresponding Authors**

Marina Campione: fax: +39-049-8276040; tel: +39-049-8276031;

E-mail: campione@bio.unipd.it ;

Francesco Acquati: fax: +39-0332-421500; tel: +39-0332-421512;

E-mail: francesco.acquati@uninsubria.it

Simonetta Ausoni: fax +39-049-8276040; tel: +39-049-8276036;

E-mail: simonetta.ausoni@unipd.it

Running title: ANKRD1 role in heart development and disease

Word count: 8560

Abstract

Aims: Increased ANKRD1 levels linked to gain of function mutations have been associated to total anomalous pulmonary venous return and adult cardiomyopathy occurrence in humans. The link between increased ANKRD1 level and cardiac structural and functional disease is not understood. To get insight into this problem, we have generated a gain of function ANKRD1 mouse model by overexpressing ANKRD1 in the myocardium.

Methods and Results: Ankrd1 is expressed non homogeneously in the embryonic myocardium, with a dynamic nucleo-sarcomeric localization in developing cardiomyocytes. ANKRD1 transgenic mice present sinus venosus defect, which originates during development by impaired remodeling of early embryonic heart. Adult transgenic hearts develop diastolic dysfunction with preserved ejection fraction, which progressively evolves into heart failure, as shown histologically and hemodynamically. Transgenic cardiomyocyte structure, sarcomeric assembly and stability are progressively impaired from embryonic to adult life. Postanatal transgenic myofibrils also present characteristic functional alterations: impaired compliance at neonatal stage and impaired lusitropism in adult hearts. Altogether, our combined analyses suggest that impaired embryonic remodeling and adult heart dysfunction in ANKRD1 transgenic mice present a common ground of initial cardiomyocyte defects, which are exacerbated postnatally. Molecular analysis showed transient activation of *GATA4-Nkx2.5* transcription in early transgenic embryos and subsequent dynamic transcriptional modulation within titin gene.

Conclusions: ANKRD1 is a fine mediator of cardiomyocyte response to hemodynamic load in the developing and adult heart. Increased ANKRD1 levels are sufficient to initiate an altered cellular phenotype, which is progressively exacerbated into a pathological organ response by the high ventricular workload during postnatal life. Our study defines for the first time a unifying picture for ANKRD1 role in heart development and disease and provides the first mechanistic link between ANKRD1 overexpression and cardiac disease onset.

1. Introduction

Ankyrin Repeat Domain 1 (ANKRD1, also known as Cardiac Ankyrin Repeat Protein, CARP) is a member of the muscle specific ankyrin repeat proteins (MARP) family, which also includes ANKRD2/Arpp and DARP[1,2]. MARP proteins are involved in muscle stress response and are structurally characterized by four ankirin repeats, a coiled-coil domain, a nuclear localization signal and a PEST degradation sequence, which mediates its rapid turnover via the ubiquitin-proteasome pathway[3,4].

ANKRD1 is highly expressed during heart development and down-regulated in adult life[5–7]. In the developing heart, ANKRD1 has been proposed to work as transcriptional cofactor and negative regulator of myocardial gene expression[5–7]. ANKRD1 is a target of Nkx2.5 *in vivo*[5] and its promoter can be cooperatively activated by Nkx2.5 and GATA4 [6].

In adult cardiomyocytes, ANKRD1 is normally located at the sarcomere, but it has been shown to translocate to the nucleus upon mechanical stimulation *in vitro*[2]. In the sarcomere, ANKRD1 is found at the I-band where it is a component of titin N2A-linked signalling complex[2,8]. Physical interaction between ANKRD1 and titin N2A spring domain has been shown to reduce PKA phosphorylation and titin compliance[1]. ANKRD1 has additionally been shown to functionally interact with GATA4 in the I band and the nucleus, thereby modulating GATA4-mediated sarcomeric gene expression and sarcomeric organization[9,10]. Interactions with several additional partners involved in modulation of muscle structure and function have been reported[3,8]. ANKRD1 is therefore part of a stretch-sensing unit capable of relaying biomechanical stress signals to the regulation of gene expression. In line, ANKRD1 expression is up-regulated in response to hypertrophy and in heart failure[6,11–13].However, the absence of cardiac phenotype in ANKRD1 knock-out mouse models[10,14], combined with contradictory results from loss and gain of function approaches[3,9,15,16], have precluded a clear understanding of ANKRD1 role in adult heart.

Genetic mutations in *ANKRD1*, mostly associated to a gain of function condition, have been correlated to several types of cardiac disease in humans. *ANKRD1* missense mutations have been identified in patients with hypertrophic and dilated cardiomyopathy (HCM, DCM)[17–19]. *ANKRD1* has additionally been identified as a candidate gene for total anomalous pulmonary venous return (TAPVR) in

isolated patients[20,21]. TAPVR is a congenital heart disease (CHD) which affects 1:15000 live births, and is characterized by incorrect pulmonary vein (PV) drainage into the heart[22]. TAPVR leads to high mortality rate in the first year of life, unless surgically corrected. Reported TAPVR patients presented either chromosomal rearrangement or T116M–*ANKRD1* mutation, leading respectively to a 3-4 fold increase in *ANKRD1* transcript levels or 10-20% increase in protein stability[4,23], suggesting that *ANKRD1* expression levels must be tightly regulated during embryogenesis.

Here we show that Ankrd1 is heterogenously expressed in the developing heart, with a dynamic nucleo-sacroplasmic sublocalization. Myocardial-overexpressing ANKRD1 transgenic (Tg) mice are born with congenital sinus venosus (SV) defect. In postnatal life, diastolic dysfunction and progressive transition from adaptive to maladaptive response occurs. Increased ANKRD1 levels are sufficient to initiate an altered cellular phenotype in the embryonic heart, which is exacerbated postnatally by high ventricular workload.

2. Methods

2.1 Mouse lines

Human wt-ANKRD1-FLAG tagged cDNA[4] was cloned downstream of the 5kb *Myh6* promoter[24]. Two Tg lines were generated by pronuclear microinjection of linearized constructs into FVB oocytes. Transgene expression was characterized by Western blotting and immunofluorescence (Figure S1). Genomic DNA was PCR-genotyped from tails of anesthetized mice (Zoletil, 30mg/kg, i.p) or the amniotic sac of embryos isolated after sacrifice by cervical dislocation of the anesthetized mother. Isolated embryos, neonatal and adult hearts were isolated and processed using standard procedures for subsequent histological, biochemical or molecular analysis. Animal procedures used conformed to the guidelines from Directive 2010/63/EU of the European Parliament on the protection of animals used for scientific purposes.

2.2 PCR analysis

RNA isolation, cDNA transcription and quantitative PCR were conducted using standard procedures. Primers for titin PCR amplification were selected to avoid regions with repetitive nucleotide sequences and potential incorrect priming. All primer sequences are available in Supplementary material online, Table S1.

2.3 Isolated myofibril analysis

Myofibrils were prepared by homogenization of permeabilized strips of frozen ventricular tissue in relaxing solution on ice[25]. Mechanical measurements from myofibrils in isometric conditions were performed during activation-relaxation cycles achieved by fast solution switching[26]. SL-resting tension relations were determined as previously described[27].

2.4 Echocardiographic analysis

Transthoracic echocardiography was performed using a high resolution echo machine with a 30 Mhz probe (VEVO 2100 Visualsonics). Both males and females mice were analyzed. Mice were chest shaved and anesthetized with 3% isoflurane, and temperature controlled anesthesia was maintained with 1.5% isoflurane. Two-dimensional cine loops and M-mode cine loops of a long-axis view and a short-axis view of the LV were recorded. Interventricular septum thickness (IVS), left ventricle internal diameter (LVID) and left ventricle posterior wall thickness (LVPW) were measured in diastole and systole from M-mode long axis view. Ejection fraction (EF) and fractional shortening (FS) were automatically calculated by the machine software.

2.5 Doppler analysis of LV and PV flow

Doppler analysis of LV flow was performed from the long axis B-mode image placing the sample volume in the left ventricle, below the mitral annulus. Isovolumetric contraction and relaxation times (IVCT, IVRT) and ejection time (ET) were measured from transmitral Doppler analysis. Myocardial performance index was calculated using the following formula: MPI= IVCT+IVRT/ET. E wave, A wave and E wave deceleration time (DT) were measured from transmitral Doppler flow profile.

Doppler analysis of PV flow was performed from a corrected long axis B-mode image placing the sample volume just before the entry of the PV in the left aria (Figure S2). The maximal velocity of PV atrial (a), systolic (s) and diastolic (d) flow waves were measured.

2.6 Statistical analysis

Data are presented as mean ± standard deviation. Comparisons between groups were performed by Students unpaired t-test, Mann-Wilcoxon W test, or Wilcoxon signed-rank test where appropriate, based on experimental design. $P<0.05$ was considered statistically significant.

Detailed Methods are available in Supplementary data online

3.Results

3.1 Ankrd1 is heterogeneously expressed in the developing myocardium

We initially examined *Ankrd1* expression in embryonic hearts. *In situ* hybridization (ISH) on sections showed that *Ankrd1* mRNA is expressed in the myocardium from E7.5 onwards, although not homogeneously (Figure 1A).

At the venous pole of the heart, at E10.0 differential *Ankrd1* mRNA levels were observed at the left and right pulmonary ridge and the sinus horns (white arrows, Figure 1Bb). By E10.5, heterogeneous mRNA staining was visible also within the developing septum primum (black arrow, Figure 1Bd), around the PV (white arrowhead, Figure 1Bd) and systemic veins entrance (red arrowheads, Fig. 1Ac and 1Bd). This expression profile was maintained at E12.5 (Figure 1Ad and 1Be,f) and E14.5 (Figure 1Bg,h).

Heterogeneous *Ankrd1* mRNA expression was detected also within the compact and trabecular layers of the left and right atrial chambers (LA, RA) (green arrows, Figure 1Cb,e), and the atrioventricular canal (red asterisk, Figure 1Bh and 1Ce). Stronger *Ankrd1* expression was visible in the outflow tract and the right ventricle (RV) (Figure 1Ac-e), whereas weaker and more heterogeneous expression was detected in the left ventricle (LV) and the interventricular septum (yellow arrows, Figure 1Ac,d and 1Cd,f).

Antibody staining confirmed heterogeneous Ankrd1 protein expression in developing cardiomyocytes (Figure 1D). Subcellular protein localization was always detected at the sarcomeric I band (Figure 1E); additional nuclear localization was frequently observed in E10.5 cardiomyocytes (Figure 1Ea,b), but was no more detectable by E14.5 (Figure 1Ec,d).

3.2 ANKRD1 finely modulates rotation and remodeling in the early myocardium

We next aimed to assess the effects of a genetically-based increase in ANKRD1 levels on cardiac structure and functionality. Thus, we generated two transgenic (Tg) mouse lines overexpressing human ANKRD1 in the myocardium under *Myh6* gene promoter (Figure S1A), which is active from E7.5 onwards[28]. Transgene protein levels were very modest in E10.5 and E14.5 embryos (Figure S1A,B and not shown),

but increased, to a similar order of magnitude, in neonatal and 10M Tg hearts (Figure S1A). ANKRD1 transgene presented always a sarcomeric sub-localization, however some nuclear signal was additionally visible in adult Tg hearts (Figure S1C). Preliminary analysis did not reveal phenotypic differences between the two Tg lines (not shown), thus detailed analysis was performed on a single line.

We initially investigated early cardiac development. E10.5 Tg hearts presented well developed atrial and ventricular chambers, which however appeared more compressed along the cranio-caudal and dorso-ventral axes, were laterally displaced and presented a reduced rotational angle if compared to wt littermates (Figure 2Aa,e). In particular, the sino-atrial region was more caudally oriented in Tg hearts, similarly to E9.5 wt embryos (Figure 2Be). Compressed shape and malrotation affected both internal remodeling and the relative orientation between sino-atrial myocardium, the flanking dorsal mesocardium and the proepicardium (Figure 2Aa,e). This resulted in malpositioning of the developing septum primum, of the pulmonary ridges, as well as of the sinus horns myocardium, visualized by Tbx18 expression[29] (Figure 2Ac,d,g,h). The sinus horns confluence, which defines the entrance of the cardinal veins into the sino-atrial region, and the pulmonary pit, delineating the route of canalization of the PV, were distinct in Tg hearts as in wt embryos. However, in Tg hearts, a mesh of $Tbx18^{+}$ mesenchyme was additionally detected within the dorsal mesocardium. $Tbx18^{+}$ mesenchyme was more abundant caudally, in proximity of the differentiating sinus horns myocardium (Figure 2Ba-d) and extended cranially up to the pulmonary ridges (Figure 2Ag,h). Remarkably, a corresponding situation could be detected in E9.5 wt embryos, which presented some $Tbx18^{+}$ cells within the loosely arranged dorsal mesocardium at the proepicardial border (Figure 2Bf,g).

In conclusion, E10.5 Tg hearts, although apparently progressed in development, are “cast” into a more immature topological arrangement that strongly affects venous pole remodeling.

3.3 ANKRD1 Tg hearts present SV defects

By mid fetal stages, most Tg hearts presented a misshapen sino-atrial region. 3D anatomically-based reconstruction outlined the malpositioning of venous inlets, which however drained in the correct atrial chamber **(**Figure 3A). Additionally, Tg hearts presented a network of microcanalizations, delineating a fine network of ectopic

connections between the PV and systemic veins, which partially drained into the vestibular region through small fenestrations (Figure 3Ad,f and Figure S3**).** These anomalous veno-atrial connections have been associated to SV defects in humans[30]. Anomalous veno-atrial connections were normally accompanied (20/27 embryos) by atrio-ventricular rotational defects and compressed appearance of the vestibular region (Figure 3Ad and Figure S3). However, in a minority of Tg embryos (7/27) SV defects occurred in the absence of morphogenetic impairment (not shown), thus indicating higher venous pole sensitivity to increased *ANKRD1* expression.

At the early postnatal life, only subtle differences could be detected between wt and Tg hearts by external anatomical observation (Figure 3Ba,e), however SV defects could be clearly outlined histologically (Figure 3Bb-d,f-h). A misshapen fossa ovalis was also clearly recognizable (Figure 3Bg).

In conclusion, ANKRD1 Tg hearts present SV defects. Fine alterations in cardiac venous pole remodeling impact both systemic and pulmonary vein development, which are closely interwined[31]. Our data support the hypothesis that SV defects are likely originated by impaired remodeling of the sino-atrial myocardium during embryonic development.

To investigate the mechanisms for SV defects, we initially wondered whether master transcription factors *GATA4* and *Nkx2.5*, functionally associated to ANKRD1, could be transcriptionally affected in early Tg embryos**.** qPCR analysis showed that *GATA4* and *Nkx2.5* mRNA levels were increased in E10.5 Tg hearts ($p<0.05$ for *Nkx2.5*), however this difference was blunted at E14.5 (Figure 4A). These results indicate that very low ANKRD1 overexpression is sufficient to affect *GATA4* and *Nkx2.5* transcription, however exclusively within the short time window of ANKRD1 nuclear localization. Thus, *GATA4-Nkx2.5* transcriptional modulation could be involved in SV defects onset.

As cardiac remodeling occurs thought the entire fetal period, these results raise the possibility that additional ANKRD1-mediated mechanisms should account for phenotype progression in Tg hearts, including altered chamber morphology. ISH analysis of E14.5 Tg hearts did not show differences in regional distribution of genes which delineate and/or define myocardial landmarks and compartments, such as *Pitx2* (left–right identity)[32], *Tbx3* (primary myocardium)[33], *Nppa, Gja5* (chamber myocardium)[33,34], *Mlc2v* (ventricular myocardium)[34], *Bmp10* (trabecular

myocardium) [35], *Tbx18* (SH myocardium)[29] (Figure 4B), thus ruling out late transcriptional effects on myocardial patterning.

3.4 Adult ANKRD1 Tg mice develop progressive ventricular diastolic dysfunction

We next investigated the consequences of ANKRD1 overexpression in adult life. Tg mice were born according to Mendelian ratio, however by 10 months (10M) they presented a reduced viability (88,5%Tg *vs* 96,9%wt; $p<0.05$). Histological analysis uncovered a severely dilated LA in all Tg hearts (Figure 5A). LA thrombi, patent foramen ovale (PFO), ventricular dilatation and altered chamber geometry could additionally be detected as isolated or combined defects (Figure 5A). Moderate fibrosis was detected in ventricular (Figure 5Am,n), but not atrial chambers, except for the organized thrombi (Figure 5Ag,h). Accordingly, TGFβ levels and TGFβ–activated ERK1/2 phosphorylation[36] were moderately increased in Tg hearts (Figure S4).

We compared wt and Tg cardiac function by echocardiography and hemodynamic analysis at 2M and 10M (Table 1). Echocardiography indicated preserved LV systolic function (*ie* EF and FS values) in 2 and 10M Tg mice, and absence of ventricular hypertrophy at 10M. However, transmitralic flow analysis in 2M mice revealed comparable E/A ratio but higher DT values in Tg animals, suggesting an initial diastolic dysfunction. By 10M, remarkably increased E/A ratio and reduced DT value were found in Tg mice, indicating progression of diastolic dysfunction with aging. Remarkably increased MPI[37] in 10M Tg *vs* wt mice supports this notion.

PV flow analysis revealed the presence of a small late diastolic wave (*d2*) in 2M Tg mice (6/8) (Figure 5B), indicating additional blood inflow into the LA, presumably via the identified cavo-pulmonary shunts (Figure 3B and Figure 5A). We hypothesize that cavo-pulmonary shunts became hemodynamically significant only in late diastole due to onset of a temporary pressure gradient which favors the R to L shunt. The *d2* wave was no longer detected in 10M Tg, indicating a change in L/R atrial chamber pressure gradients with age.

At 2M, *a* wave value was significantly higher in Tg than wt mice, indicating more effective atrial contraction (Table 1 and Figure 5B). *s* and *d* wave values were

294 also higher in Tg than wt mice (Table 1 and Figure 5B), indicating ventricular systolic
295 compensation according to Frank Starling law. Comparable *a/d* ratio indicated similar
296 hemodynamics in 2M wt *vs* Tg mice during atrial systole and ventricular diastole;
297 however, *s/d* ratio was <1 in 2M Tg mice, as it occurs in early diastolic dysfunction[38].
298 By 10M, decreased *a* and *s* values, as well as *s/d* and *a/d* ratio indicated less effective
299 atrial contraction and very different hemodynamics in Tg *vs* wt mice, underlying a
300 severe diastolic dysfunction and loss in LA contractility. Doppler visualization
301 confirmed this latter finding. Visual assessment of mitral valve flow did not reveal
302 anomalies in valve functionality, thus ruling out valvular impairment as the leading
303 cause for diastolic dysfunction.
304 Overall, functional analysis indicates that 2M Tg mice present initial
305 ventricular diastolic dysfunction accompanied by increased atrial contractility; by
306 10M, diastolic dysfunction progresses into diastolic heart failure (HF), associated to
307 LA enlargement and loss of LA contractility. In line, cardiac disease marker BNP was
308 also significantly increased in 10M Tg hearts (Figure 5Ao).
309 Atrial dilatation and diastolic HF together can lead to pulmonary edema,
310 whereas diastolic HF can occasionally lead to ventricular fibrillation. Thrombi
311 formation in 10M Tg mice indicates altered atrial hemodynamics, possibly caused by
312 HF and/or PFO defects[39]. All these co-morbidities can have a fatal outcome, therefore
313 they likely account, as single or combined events, for the reduced viability in 10M Tg
314 mice.
315
316 **3.5 Cardiomyocyte contractility is impaired in ANKRD1 Tg hearts**
317 We tested the hypothesis that impaired cardiomyocyte contractility could contribute
318 to CHD and adult diastolic dysfunction in Tg hearts. Isolated myofibrils from mid-
319 fetal, early postnatal and 10M hearts were tested for passive tension. Neonatal and
320 10M myofibrils were additionally tested for active mechanical properties.
321 Sarcomere length-resting tension (SL-RT) relations (*ie* passive mechanical
322 properties) of wt and Tg myofibrils were comparable at E14.5 (Figure 6Aa) and 10M
323 (Figure 6Ac), but not in newborns (Figure 6Ab). Interestingly, neonatal wt myofibrils
324 retained passive properties of fetal stage, as expected[40], whereas Tg myofibrils
325 presented a functional shift towards the stiffer phenotype of adult wt (Figure 6Ab,c).

Regarding active mechanical properties (Figure 6Ad), the maximally calcium activated isometric force value (P_0) was significantly higher in neonatal Tg than wt myofibrils, and comparable to adult wt value. Kinetics of force rise (k_{ACT}) and relaxation (slow and fast k_{REL}) and tension relaxation parameters (D_{slow}) were comparable in neonatal Tg and wt myofibrils. Interestingly, adult wt and Tg myofibrils showed comparable k_{ACT}, while force relaxation was clearly impaired in Tg, as shown by significantly increased D_{slow} and decreased fast k_{REL}. Thus, Tg myofibrils present a differential modulation of passive and active contractile properties during life time, *ie* reduced compliance at neonatal stage and overall slowed down relaxation at 10M.

We investigated the molecular basis for early functional changes observed in Tg myofibrils. Regulation of passive mechanical properties is mainly due to modulation of titin compliance either post-transcriptionally, or at the transcriptional level via alternative splicing[41,42]. Here, we tested the hypothesis that titin transcription could be affected in ANKRD1 Tg hearts. Titin splicing regulation involves N2B/N2BA isoforms ratio modulation and N2BA length modification via exons inclusion at the middle Ig and PEVK spring regions[41,42].

In E14.5 Tg hearts the transcripts levels of titin did not show significant differences, similar to representative thick, thin and Z band components (Figure 6B). The N2B/N2BA isoform ratio was slightly, though not significantly, increased (Figure 6C). In neonatal Tg hearts, expression of analysed transcripts were unchanged (Figure 6B). However, N2B/N2BA ratio was now clearly modified and significantly reduced in Tg samples (Figure 6C), indicating a transcriptional shift towards the more compliant N2BA isoform. This result was somehow surprising, since functional data indicated a reduced compliance in neonatal Tg myofibrils (Figure 6Ab). Intriguingly, when we performed PCR scanning analysis of N2BA exon usage within middle Ig and PEVK regions, we found that Tg hearts used a different exon combination, leading to expression of shorter, therefore less compliant, N2BA titin isoforms (Figure 6C and Figure S5). Thus, a wide modulation within titin gene transcription accompanies the biomechanical changes of neonatal Tg myofibrils.

3.6 Cardiomyocyte organization and ultrastructure are progressively impaired in ANKRD1 Tg mice

Having established that ANKRD1 overexpression impairs sarcomeric function, we next explored the impact of these alterations on cellular organization. Cardiomyocyte disorganization was visible in Tg hearts from E10.5 onwards (Figure 7A). Confocal analysis showed that E14.5 Tg cardiomyocytes were mostly distorted and presented sarcomeric disaligment (Figure 7Ai,l, Supplementary videos 1,2). Electron microscopy analysis of neonatal Tg ventricles confirmed sarcomeric disorganization and additionally showed focal areas of myofibrillar disruption (Figure 7Bf,i). Swollen mitochondria with abnormal cristae (Figure 7Bi) and rare lipid droplets in the cytoplasm (Figure 7Bf) were also found. By 10M, ultrastructural disorganization progressed in Tg ventricles, as indicated by the increased myofibril loss, mitochondrial damage and accumulation of lipid droplets. Myofibrillar loss was not detected in adult Tg LA (Figure 7).

In conclusion, tight regulation of *ANKRD1* expression is required for proper modulation of cardiomyocyte structure and of sarcomeric assembly and stability, from early development to adult life. Impaired embryonic remodeling and contractility in ANKRD1 Tg mice are therefore underlined by a common cellular basis.

4. Discussion

Here, we have presented the first longitudinal study aiming to assess the consequences of ANKRD1 myocardial overexpression from development to adult stage. Novel findings of our study are: 1) The presence of SV defects in ANKRD1 Tg mice. To our knowledge, this is the first mouse model for such congenital heart disease. 2) The pathological phenotype of adult ANKRD1 Tg hearts in the absence of pharmacological stimuli or pressure overload. This feature has not been highlighted before[16], possibly because of late appearance of gross cardiac abnormalities. The mechanistic link between ANKRD1 overexpression, CHD and adult cardiomyopathy are hereafter discussed, in relation to ANKRD1 expression and subcellular localization.

4.1 ANKRD1 expression and overexpression

We have here shown a discrete sub-compartmentalization of *Ankrd1* expression and dynamic nucleo-sarcomeric localization in the developing heart, not recognized in previous studies[5,7]. The limited time window of nuclear localization suggests that

ANKRD1 can sense ongoing hemodynamic changes[43] and respond by fine tuning its interacting partners (Figure 8A).

Extreme sensitivity to increased ANKRD1 levels in Tg hearts is therefore not surprising. Very low levels of Tg expression in E10.5 Tg hearts were sufficient for morphological and cellular phenotype onset and for transient *GATA4* and *Nkx2.5* transcriptional up-regulation. ANKRD1 expression can in turn be regulated by Nkx2.5 and GATA4[5,6,9]. Thus, our data suggest a novel *in vivo* autoregulatory loop for increased *GATA4* and *Nkx2.5* transcription, mediated by ANKRD1 binding. We cannot rule out that GATA4 could be directly involved in *Nkx2.5* transcriptional activation[44]. GATA4-ANKRD1 functional interaction can lead to increased GATA4-mediated sarcomeric gene expression and has been proposed to contribute to sarcomere homeostasis[9,10]. On the other hand, GATA4 and Nkx2.5 together can co-activate target genes regulating cardiac development[45]. We propose that ANKRD1-mediated *GATA4* and *Nkx2.5* transcriptional modulation contributes both to cellular phenotype onset and to early abnormal venous pole remodeling, leading to SV defects (Figure 8B~~A~~).

The extreme sensitivity to ANKRD1 levels in our Tg mice is in line with TAPVR occurrence in patients presenting a mild increase in ANKRD1 transcripts and/or protein stability[4,23]. TAPVR and SV defects present a common feature, *ie* abnormal pulmonary venous connections: PV are not connected to the LA in TAPVR, whereas partial anomalous PV connections characterize SV defects[46]. Our data support the hypothesis that both diseases can stem from a common developmental defect, *ie* reduced cardiac venous pole remodeling[31,46].

The limited time-window of *GATA4-Nkx2*.5 transcriptional modulation cannot account for the full, complex phenotypic spectrum of Tg mice. Dynamic titin isoform alterations in Tg hearts and reduced myofibrillar compliance accompanied by increased max force in neonatal Tg myofibrils[1,47,48] (Figure 8B~~A~~-D~~C~~), altogether indicate a correlation between increased ANKRD1 levels and titin response. Transgene expression was exclusively sarcomeric in fetal and neonatal hearts, suggesting that altered ANKRD1 stoichiometry could directly affect titin mechanosensing properties at these stages. However, as titin compliance can be finely modulated by ANKRD1 binding[1,49], its mechanosensing properties could be affected already in early Tg embryos. We cannot additionally rule out that ANKRD1-

Field Code Changed

GATA4(-Nkx2.5)-mediated cardiomyocyte disorganization can contribute to trigger an initial titin response (Figure 8BA). Titin can finely respond to changes in sarcomere stretch by differential splicing of its spring elements, resulting in either increased or decreased passive stiffness[41,50] and can additionally regulate sarcomere assembly[51] and stability[42] from development to adult life[41,50,52]. Thus, our data suggest that titin-mediated mechanotransduction impairment plays a relevant role in Tg cardiomyocyte phenotype functional modulation (Figure 8BA).

Altogether, our results show that activation of *GATA4-Nkx2.5* transcription and titin gene modulation are temporally distinct but integrated systems of rapid response to changes in ANKRD1 levels and in hemodynamic load**.**

4.2 ANKRD1 overexpression and cardiac functional disease

Early postnatal transgenic cardiomyocytes presented signs (functional, molecular and ultrastructural changes) of ongoing cardiac disease. They are likely the result of mechanotransduction impairment, due to changes in hemodynamic load and increased Tg expression at birth.

Disease progression in postnatal life is triggered by both the cellular/functional and the anatomical substrates. 2M Tg hearts presented an early adaptive response, likely triggered by small volume overload due to the R-L shunt and impaired compliance of ventricular cardiomyocytes (Figure 8CB). Progressively, altered hemodynamics and impaired functionality in Tg cardiomyocytes initiate a vicious loop, that peaks to the maladaptive organ response observed at 10M (Figure 8B). Dramatic worsening of Tg ventricular cardiomyocyte ultrastructure in adult hearts could be caused by their altered mechanosensing properties combined to the high workload of ventricular chambers. As a support to our hypothesis, myofibrillar loss was absent in adult Tg LA, in line with its major function as a reservoir chamber.

Functional analysis demonstrated a significant slowing down in the fast component of myofibrillar relaxation kinetics in 10M Tg hearts. This finding indicates an impairment in inter-sarcomeric dynamics, likely due to the altered load conditions[53]. Comparable passive properties of 10M wt and Tg indicated that late diastolic dysfunction is due to impaired ventricular relaxation (lusitropy), not impaired passive stiffness (Figure 8DC). Additional possible contributors to

Field Code Changed
Field Code Changed
Field Code Changed
Field Code Changed
Field Code Changed
Field Code Changed
Field Code Changed
Field Code Changed

cardiomyocyte dysfunction, such as altered intracellular Ca^{2+} dynamics and impaired energetic costs[54,55] most likely contribute to the diastolic impairment.

The mechanistic links between ANKRD1 overexpression and cardiac disease progression can only partially be elucidated. However, transgene nucleo-sarcomeric sublocalization during postnatal life indicates that ANKRD1 can sense the altered cardiomyocyte status and, once a certain threshold is reached, can respond by modulating its interacting partners.

ANKRD1 gain of function mutations have been identified in HCM and DCM patients[18,19]. DCM-associated features are ventricular dilatation, wall thinning and reduced systolic function, whereas HCM presents with normal or increased systolic function and strong variability: a subset of patients develop HF, a minority further progresses to end stage HF, which resembles DCM[56]. At the organ level, ANKRD1 Tg hearts present typical features of HCM, *ie* diastolic dysfunction with preserved systolic functionality and phenotypic variability associated to disease progression[57]. Hypertrophic response, the hallmark of human HCM disease, was not present in *ANKRD1* Tg mice, however this is a shared characteristic of Tg mouse models of sarcomere-associated HCM mutations[58,59].

Contractile dysfunction plays a central role in cardiomyopathies onset and progression. Increased contraction is associated to HCM onset, whereas disruption of sarcomeric function and/or structure has been suggested as early landmark of DCM[56]. ANKRD1 Tg neonatal hearts presented both features, *ie* increased myofibrils maximal force and an initial sarcomeric loss (Figure 8C~~B~~,D~~C~~). Cardiac disease progression is characterized by increased cardiomyocyte compliance, which is generally higher in DCM and end-stage HF, compared to early-stage patients[60,61]. In this line, the dynamic alteration of contractile properties in Tg myofibrils parallels functional changes observed in human disease.

5. Conclusions and perspectives

Our study defines for the first time a unifying picture for ANKRD1 role in heart development, CHD and adult cardiomyopathy occurrence. The complexity and multifactorial components of human disease suggests a note of caution for any direct extrapolation from animal models to humans. Phenotypic variability of our Tg mice allows to speculate that fine modulation of interacting partners and signalling

Field Code Changed
Field Code Changed
Field Code Changed
Field Code Changed
Field Code Changed
Field Code Changed
Field Code Changed
Field Code Changed
Field Code Changed

pathways could results in different disease outcome in humans, as previously proposed[62]. Our results open the perspective that gain of function mutations of *ANKRD1* gene could be a prognostic early genetic marker for adult cardiomyopathy, in addition to congenital malformations, such as SV defects and TAPVR.

Funding

This work was supported by European Union's Horizon 2020 research and innovation program under grant agreement no. 777204 (SILICOFCM) to C.P, University of Insubria (FAR 2016-2018) and Federico Ghidoni Memorial Fund to F.A., Italian Ministry of Education, University and Research (DOR 2018) to SA.

Acknowledgements

We thank Cinzia Parolini for help and support in animal handling and tissue harvesting, Walter Giuriati for histological analysis, Sandra Furlan and Marco Sandri for help in data analysis, Marta Murgia for critical reading of the manuscript and for discussion.

Conflict of interests

None declared.

References

1. Lun AS, Chen J, Lange S. Probing muscle ankyrin-repeat protein (MARP) structure and function. *Anat Rec (Hoboken)* 2014;**297**:1615–1629.
2. Miller MK, Bang M-L, Witt CC, Labeit D, Trombitas C, Watanabe K, Granzier H, McElhinny AS, Gregorio CC, Labeit S. The muscle ankyrin repeat proteins: CARP, ankrd2/Arpp and DARP as a family of titin filament-based stress response molecules. *J Mol Biol* 2003;**333**:951–964.
3. Ling SSM, Chen Y-T, Wang J, Richards AM, Liew OW. Ankyrin Repeat Domain 1 Protein: A Functionally Pleiotropic Protein with Cardiac Biomarker Potential. *Int J Mol Sci* 2017;**18**:1362.
4. Badi I, Cinquetti R, Frascoli M, Parolini C, Chiesa G, Taramelli R, Acquati F. Intracellular ANKRD1 protein levels are regulated by 26S proteasome-mediated degradation. *FEBS Lett* 2009;**583**:2486–2492.

5. Zou Y, Evans S, Chen J, Kuo HC, Harvey RP, Chien KR. CARP, a cardiac ankyrin repeat protein, is downstream in the Nkx2-5 homeobox gene pathway. *Development* 1997;**124**:793–804.
6. Kuo H, Chen J, Ruiz-Lozano P, Zou Y, Nemer M, Chien KR. Control of segmental expression of the cardiac-restricted ankyrin repeat protein gene by distinct regulatory pathways in murine cardiogenesis. *Development* 1999;**126**:4223–4234.
7. Jeyaseelan R, Poizat C, Baker RK, Abdishoo S, Isterabadi LB, Lyons GE, Kedes L. A novel cardiac-restricted target for doxorubicin. CARP, a nuclear modulator of gene expression in cardiac progenitor cells and cardiomyocytes. *J Biol Chem* 1997;**272**:22800–22808.
8. Bang ML, Mudry RE, McElhinny AS, Trombitás K, Geach AJ, Yamasaki R, Sorimachi H, Granzier H, Gregorio CC, Labeit S. Myopalladin, a novel 145-kilodalton sarcomeric protein with multiple roles in Z-disc and I-band protein assemblies. *J Cell Biol* 2001;**153**:413–427.
9. Chen B, Zhong L, Roush SF, Pentassuglia L, Peng X, Samaras S, Davidson JM, Sawyer DB, Lim CC. Disruption of a GATA4/Ankrd1 Signaling Axis in Cardiomyocytes Leads to Sarcomere Disarray: Implications for Anthracycline Cardiomyopathy. Capogrossi MC, ed. *PLoS One* 2012;**7**:e35743.
10. Zhong L, Chiusa M, Cadar AG, Lin A, Samaras S, Davidson JM, Lim CC. Targeted inhibition of ANKRD1 disrupts sarcomeric ERK-GATA4 signal transduction and abrogates phenylephrine-induced cardiomyocyte hypertrophy. *Cardiovasc Res* 2015;**106**:261–271.
11. Aihara Y, Kurabayashi M, Saito Y, Ohyama Y, Tanaka T, Takeda S, Tomaru K, Sekiguchi K, Arai M, Nakamura T, Nagai R. Cardiac ankyrin repeat protein is a novel marker of cardiac hypertrophy: role of M-CAT element within the promoter. *Hypertens (Dallas, Tex 1979)* 2000;**36**:48–53.
12. Wei Y-J, Cui C-J, Huang Y-X, Zhang X-L, Zhang H, Hu S-S. Upregulated expression of cardiac ankyrin repeat protein in human failing hearts due to arrhythmogenic right ventricular cardiomyopathy. *Eur J Heart Fail* 2009;**11**:559–566.
13. Kempton A, Cefalu M, Justice C, Baich T, Derbala M, Canan B, Janssen PML, Mohler PJ, Smith SA. Altered regulation of cardiac ankyrin repeat protein in

heart failure. *Heliyon* 2018;**4**:e00514.

14. Bang M-L, Gu Y, Dalton ND, Peterson KL, Chien KR, Chen J. The muscle ankyrin repeat proteins CARP, Ankrd2, and DARP are not essential for normal cardiac development and function at basal conditions and in response to pressure overload. Xu X, ed. *PLoS One* 2014;**9**:e93638.
15. Shen L, Chen C, Wei X, Li X, Luo G, Zhang J, Bin J, Huang X, Cao S, Li G, Liao Y. Overexpression of ankyrin repeat domain 1 enhances cardiomyocyte apoptosis by promoting p53 activation and mitochondrial dysfunction in rodents. *Clin Sci* 2015;**128**:665–678.
16. Song Y, Xu J, Li Y, Jia C, Ma X, Zhang L, Xie X, Zhang Y, Gao X, Zhang Y, Zhu D. Cardiac Ankyrin Repeat Protein Attenuates Cardiac Hypertrophy by Inhibition of ERK1/2 and TGF-β Signaling Pathways. Hirsch E, ed. *PLoS One* 2012;**7**:e50436.
17. Arimura T, Bos JM, Sato A, Kubo T, Okamoto H, Nishi H, Harada H, Koga Y, Moulik M, Doi YL, Towbin JA, Ackerman MJ, Kimura A. Cardiac Ankyrin Repeat Protein Gene (ANKRD1) Mutations in Hypertrophic Cardiomyopathy. *J Am Coll Cardiol* 2009;**54**:334–342.
18. Duboscq-Bidot L, Charron P, Ruppert V, Fauchier L, Richter A, Tavazzi L, Arbustini E, Wichter T, Maisch B, Komajda M, Isnard R, Villard E, EUROGENE Heart Failure Network. Mutations in the ANKRD1 gene encoding CARP are responsible for human dilated cardiomyopathy. *Eur Heart J* 2009;**30**:2128–2136.
19. Moulik M, Vatta M, Witt SH, Arola AM, Murphy RT, McKenna WJ, Boriek AM, Oka K, Labeit S, Bowles NE, Arimura T, Kimura A, Towbin JA. ANKRD1, the gene encoding cardiac ankyrin repeat protein, is a novel dilated cardiomyopathy gene. *J Am Coll Cardiol* 2009;**54**:325–333.
20. Acquati F, Russo A, Taramelli R, Tibiletti MG, Taborelli M, Camesasca C, Papa M. Nonsyndromic total anomalous venous return associated with a de novo translocation inolving chromosomes 10 and 21 t(10;21)(q23.1;q11.2). *Am J Med Genet* 2000;**95**:285–286.
21. Cinquetti R, Badi I, Campione M, Bortoletto E, Chiesa G, Parolini C, Camesasca C, Russo A, Taramelli R, Acquati F. Transcriptional deregulation and a missense mutation define ANKRD1 as a candidate gene for total

anomalous pulmonary venous return. *Hum Mutat* 2008;**29**:468–474.

22. Correa-Villaseñor A, Ferencz C, Boughman JA, Neill CA. Total anomalous pulmonary venous return: familial and environmental factors. The Baltimore-Washington Infant Study Group. *Teratology* 1991;**44**:415–428.

23. Cinquetti R, Badi I, Campione M, Bortoletto E, Chiesa G, Parolini C, Camesasca C, Russo A, Taramelli R, Acquati F. Transcriptional deregulation and a missense mutation define ANKRD1 as a candidate gene for total anomalous pulmonary venous return. *Hum Mutat* 2008;**29**.

24. Subramaniam A, Jones WK, Gulick J, Wert S, Neumann J, Robbins J. Tissue-specific regulation of the alpha-myosin heavy chain gene promoter in transgenic mice. *J Biol Chem* 1991;**266**:24613–24620.

25. Piroddi N, Belus A, Eiras S, Tesi C, Velden J van der, Poggesi C, Stienen GJM. No direct effect of creatine phosphate on the cross-bridge cycle in cardiac myofibrils. *Pflügers Arch* 2006;**452**:3–6.

26. Colomo F, Piroddi N, Poggesi C, Kronnie G te, Tesi C. Active and passive forces of isolated myofibrils from cardiac and fast skeletal muscle of the frog. *J Physiol* 1997;**500 (Pt 2)**:535–548.

27. Scellini B, Piroddi N, Flint G V., Regnier M, Poggesi C, Tesi C. Impact of tropomyosin isoform composition on fast skeletal muscle thin filament regulation and force development. *J Muscle Res Cell Motil* 2015;**36**:11–23.

28. Lange FJ de, Moorman AFM, Anderson RH, Männer J, Soufan AT, Gier-de Vries C de, Schneider MD, Webb S, Hoff MJB van den, Christoffels VM. Lineage and morphogenetic analysis of the cardiac valves. *Circ Res* 2004;**95**:645–654.

29. Christoffels VM, Mommersteeg MTM, Trowe M-O, Prall OWJ, Gier-de Vries C de, Soufan AT, Bussen M, Schuster-Gossler K, Harvey RP, Moorman AFM, Kispert A. Formation of the Venous Pole of the Heart From an *Nkx2–5* – Negative Precursor Population Requires *Tbx18*. *Circ Res* 2006;**98**:1555–1563.

30. Tretter JT, Chikkabyrappa S, Spicer DE, Backer CL, Mosca RS, Anderson RH, Bhatla P. Understanding the spectrum of sinus venosus interatrial communications. *Cardiol Young* 2017;**27**:418–426.

31. Berg G van den, Moorman AFM. Development of the pulmonary vein and the systemic venous sinus: An interactive 3D overview. *PLoS One* 2011;**6**.

Formatted: English (United States)

32. Campione M, Ros MA, Icardo JM, Piedra E, Christoffels VM, Schweickert A, Blum M, Franco D, Moorman AFM. Pitx2 expression defines a left cardiac lineage of cells: Evidence for atrial and ventricular molecular isomerism in the iv/iv mice. *Dev Biol* Academic Press Inc.; 2001;**231**:252–264.
33. Hoogaars WMH, Tessari A, Moorman AFM, Boer PAJ de, Hagoort J, Soufan AT, Campione M, Christoffels VM. The transcriptional repressor Tbx3 delineates the developing central conduction system of the heart. *Cardiovasc Res* 2004;**62**:489–499.
34. Christoffels VM, Habets PE, Franco D, Campione M, Jong F de, Lamers WH, Bao ZZ, Palmer S, Biben C, Harvey RP, Moorman AF. Chamber formation and morphogenesis in the developing mammalian heart. *Dev Biol* 2000;**223**:266–278.
35. Chen H, Shi S, Acosta L, Li W, Lu J, Bao S, Chen Z, Yang Z, Schneider MD, Chien KR, Conway SJ, Yoder MC, Haneline LS, Franco D, Shou W. BMP10 is essential for maintaining cardiac growth during murine cardiogenesis. *Development* 2004;**131**:2219–2231.
36. Heldin C-H, Moustakas A. Signaling Receptors for TGF-β Family Members. *Cold Spring Harb Perspect Biol* 2016;**8**.
37. Broberg CS, Pantely GA, Barber BJ, Mack GK, Lee K, Thigpen T, Davis LE, Sahn D, Hohimer AR. Validation of the myocardial performance index by echocardiography in mice: a noninvasive measure of left ventricular function. *J Am Soc Echocardiogr* 2003;**16**:814–823.
38. Faggiano P, Vizzardi E, Pulcini E, Maffeo D, Fracassi F, Nodari S, Dei Cas L. The study of left ventricular diastolic function by Doppler echocardiography: the essential for the clinician. *Heart Int* 2007;**3**:42.
39. Rigatelli G, Zuin M, Dell'Avvocata F. Atrial fibrillation and patent foramen potentially share same atrial flow dynamic profile and thrombotic mechanism. *Eur J Intern Med* 2017;**44**:e20–e21.
40. LINKE W. Sense and stretchability: The role of titin and titin-associated proteins in myocardial stress-sensing and mechanical dysfunction. *Cardiovasc Res* Oxford University Press; 2008;**77**:637–648.
41. Granzier HL, Labeit S. The Giant Protein Titin. *Circ Res* 2004;**94**:284–295.
42. Linke WA, Hamdani N. Gigantic Business. *Circ Res* 2014;**114**:1052–1068.

Formatted: English (United States)

43. Gui Y-H, Linask KK, Khowsathit P, Huhta JC. Doppler Echocardiography of Normal and Abnormal Embryonic Mouse Heart. *Pediatr Res* 1996;**40**:633–642.
44. Brewer AC, Alexandrovich A, Mjaatvedt CH, Shah AM, Patient RK, Pizzey JA. GATA Factors Lie Upstream of Nkx 2.5 in the Transcriptional Regulatory Cascade That Effects Cardiogenesis. *Stem Cells Dev* 2005;**14**:425–439.
45. McCulley DJ, Black BL. Transcription Factor Pathways and Congenital Heart Disease. *Current Topics in Developmental Biology* Academic Press Inc.; 2012. p. 253–277.
46. Butts RJ, Crean AM, Hlavacek AM, Spicer DE, Cook AC, Oechslin EN, Anderson RH. Veno-venous bridges: the forerunners of the sinus venosus defect. *Cardiol Young* 2011;**21**:623–630.
47. Elhamine F, Radke MH, Pfitzer G, Granzier H, Gotthardt M, Stehle R. Deletion of the titin N2B region accelerates myofibrillar force development but does not alter relaxation kinetics. *J Cell Sci* 2014;**127**:3666–3674.
48. Sequeira V, Velden J van der. The Frank–Starling Law: a jigsaw of titin proportions. *Biophys Rev* 2017;**9**:259–267.
49. Zhou T, Fleming JR, Franke B, Bogomolovas J, Barsukov I, Rigden DJ, Labeit S, Mayans O. CARP interacts with titin at a unique helical N2A sequence and at the domain Ig81 to form a structured complex. *FEBS Lett* 2016;**590**:3098–3110.
50. Anderson BR, Granzier HL. Titin-based tension in the cardiac sarcomere: molecular origin and physiological adaptations. *Prog Biophys Mol Biol* 2012;**110**:204–217.
51. Walker JS, Tombe PP de. Titin and the Developing Heart. *Circ Res* 2004;**94**:860–862.
52. Opitz CA, Leake MC, Makarenko I, Benes V, Linke WA. Developmentally Regulated Switching of Titin Size Alters Myofibrillar Stiffness in the Perinatal Heart. *Circ Res* 2004;**94**:967–975.
53. Poggesi C, Tesi C, Stehle R. Sarcomeric determinants of striated muscle relaxation kinetics. *Pflugers Arch* 2005;**449**:505–517.
54. Borlaug BA, Kass DA. Mechanisms of Diastolic Dysfunction in Heart Failure. *Trends Cardiovasc Med* 2006;**16**:273–279.

55. Lopes LR, Elliott PM. A straightforward guide to the sarcomeric basis of cardiomyopathies. *Heart* 2014;**100**:1916–1923.
56. Garfinkel AC, Seidman JG, Seidman CE. Genetic Pathogenesis of Hypertrophic and Dilated Cardiomyopathy. *Heart Fail Clin* 2018;**14**:139–146.
57. Velden J van der, Ho CY, Tardiff JC, Olivotto I, Knollmann BC, Carrier L. Research priorities in sarcomeric cardiomyopathies. *Cardiovasc Res* 2015;**105**:449–456.
58. Moore RK, Grinspan LT, Jimenez J, Guinto PJ, Ertz-Berger B, Tardiff JC. HCM-linked Δ160E cardiac troponin T mutation causes unique progressive structural and molecular ventricular remodeling in transgenic mice. *J Mol Cell Cardiol* 2013;**58**:188–198.
59. Michele DE, Gomez CA, Hong KE, Westfall M V, Metzger JM. Cardiac dysfunction in hypertrophic cardiomyopathy mutant tropomyosin mice is transgene-dependent, hypertrophy-independent, and improved by beta-blockade. *Circ Res* 2002;**91**:255–262.
60. Heerebeek L van, Borbély A, Niessen HWM, Bronzwaer JGF, Velden J van der, Stienen GJM, Linke WA, Laarman GJ, Paulus WJ. Myocardial Structure and Function Differ in Systolic and Diastolic Heart Failure. *Circulation* 2006;**113**:1966–1973.
61. Vikhorev P, Vikhoreva N. Cardiomyopathies and Related Changes in Contractility of Human Heart Muscle. *Int J Mol Sci* 2018;**19**:2234.
62. Lange S, Gehmlich K, Lun AS, Blondelle J, Hooper C, Dalton ND, Alvarez EA, Zhang X, Bang M-L, Abassi YA, Remedios CG Dos, Peterson KL, Chen J, Ehler E. MLP and CARP are linked to chronic PKCα signalling in dilated cardiomyopathy. *Nat Commun* 2016;**7**:12120.

Formatted: English (United States)

Figure legends

Figure 1: *Ankrd1* mRNA and protein expression in cardiac development. A-C: *Ankrd1* mRNA expression in E8.5-E14.5 hearts, ISH analysis. Myocardium is identified by *Mhc* transcripts. A: E8.5(a,b), E10.5(c), E12.5(d), E14.5(h) hearts, global view. Dotted areas in e are magnified below. B: *Ankrd1* expression at venous pole of E10(a,b), E10.5(c,d), E12.5(e,f), E14.5(g,h) embryos. C: *Ankrd1* expression in atrial and ventricular chambers of E10.5(a-d) and E14.5(e,f) embryos. D-E: Ankrd1

721 protein expression and sub-cellular localization in E10.5 and E14.5 hearts, double
722 immunofluorescence and confocal analysis. D: E10.5(a,b) and E14.5(c,d) hearts,
723 overview pictures. Note heterogeneous reaction of α-Ankrd1(a,c) *vs* α-actinin(b,d)
724 antibody. E: at E10.5(a,b) Ankrd1 presents sarcomeric and nuclear (arrows) co-
725 localization; at E14.5(c,d) Ankrd1 is exclusively sarcomeric. Note strong (yellow star)
726 or low (white star) α-Ankrd1 antibody reaction in neighboring cardiomyocytes. ca:
727 common atrium; v: primitive ventricle; avc: atrioventricular canal; oft: outflow tract;
728 rv: right ventricle; lv: left ventricle; r,l-pr: right,left pulmonary ridge; rsh,lsh: righ,left
729 sinus horn; sp: septum primum; ivs: interventricular septum; vv: venous valves; icv:
730 inferior caval vein; pv: pulmonary vein; lscv, rscv: left, right superior caval vein.
731 Scale bar: A-C=100 μm; D=100 μm, E=10μm.
732
733 **Figure 2: ANKRD1 overexpression affects fine rotation and remodeling in the**
734 **early myocardium. A**: abnormal rotation and remodeling in E10.5 Tg compared to
735 wt embryos, ISH whole mount (a,e) and on sections (b-d, f-h,) analysis. Dotted lines
736 in a,e show LA-LV angle in wt (white) and Tg (red); double-headed arrow shows
737 cranio-caudal extension of the heart from the LV base to the outflow tract. b,f:
738 abnormal shape and position of cardiac chambers, atrioventricular canal (asterisk) and
739 septum primum (dotted box) in Tg. Red dotted lines in c,d,g,h indicate the
740 myocardium of the pulmonary ridges. Black arrow indicates the pulmonary pit,
741 misplaced in Tg embryos. Yellow arrowheads indicate $Tbx18^{+}$ cells within the dorsal
742 mesocardium (dm). B: Venous pole organization in E10.5 Tg (a-d) and E9.5 wt (e-g)
743 embryos, ISH on sections (a-d,f,g) and whole mount (e). Red dotted lines delineate
744 the sino-atrial myocardium. Yellow arrowheads indicate *Tbx18*$^{+}$ cells within the dm.
745 Black dotted circle in f'-g highlights the base of the dm where some $Tbx18^{+}$ cells are
746 visible, flanking the loosely arranged mesoderm (red asterisks). fg: foregut; pe:
747 proepicardium. See Figure legend 1 for other abbreviations. Scale bar:A,B=100μm.
748
749 **Figure 3: SV defects in mid-fetal and neonatal ANKRD1 Tg hearts**. A: 3D
750 reconstruction of the sino-atrial region and venous system lumen in E13.5 hearts,
751 highlighting anomalous venous pole organization in Tg hearts. Note in d, the
752 canalizations around PV and systemic veins and a compressed shape of the vestibular
753 region; b,c,e,f: virtual sections at the venous pole. In Tg embryos, the

754 communications between PV and systemic veins around the vestibular regions define
755 the SV defects. Black lines delineate splanchnopleure. B: neonatal hearts, freshly
756 isolated (a,e) and H/E analysis (b-d, f-h). c: white arrow indicates atrial malrotation,
757 yellow arrow indicates rounded ventricular apex. g-h: SV defects in Tg hearts.
758 Confluence of RSCV and PV at the dorsal atrial wall (asterisk in g) and into the RA
759 (h) are clearly recognizable. Black arrowhead in g indicates the misshapen fossa
760 ovalis. See Figure legend 1 for abbreviations. Scale bar: Aa-f=100μm;
761 Ba,b,e,f=500μm; Bc,d,g,h=200 μm.
762
763 **Figure 4: Timed transcriptional modulation in ANKRD1 Tg embryos.** A: *GATA4*
764 and *Nkx2.5* mRNA expression levels in E10.5 (wt=5, Tg=4) and E14.5 (wt=4,Tg=5)
765 hearts, *p<0.05 , Student unpaired t-test; values are compared to the mean wt level at
766 each stage. B: ISH analysis shows that molecular patterning is not affected in E14.5
767 Tg hearts. san: sino-atrial node; avn: atrio-ventricular node; icv: inferior caval vein;
768 for other abbreviations see Figure legend 1. Scale bar: a–h:20 μm; i-r:10 μm.
769
770 **Figure 5: Adult ANKRD1 Tg hearts analysis**. A: Phenotypic variability in 10M Tg
771 hearts. a-d: freshly isolated hearts; e-n: histological analysis, sino-atrial (e-h) and
772 ventricular (i-n) regions; H/E (e-g, i-l) and Sirius red (h,m,n) staining. Black
773 arrowhead indicates the enlarged Tg LA, asterisk indicates thrombus. e-h: note in (f)
774 anomalous confluence of PV (red dotted arrow) and RSCV (black arrow) at the dorsal
775 atrial wall. g: dotted box indicates PFO, associated to thrombus formation. h: fibrotic
776 infiltration within LA thrombus. i-l: dilatation and altered geometry in Tg LV; m-n:
777 moderate fibrosis in Tg LV. o: Western blot analysis of BNP *vs* GADPH expression
778 in 10M wt (n=4) and Tg (n=5) hearts, representative results and box plot
779 quantification; *p<0.05 , Student unpaired t-test. Scale bar: a-d=1mm, e-g, i-l=
780 0.5mm, g-i=100μm. B: *In vivo* analysis. a,b: PV Doppler flow profile of a
781 representative 2M wt (a) and Tg (b) mouse. Red arrows indicate *d2* wave in Tg. c,d:
782 representation of mean PV Doppler flow curves in wt and Tg mice at 2 and 10M.
783 Mean *a*, *s* and *d* values are from Table 1. e,f: echocardiographic view of a 10M wt (e)
784 and Tg (f) heart. Note strongly enlarged LA in Tg (red line).
785

Figure 6: Modulation of contractile properties in ANKRD1 Tg hearts. A: functional analysis on isolated myofibrils. a-c: average sarcomere length-resting tension relation of myofibrils from E14.5 (a) newborn (b) and adult (c) hearts; wt, *black circle;* Tg, *red circle.* Vertical and horizontal bars are SEM. (d) Mechanical properties of myofibrils from newborn and adult hearts (myofibrils number in brackets). SL: sarcomere length, P_0 : maximum isometric tension, k_{ACT} : rate constant of force development following maximal Ca^{2+}-activation, D_{slow} : duration of the slow linear phase of relaxation, Slow-Fast k_{REL} : rate constants of tension relaxation for slow and fast relaxation phases. $^{*}p < 0.001$, $^{\#}p < 0.02$, Student unpaired t-test. B**:** qPCR results of sarcomeric genes expression in E14.5 and newborn hearts. wt *vs* Tg: p>0.05 for each stage, Student unpaired t-test; values are compared to the mean wt level at each stage. C: titin splice variant analysis. Top: schematic representation of titin N2BA and N2B structure; arrows indicate position of primers used for N2BA combinatorial exon analysis, red arrows: regions with differential exon inclusion in newborn wt/Tg. Bottom left: N2B/N2BA isoform ratio analysis. $^{*}p < 0.05$, Student unpaired t-test; values are compared to the mean wt level at each stage. Bottom right: PCR amplification of exons 72-80 and exons 137-156 from wt and Tg hearts (n=5) results in multiple amplicons (square boxes) of different length. The longest amplicons are mostly detected in wt hearts. Y axis: amplicons length (bp); X axis: count of wt and Tg samples which present the specified amplicon (see Figure S5 for original data).

Figure 7: Impairment of cardiomyocyte organization and ultrastructure in ANKRD1 Tg hearts. A: Cardiomyocyte organization in embryonic wt and Tg hearts. H/E analysis at E10.5 (a,f) and confocal analysis of E14.5 RV wall (b,c,g,h), trabeculae (d,i) and atria (e,l);. b,g: bright field and nuclei, merged; c-e,h-l: actinin. b,c and g,h are adjacent sections. Scale bar: a,f=20µm; b-e,g-l=10µm B: TEM analysis of neonatal and adult ventricles and of adult atria, at low (a-c,f-h) and high magnification (d,e,i,l). Red asterisk: focal sarcomeric loss, red arrow: sarcomeric disorganization, double headed arrow: extensive sarcomeric loss, green asterisk: damaged mitocondria; yellow arrowheads: lipid droplets. Scale bar: a-c,f,h= 5µm; d,e,i,l= 1µm.

Figure 8: Working model linking ANKRD1 expression, ~~-~~overexpression ~~and~~and cardiac disease. A: Ankrd1 role in heart development. Heterogeneous Ankrd1 expression and its dynamic nucleo-sarcomeric sub-localization modulate developmental cardiac remodeling in response to hemodynamics by finely regulating cardiomyocyte transcription and mechanotransduction; ~~-~~ the initially contiguous PV (yellow, dotted lines) and systemic veins (red, dotted lines) precursors become spatially separated by mid-fetal stage. B~~A~~: temporally distinct transcriptional modulation scored in embryonic and neonatal Tg hearts (red arrows) and their proposed link with disease onset and early progression at the cellular and organ levels (black arrows). C~~B~~,D~~C~~: disease onset and progression in Tg hearts, with the underlying cardiomyocyte defects (C~~B~~) and ~~corresponding~~ myofibrillar functional modifications (D~~C~~) ~~during disease onset and progression in Tg hearts~~. ~~-~~Embryos: impaired myocardial remodeling retains the contiguity of the regions where PV ~~(yellow)~~ and systemic veins ~~(red)~~ precursors are located, ~~(dotted lines),~~ thereby causing SV defect~~; this is driven by an initial cardiomyocyte structural/functional defect, in the presence of low hemodynamic load.~~ . ~~-~~Postnatal life: ~~in~~ neonatal Tg hearts present ~~, higher hemodynamic load leads to~~ overt cardiomyocyte structural and functional impairment. A~~A~~ltered A-V hemodynamic cross talk (double headed arrow), due to SV defect and impaired functionality in Tg cardiomyocytes, initiates a vicious loop that progressively leads to diastolic dysfunction (dd), then heart failure (dHF). D~~C~~: Tg myofibrillar functional properties (compliance, lusitropism and maximal force) present substantial modifications in prenatal and postnatal life, as shown by reduced and then increased compliance, progressive reduction of lusitropism and persistent higher maximal force. Color code: green, values in Tg myofibrils comparable to corresponding wt; red: values higher than wt.

Tables

Table 1: Ecocardiographic (top) and hemodynamic (botton) analysis of wt and ANKRD1 Tg mice at 2 and 10 months; n= number of animal analyzed (2M: wt=6 males, 4 females; Tg= 3 males, 5 females; 10M:wt=6 males, 3 females, Tg= 2 males, 5 females). Values are indicated as mean ± SE. *np*: not present; Legend: LV%EF: LV ejection fraction; LV%FS: LV fractional shortening; IVSd: interventricular septum

Formatted: Not Highlight
Formatted: Not Highlight
Formatted: Font: Not Bold
Formatted: Font: Not Bold, Not Highlight
Formatted: Font: Not Bold
Formatted: Font: Not Bold, Not Highlight
Formatted: Font: Not Bold
Formatted: Font: Not Bold, Not Italic, Not Highlight
Formatted: Font: Not Bold
Formatted: Font: Not Bold, Not Italic, Not Strikethrough
Formatted: Font: Not Bold
Formatted: Not Highlight
Formatted: Not Highlight
Formatted: Strikethrough
Formatted: Strikethrough
Formatted: Not Highlight
Formatted: Strikethrough
Formatted: Strikethrough
Formatted: Strikethrough
Formatted: Highlight
Formatted: Highlight

diastolic thickness; IVSs: interventricular septum systolic thickness; LVIDd: LV internal diameter, diastolic; LVIDs: LV internal diameter, systolic; LVPWd: LV posterior wall, diastolic; LVPWs: LV posterior wall, systolic; MPI: myocardial performance index. See text and supplementary methods for other abbreviations. Wt *vs* Tg data comparison at each stage (2M, 10M) was performed by Mann-Wilcoxon W test; 2M *vs* 10M data comparison for each experimental group (wt and Tg) was performed by Wilcoxon signed-rank test.

884
885
886

Formatted: English (United States)

	Wt 2M (n=10)	Tg 2M (n=8)	Wt10M (n=9)	Tg 10M (n=7)	Wt *vs Tg* @2M (p)	Wt *vs* Tg @10M (p)	Wt: 2M *vs* 10M (p)	Tg: 2M *vs* 10M (p)
LV%EF	56,80 ±3,64	**63,75 ±4,87**	58,25 ±2,94	**63,29 ±4,03**	0,23	**0,22**	0,87	1
LV%FS	29,40 ±2,53	**34,50 ±3,39**	30,25 ±1,91	**34,43 ±2,90**	0,25	**0,20**	0,93	1
IVSd	-	-	1,05 ±0,05	**0,96 ±0,07**	-	**0,31**		-
IVSs	-	-	1,48 ±0,03	**1,43 ±0,05**	-	**0,56**	-	-
LVIDd	-	-	3,89 ±0,14	**3,81 ±0,15**	-	**1**	-	-
LVIDs	-	-	2,69 ±0,15	**2,50 ±0,19**	-	**0,30**	-	-
LVPWd	-	-	0,97 ±0,04	**0,94 ±0,06**	-	**0,90**	-	-
LVPWs	-	-	1,36 ±0,04	**1,15 ±0,10**	-	**0,05***	-	
E/A	2,13 ±0,21	**2,04 ±0,27**	2,06 ±0,23	**3,13 ± 0,57**	0,95	0,10	1	0,06
DT	19,05 ±2,12	**23,01 ±3,12**	14,90 ±1,66	**14,26 ±2,14**	0,41	0,79	0,23	0,06
MPI	0,79 ± 0,04	**0,80 ± 0,07**	0,71 ± 0,04	**0,86 ± 0,06**	0,89	0,06	0,55	0,45
d	363,20 ± 63,65	**507,25 ± 75,27**	587,13 ±121,23	**629,43 ±132,17**	0,14	0,86	0,91	0,19
d2	*np*	**298,5 ± 39,90**	*np*	***np***	-	-	-	-
a	-111,40 *± 13,18*	**-187,63 *± 30,36***	-191,13 *±71,75*	**-132,57 *±37,56***	0,03*	0,86	0,91	0,12
s	271,20 ± 13,18	**371,88 ± 30,36**	311,00 ±71,75	**203,86 ± 37,56**	0,17	0,02*	0,41	0,03*
s/d	1,01 ±0,22	**0,66 ±0,08**	0,80 ±0,22	**0,34 ±0,04**	0,45	0,01*	1	0,02*

a/d	-0,37 ±0,05	**-0,40** **±0,07**	-0,30 ±0,06	**-0,21** **±0,03**	0,82	0,22	1	0,08
a/s	-0,45 ±0,08	**-0,60** **±0,08**	-0,49 ±0,12	**-0,62** **±0,08**	0,12	0,32	0,32	0,67

887

Myocardial overexpression of ANKRD1 causes sinus venosus defects and progressive diastolic dysfunction

Nicoletta Piroddi[1], Paola Pesce[2], Beatrice Scellini[1], Stefano Manzini[3], Giulia S. Ganzetti[3], Ileana Badi[4,5], Michela Menegollo[6], Virginia Cora[6], Simone Tiso[6], Raffaella Cinquetti[4], Laura Monti[4] , Giulia Chiesa[3], Steven B. Bleyl[7], Marco Busnelli[3], Federica Dellera[3], Daniele Bruno[4], Federico Caicci[8], Annalisa Grimaldi[4], Roberto Taramelli[4], Lucia Manni[8], David Sacerdoti[2], Chiara Tesi[1], Corrado Poggesi[1], Simonetta Ausoni[6*], Francesco Acquati[4*], Marina Campione[6,9*].

[1]Department of Experimental and Clinical Medicine, University of Florence, 50134 Florence, Italy; [2]Department of Medicine, University of Padua, 35121 Padua, Italy; [3]Dept. of Pharmacological and Biomolecular Sciences, University of Milan, 20133 Milan, Italy; [4]Dept. of Biotechnology and Life Sciences, University of Insubria, 21100 Varese, Italy; [6]Dept. of Biomedical Sciences, University of Padua, 35121 Padua, Italy; [7] Dept. of Pediatrics, University of Utah, Salt Lake City, 84132 Utah, USA; [8]Dep. of Biology, University of Padua, 35121 Padua, Italy; [9]CNR-Neuroscience Institute, 35121 Padua, Italy.

[5]**Present address:** Division of Cardiovascular Medicine, Radcliffe Department of Medicine, University of Oxford, John Radcliffe Hospital, Oxford OX3 9DU, UK.

***: corresponding Authors**

Marina Campione: fax: +39-049-8276040; tel: +39-049-8276031;

E-mail: campione@bio.unipd.it ;

Francesco Acquati: fax: +39-0332-421500; tel: +39-0332-421512;

E-mail: francesco.acquati@uninsubria.it

Simonetta Ausoni: fax +39-049-8276040; tel: +39-049-8276036;

E-mail: simonetta.ausoni@unipd.it

Running title: ANKRD1 role in heart development and disease

Word count: 8560

Abstract

Aims: Increased ANKRD1 levels linked to gain of function mutations have been associated to total anomalous pulmonary venous return and adult cardiomyopathy occurrence in humans. The link between increased ANKRD1 level and cardiac structural and functional disease is not understood. To get insight into this problem, we have generated a gain of function ANKRD1 mouse model by overexpressing ANKRD1 in the myocardium.

Methods and Results: Ankrd1 is expressed non homogeneously in the embryonic myocardium, with a dynamic nucleo-sarcomeric localization in developing cardiomyocytes. ANKRD1 transgenic mice present sinus venosus defect, which originates during development by impaired remodeling of early embryonic heart. Adult transgenic hearts develop diastolic dysfunction with preserved ejection fraction, which progressively evolves into heart failure, as shown histologically and hemodynamically. Transgenic cardiomyocyte structure, sarcomeric assembly and stability are progressively impaired from embryonic to adult life. Postanatal transgenic myofibrils also present characteristic functional alterations: impaired compliance at neonatal stage and impaired lusitropism in adult hearts. Altogether, our combined analyses suggest that impaired embryonic remodeling and adult heart dysfunction in ANKRD1 transgenic mice present a common ground of initial cardiomyocyte defects, which are exacerbated postnatally. Molecular analysis showed transient activation of *GATA4-Nkx2.5* transcription in early transgenic embryos and subsequent dynamic transcriptional modulation within titin gene.

Conclusions: ANKRD1 is a fine mediator of cardiomyocyte response to hemodynamic load in the developing and adult heart. Increased ANKRD1 levels are sufficient to initiate an altered cellular phenotype, which is progressively exacerbated into a pathological organ response by the high ventricular workload during postnatal life. Our study defines for the first time a unifying picture for ANKRD1 role in heart development and disease and provides the first mechanistic link between ANKRD1 overexpression and cardiac disease onset.

1. Introduction

Ankyrin Repeat Domain 1 (ANKRD1, also known as Cardiac Ankyrin Repeat Protein, CARP) is a member of the muscle specific ankyrin repeat proteins (MARP) family, which also includes ANKRD2/Arpp and DARP[1,2]. MARP proteins are involved in muscle stress response and are structurally characterized by four ankirin repeats, a coiled-coil domain, a nuclear localization signal and a PEST degradation sequence, which mediates its rapid turnover via the ubiquitin-proteasome pathway[3,4].

ANKRD1 is highly expressed during heart development and down-regulated in adult life[5–7]. In the developing heart, ANKRD1 has been proposed to work as transcriptional cofactor and negative regulator of myocardial gene expression[5–7]. ANKRD1 is a target of Nkx2.5 *in vivo*[5] and its promoter can be cooperatively activated by Nkx2.5 and GATA4 [6].

In adult cardiomyocytes, ANKRD1 is normally located at the sarcomere, but it has been shown to translocate to the nucleus upon mechanical stimulation *in vitro*[2]. In the sarcomere, ANKRD1 is found at the I-band where it is a component of titin N2A-linked signalling complex[2,8]. Physical interaction between ANKRD1 and titin N2A spring domain has been shown to reduce PKA phosphorylation and titin compliance[1]. ANKRD1 has additionally been shown to functionally interact with GATA4 in the I band and the nucleus, thereby modulating GATA4-mediated sarcomeric gene expression and sarcomeric organization[9,10]. Interactions with several additional partners involved in modulation of muscle structure and function have been reported[3,8]. ANKRD1 is therefore part of a stretch-sensing unit capable of relaying biomechanical stress signals to the regulation of gene expression. In line, ANKRD1 expression is up-regulated in response to hypertrophy and in heart failure[6,11–13].However, the absence of cardiac phenotype in ANKRD1 knock-out mouse models[10,14], combined with contradictory results from loss and gain of function approaches[3,9,15,16], have precluded a clear understanding of ANKRD1 role in adult heart.

Genetic mutations in *ANKRD1*, mostly associated to a gain of function condition, have been correlated to several types of cardiac disease in humans. *ANKRD1* missense mutations have been identified in patients with hypertrophic and dilated cardiomyopathy (HCM, DCM)[17–19]. *ANKRD1* has additionally been identified as a candidate gene for total anomalous pulmonary venous return (TAPVR) in

isolated patients[20,21]. TAPVR is a congenital heart disease (CHD) which affects 1:15000 live births, and is characterized by incorrect pulmonary vein (PV) drainage into the heart[22]. TAPVR leads to high mortality rate in the first year of life, unless surgically corrected. Reported TAPVR patients presented either chromosomal rearrangement or T116M–*ANKRD1* mutation, leading respectively to a 3-4 fold increase in *ANKRD1* transcript levels or 10-20% increase in protein stability[4,23], suggesting that *ANKRD1* expression levels must be tightly regulated during embryogenesis.

Here we show that Ankrd1 is heterogenously expressed in the developing heart, with a dynamic nucleo-sacroplasmic sublocalization. Myocardial-overexpressing ANKRD1 transgenic (Tg) mice are born with congenital sinus venosus (SV) defect. In postnatal life, diastolic dysfunction and progressive transition from adaptive to maladaptive response occurs. Increased ANKRD1 levels are sufficient to initiate an altered cellular phenotype in the embryonic heart, which is exacerbated postnatally by high ventricular workload.

2. Methods

2.1 Mouse lines

Human wt-ANKRD1-FLAG tagged cDNA[4] was cloned downstream of the 5kb *Myh6* promoter[24]. Two Tg lines were generated by pronuclear microinjection of linearized constructs into FVB oocytes. Transgene expression was characterized by Western blotting and immunofluorescence (Figure S1). Genomic DNA was PCR-genotyped from tails of anesthetized mice (Zoletil, 30mg/kg, i.p) or the amniotic sac of embryos isolated after sacrifice by cervical dislocation of the anesthetized mother. Isolated embryos, neonatal and adult hearts were isolated and processed using standard procedures for subsequent histological, biochemical or molecular analysis. Animal procedures used conformed to the guidelines from Directive 2010/63/EU of the European Parliament on the protection of animals used for scientific purposes.

2.2 PCR analysis

RNA isolation, cDNA transcription and quantitative PCR were conducted using standard procedures. Primers for titin PCR amplification were selected to avoid regions with repetitive nucleotide sequences and potential incorrect priming. All primer sequences are available in Supplementary material online, Table S1.

2.3 Isolated myofibril analysis

Myofibrils were prepared by homogenization of permeabilized strips of frozen ventricular tissue in relaxing solution on ice[25]. Mechanical measurements from myofibrils in isometric conditions were performed during activation-relaxation cycles achieved by fast solution switching[26]. SL-resting tension relations were determined as previously described[27].

2.4 Echocardiographic analysis

Transthoracic echocardiography was performed using a high resolution echo machine with a 30 Mhz probe (VEVO 2100 Visualsonics). Both males and females mice were analyzed. Mice were chest shaved and anesthetized with 3% isoflurane, and temperature controlled anesthesia was maintained with 1.5% isoflurane. Two-dimensional cine loops and M-mode cine loops of a long-axis view and a short-axis view of the LV were recorded. Interventricular septum thickness (IVS), left ventricle internal diameter (LVID) and left ventricle posterior wall thickness (LVPW) were measured in diastole and systole from M-mode long axis view. Ejection fraction (EF) and fractional shortening (FS) were automatically calculated by the machine software.

2.5 Doppler analysis of LV and PV flow

Doppler analysis of LV flow was performed from the long axis B-mode image placing the sample volume in the left ventricle, below the mitral annulus. Isovolumetric contraction and relaxation times (IVCT, IVRT) and ejection time (ET) were measured from transmitral Doppler analysis. Myocardial performance index was calculated using the following formula: MPI= IVCT+IVRT/ET. E wave, A wave and E wave deceleration time (DT) were measured from transmitral Doppler flow profile.

Doppler analysis of PV flow was performed from a corrected long axis B-mode image placing the sample volume just before the entry of the PV in the left aria (Figure S2). The maximal velocity of PV atrial (a), systolic (s) and diastolic (d) flow waves were measured.

2.6 Statistical analysis

Data are presented as mean ± standard deviation. Comparisons between groups were performed by Students unpaired t-test, Mann-Wilcoxon W test, or Wilcoxon signed-rank test where appropriate, based on experimental design. $P<0.05$ was considered statistically significant.

Detailed Methods are available in Supplementary data online

3.Results

3.1 Ankrd1 is heterogeneously expressed in the developing myocardium

We initially examined *Ankrd1* expression in embryonic hearts. *In situ* hybridization (ISH) on sections showed that *Ankrd1* mRNA is expressed in the myocardium from E7.5 onwards, although not homogeneously (Figure 1A).

At the venous pole of the heart, at E10.0 differential *Ankrd1* mRNA levels were observed at the left and right pulmonary ridge and the sinus horns (white arrows, Figure 1Bb). By E10.5, heterogeneous mRNA staining was visible also within the developing septum primum (black arrow, Figure 1Bd), around the PV (white arrowhead, Figure 1Bd) and systemic veins entrance (red arrowheads, Fig. 1Ac and 1Bd). This expression profile was maintained at E12.5 (Figure 1Ad and 1Be,f) and E14.5 (Figure 1Bg,h).

Heterogeneous *Ankrd1* mRNA expression was detected also within the compact and trabecular layers of the left and right atrial chambers (LA, RA) (green arrows, Figure 1Cb,e), and the atrioventricular canal (red asterisk, Figure 1Bh and 1Ce). Stronger *Ankrd1* expression was visible in the outflow tract and the right ventricle (RV) (Figure 1Ac-e), whereas weaker and more heterogeneous expression was detected in the left ventricle (LV) and the interventricular septum (yellow arrows, Figure 1Ac,d and 1Cd,f).

Antibody staining confirmed heterogeneous Ankrd1 protein expression in developing cardiomyocytes (Figure 1D). Subcellular protein localization was always detected at the sarcomeric I band (Figure 1E); additional nuclear localization was frequently observed in E10.5 cardiomyocytes (Figure 1Ea,b), but was no more detectable by E14.5 (Figure 1Ec,d).

3.2 ANKRD1 finely modulates rotation and remodeling in the early myocardium

We next aimed to assess the effects of a genetically-based increase in ANKRD1 levels on cardiac structure and functionality. Thus, we generated two transgenic (Tg) mouse lines overexpressing human ANKRD1 in the myocardium under *Myh6* gene promoter (Figure S1A), which is active from E7.5 onwards[28]. Transgene protein levels were very modest in E10.5 and E14.5 embryos (Figure S1A,B and not shown),

but increased, to a similar order of magnitude, in neonatal and 10M Tg hearts (Figure S1A). ANKRD1 transgene presented always a sarcomeric sub-localization, however some nuclear signal was additionally visible in adult Tg hearts (Figure S1C). Preliminary analysis did not reveal phenotypic differences between the two Tg lines (not shown), thus detailed analysis was performed on a single line.

We initially investigated early cardiac development. E10.5 Tg hearts presented well developed atrial and ventricular chambers, which however appeared more compressed along the cranio-caudal and dorso-ventral axes, were laterally displaced and presented a reduced rotational angle if compared to wt littermates (Figure 2Aa,e). In particular, the sino-atrial region was more caudally oriented in Tg hearts, similarly to E9.5 wt embryos (Figure 2Be). Compressed shape and malrotation affected both internal remodeling and the relative orientation between sino-atrial myocardium, the flanking dorsal mesocardium and the proepicardium (Figure 2Aa,e). This resulted in malpositioning of the developing septum primum, of the pulmonary ridges, as well as of the sinus horns myocardium, visualized by Tbx18 expression[29] (Figure 2Ac,d,g,h). The sinus horns confluence, which defines the entrance of the cardinal veins into the sino-atrial region, and the pulmonary pit, delineating the route of canalization of the PV, were distinct in Tg hearts as in wt embryos. However, in Tg hearts, a mesh of $Tbx18^{+}$ mesenchyme was additionally detected within the dorsal mesocardium. $Tbx18^{+}$ mesenchyme was more abundant caudally, in proximity of the differentiating sinus horns myocardium (Figure 2Ba-d) and extended cranially up to the pulmonary ridges (Figure 2Ag,h). Remarkably, a corresponding situation could be detected in E9.5 wt embryos, which presented some $Tbx18^{+}$ cells within the loosely arranged dorsal mesocardium at the proepicardial border (Figure 2Bf,g).

In conclusion, E10.5 Tg hearts, although apparently progressed in development, are “cast” into a more immature topological arrangement that strongly affects venous pole remodeling.

3.3 ANKRD1 Tg hearts present SV defects

By mid fetal stages, most Tg hearts presented a misshapen sino-atrial region. 3D anatomically-based reconstruction outlined the malpositioning of venous inlets, which however drained in the correct atrial chamber **(**Figure 3A). Additionally, Tg hearts presented a network of microcanalizations, delineating a fine network of ectopic

connections between the PV and systemic veins, which partially drained into the vestibular region through small fenestrations (Figure 3Ad,f and Figure S3**).** These anomalous veno-atrial connections have been associated to SV defects in humans[30]. Anomalous veno-atrial connections were normally accompanied (20/27 embryos) by atrio-ventricular rotational defects and compressed appearance of the vestibular region (Figure 3Ad and Figure S3). However, in a minority of Tg embryos (7/27) SV defects occurred in the absence of morphogenetic impairment (not shown), thus indicating higher venous pole sensitivity to increased *ANKRD1* expression.

At the early postnatal life, only subtle differences could be detected between wt and Tg hearts by external anatomical observation (Figure 3Ba,e), however SV defects could be clearly outlined histologically (Figure 3Bb-d,f-h). A misshapen fossa ovalis was also clearly recognizable (Figure 3Bg).

In conclusion, ANKRD1 Tg hearts present SV defects. Fine alterations in cardiac venous pole remodeling impact both systemic and pulmonary vein development, which are closely interwined[31]. Our data support the hypothesis that SV defects are likely originated by impaired remodeling of the sino-atrial myocardium during embryonic development.

To investigate the mechanisms for SV defects, we initially wondered whether master transcription factors *GATA4* and *Nkx2.5*, functionally associated to ANKRD1, could be transcriptionally affected in early Tg embryos**.** qPCR analysis showed that *GATA4* and *Nkx2.5* mRNA levels were increased in E10.5 Tg hearts ($p<0.05$ for *Nkx2.5*), however this difference was blunted at E14.5 (Figure 4A). These results indicate that very low ANKRD1 overexpression is sufficient to affect *GATA4* and *Nkx2.5* transcription, however exclusively within the short time window of ANKRD1 nuclear localization. Thus, *GATA4-Nkx2.5* transcriptional modulation could be involved in SV defects onset.

As cardiac remodeling occurs thought the entire fetal period, these results raise the possibility that additional ANKRD1-mediated mechanisms should account for phenotype progression in Tg hearts, including altered chamber morphology. ISH analysis of E14.5 Tg hearts did not show differences in regional distribution of genes which delineate and/or define myocardial landmarks and compartments, such as *Pitx2* (left–right identity)[32], *Tbx3* (primary myocardium)[33], *Nppa, Gja5* (chamber myocardium)[33,34], *Mlc2v* (ventricular myocardium)[34], *Bmp10* (trabecular

myocardium) [35], *Tbx18* (SH myocardium)[29] (Figure 4B), thus ruling out late transcriptional effects on myocardial patterning.

3.4 Adult ANKRD1 Tg mice develop progressive ventricular diastolic dysfunction

We next investigated the consequences of ANKRD1 overexpression in adult life. Tg mice were born according to Mendelian ratio, however by 10 months (10M) they presented a reduced viability (88,5%Tg *vs* 96,9%wt; $p<0.05$). Histological analysis uncovered a severely dilated LA in all Tg hearts (Figure 5A). LA thrombi, patent foramen ovale (PFO), ventricular dilatation and altered chamber geometry could additionally be detected as isolated or combined defects (Figure 5A). Moderate fibrosis was detected in ventricular (Figure 5Am,n), but not atrial chambers, except for the organized thrombi (Figure 5Ag,h). Accordingly, TGFβ levels and TGFβ–activated ERK1/2 phosphorylation[36] were moderately increased in Tg hearts (Figure S4).

We compared wt and Tg cardiac function by echocardiography and hemodynamic analysis at 2M and 10M (Table 1). Echocardiography indicated preserved LV systolic function (*ie* EF and FS values) in 2 and 10M Tg mice, and absence of ventricular hypertrophy at 10M. However, transmitralic flow analysis in 2M mice revealed comparable E/A ratio but higher DT values in Tg animals, suggesting an initial diastolic dysfunction. By 10M, remarkably increased E/A ratio and reduced DT value were found in Tg mice, indicating progression of diastolic dysfunction with aging. Remarkably increased MPI[37] in 10M Tg *vs* wt mice supports this notion.

PV flow analysis revealed the presence of a small late diastolic wave (*d2*) in 2M Tg mice (6/8) (Figure 5B), indicating additional blood inflow into the LA, presumably via the identified cavo-pulmonary shunts (Figure 3B and Figure 5A). We hypothesize that cavo-pulmonary shunts became hemodynamically significant only in late diastole due to onset of a temporary pressure gradient which favors the R to L shunt. The *d2* wave was no longer detected in 10M Tg, indicating a change in L/R atrial chamber pressure gradients with age.

At 2M, *a* wave value was significantly higher in Tg than wt mice, indicating more effective atrial contraction (Table 1 and Figure 5B). *s* and *d* wave values were

also higher in Tg than wt mice (Table 1 and Figure 5B), indicating ventricular systolic compensation according to Frank Starling law. Comparable *a/d* ratio indicated similar hemodynamics in 2M wt *vs* Tg mice during atrial systole and ventricular diastole; however, *s/d* ratio was <1 in 2M Tg mice, as it occurs in early diastolic dysfunction[38]. By 10M, decreased *a* and *s* values, as well as *s/d* and *a/d* ratio indicated less effective atrial contraction and very different hemodynamics in Tg *vs* wt mice, underlying a severe diastolic dysfunction and loss in LA contractility. Doppler visualization confirmed this latter finding. Visual assessment of mitral valve flow did not reveal anomalies in valve functionality, thus ruling out valvular impairment as the leading cause for diastolic dysfunction.

Overall, functional analysis indicates that 2M Tg mice present initial ventricular diastolic dysfunction accompanied by increased atrial contractility; by 10M, diastolic dysfunction progresses into diastolic heart failure (HF), associated to LA enlargement and loss of LA contractility. In line, cardiac disease marker BNP was also significantly increased in 10M Tg hearts (Figure 5Ao).

Atrial dilatation and diastolic HF together can lead to pulmonary edema, whereas diastolic HF can occasionally lead to ventricular fibrillation. Thrombi formation in 10M Tg mice indicates altered atrial hemodynamics, possibly caused by HF and/or PFO defects[39]. All these co-morbidities can have a fatal outcome, therefore they likely account, as single or combined events, for the reduced viability in 10M Tg mice.

3.5 Cardiomyocyte contractility is impaired in ANKRD1 Tg hearts

We tested the hypothesis that impaired cardiomyocyte contractility could contribute to CHD and adult diastolic dysfunction in Tg hearts. Isolated myofibrils from mid-fetal, early postnatal and 10M hearts were tested for passive tension. Neonatal and 10M myofibrils were additionally tested for active mechanical properties.

Sarcomere length-resting tension (SL-RT) relations (*ie* passive mechanical properties) of wt and Tg myofibrils were comparable at E14.5 (Figure 6Aa) and 10M (Figure 6Ac), but not in newborns (Figure 6Ab). Interestingly, neonatal wt myofibrils retained passive properties of fetal stage, as expected[40], whereas Tg myofibrils presented a functional shift towards the stiffer phenotype of adult wt (Figure 6Ab,c).

Regarding active mechanical properties (Figure 6Ad), the maximally calcium activated isometric force value (P_0) was significantly higher in neonatal Tg than wt myofibrils, and comparable to adult wt value. Kinetics of force rise (k_{ACT}) and relaxation (slow and fast k_{REL}) and tension relaxation parameters (D_{slow}) were comparable in neonatal Tg and wt myofibrils. Interestingly, adult wt and Tg myofibrils showed comparable k_{ACT}, while force relaxation was clearly impaired in Tg, as shown by significantly increased D_{slow} and decreased fast k_{REL}. Thus, Tg myofibrils present a differential modulation of passive and active contractile properties during life time, *ie* reduced compliance at neonatal stage and overall slowed down relaxation at 10M.

We investigated the molecular basis for early functional changes observed in Tg myofibrils. Regulation of passive mechanical properties is mainly due to modulation of titin compliance either post-transcriptionally, or at the transcriptional level via alternative splicing[41,42]. Here, we tested the hypothesis that titin transcription could be affected in ANKRD1 Tg hearts. Titin splicing regulation involves N2B/N2BA isoforms ratio modulation and N2BA length modification via exons inclusion at the middle Ig and PEVK spring regions[41,42].

In E14.5 Tg hearts the transcripts levels of titin did not show significant differences, similar to representative thick, thin and Z band components (Figure 6B). The N2B/N2BA isoform ratio was slightly, though not significantly, increased (Figure 6C). In neonatal Tg hearts, expression of analysed transcripts were unchanged (Figure 6B). However, N2B/N2BA ratio was now clearly modified and significantly reduced in Tg samples (Figure 6C), indicating a transcriptional shift towards the more compliant N2BA isoform. This result was somehow surprising, since functional data indicated a reduced compliance in neonatal Tg myofibrils (Figure 6Ab). Intriguingly, when we performed PCR scanning analysis of N2BA exon usage within middle Ig and PEVK regions, we found that Tg hearts used a different exon combination, leading to expression of shorter, therefore less compliant, N2BA titin isoforms (Figure 6C and Figure S5). Thus, a wide modulation within titin gene transcription accompanies the biomechanical changes of neonatal Tg myofibrils.

3.6 Cardiomyocyte organization and ultrastructure are progressively impaired in ANKRD1 Tg mice

Having established that ANKRD1 overexpression impairs sarcomeric function, we next explored the impact of these alterations on cellular organization. Cardiomyocyte disorganization was visible in Tg hearts from E10.5 onwards (Figure 7A). Confocal analysis showed that E14.5 Tg cardiomyocytes were mostly distorted and presented sarcomeric disaligment (Figure 7Ai,l, Supplementary videos 1,2). Electron microscopy analysis of neonatal Tg ventricles confirmed sarcomeric disorganization and additionally showed focal areas of myofibrillar disruption (Figure 7Bf,i). Swollen mitochondria with abnormal cristae (Figure 7Bi) and rare lipid droplets in the cytoplasm (Figure 7Bf) were also found. By 10M, ultrastructural disorganization progressed in Tg ventricles, as indicated by the increased myofibril loss, mitochondrial damage and accumulation of lipid droplets. Myofibrillar loss was not detected in adult Tg LA (Figure 7).

In conclusion, tight regulation of *ANKRD1* expression is required for proper modulation of cardiomyocyte structure and of sarcomeric assembly and stability, from early development to adult life. Impaired embryonic remodeling and contractility in ANKRD1 Tg mice are therefore underlined by a common cellular basis.

4. Discussion

Here, we have presented the first longitudinal study aiming to assess the consequences of ANKRD1 myocardial overexpression from development to adult stage. Novel findings of our study are: 1) The presence of SV defects in ANKRD1 Tg mice. To our knowledge, this is the first mouse model for such congenital heart disease. 2) The pathological phenotype of adult ANKRD1 Tg hearts in the absence of pharmacological stimuli or pressure overload. This feature has not been highlighted before[16], possibly because of late appearance of gross cardiac abnormalities. The mechanistic link between ANKRD1 overexpression, CHD and adult cardiomyopathy are hereafter discussed, in relation to ANKRD1 expression and subcellular localization.

4.1 ANKRD1 expression and overexpression

We have here shown a discrete sub-compartmentalization of *Ankrd1* expression and dynamic nucleo-sarcomeric localization in the developing heart, not recognized in previous studies[5,7]. The limited time window of nuclear localization suggests that

ANKRD1 can sense ongoing hemodynamic changes[43] and respond by fine tuning its interacting partners (Figure 8A).

Extreme sensitivity to increased ANKRD1 levels in Tg hearts is therefore not surprising. Very low levels of Tg expression in E10.5 Tg hearts were sufficient for morphological and cellular phenotype onset and for transient *GATA4* and *Nkx2.5* transcriptional up-regulation. ANKRD1 expression can in turn be regulated by Nkx2.5 and GATA4[5,6,9]. Thus, our data suggest a novel *in vivo* autoregulatory loop for increased *GATA4* and *Nkx2.5* transcription, mediated by ANKRD1 binding. We cannot rule out that GATA4 could be directly involved in *Nkx2.5* transcriptional activation[44]. GATA4-ANKRD1 functional interaction can lead to increased GATA4-mediated sarcomeric gene expression and has been proposed to contribute to sarcomere homeostasis[9,10]. On the other hand, GATA4 and Nkx2.5 together can co-activate target genes regulating cardiac development[45]. We propose that ANKRD1-mediated *GATA4* and *Nkx2.5* transcriptional modulation contributes both to cellular phenotype onset and to early abnormal venous pole remodeling, leading to SV defects (Figure 8B).

The extreme sensitivity to ANKRD1 levels in our Tg mice is in line with TAPVR occurrence in patients presenting a mild increase in ANKRD1 transcripts and/or protein stability[4,23]. TAPVR and SV defects present a common feature, *ie* abnormal pulmonary venous connections: PV are not connected to the LA in TAPVR, whereas partial anomalous PV connections characterize SV defects[46]. Our data support the hypothesis that both diseases can stem from a common developmental defect, *ie* reduced cardiac venous pole remodeling[31,46].

The limited time-window of *GATA4-Nkx2*.5 transcriptional modulation cannot account for the full, complex phenotypic spectrum of Tg mice. Dynamic titin isoform alterations in Tg hearts and reduced myofibrillar compliance accompanied by increased max force in neonatal Tg myofibrils[1,47,48] (Figure 8B-D), altogether indicate a correlation between increased ANKRD1 levels and titin response. Transgene expression was exclusively sarcomeric in fetal and neonatal hearts, suggesting that altered ANKRD1 stoichiometry could directly affect titin mechanosensing properties at these stages. However, as titin compliance can be finely modulated by ANKRD1 binding[1,49], its mechanosensing properties could be affected already in early Tg embryos. We cannot additionally rule out that ANKRD1-GATA4(-Nkx2.5)-mediated

cardiomyocyte disorganization can contribute to trigger an initial titin response (Figure 8B). Titin can finely respond to changes in sarcomere stretch by differential splicing of its spring elements, resulting in either increased or decreased passive stiffness[41,50] and can additionally regulate sarcomere assembly[51] and stability[42] from development to adult life[41,50,52]. Thus, our data suggest that titin-mediated mechanotransduction impairment plays a relevant role in Tg cardiomyocyte phenotype functional modulation (Figure 8B).

Altogether, our results show that activation of *GATA4-Nkx2.5* transcription and titin gene modulation are temporally distinct but integrated systems of rapid response to changes in ANKRD1 levels and in hemodynamic load**.**

4.2 ANKRD1 overexpression and cardiac functional disease

Early postnatal transgenic cardiomyocytes presented signs (functional, molecular and ultrastructural changes) of ongoing cardiac disease. They are likely the result of mechanotransduction impairment, due to changes in hemodynamic load and increased Tg expression at birth.

Disease progression in postnatal life is triggered by both the cellular/functional and the anatomical substrates. 2M Tg hearts presented an early adaptive response, likely triggered by small volume overload due to the R-L shunt and impaired compliance of ventricular cardiomyocytes (Figure 8C). Progressively, altered hemodynamics and impaired functionality in Tg cardiomyocytes initiate a vicious loop, that peaks to the maladaptive organ response observed at 10M (Figure 8B). Dramatic worsening of Tg ventricular cardiomyocyte ultrastructure in adult hearts could be caused by their altered mechanosensing properties combined to the high workload of ventricular chambers. As a support to our hypothesis, myofibrillar loss was absent in adult Tg LA, in line with its major function as a reservoir chamber.

Functional analysis demonstrated a significant slowing down in the fast component of myofibrillar relaxation kinetics in 10M Tg hearts. This finding indicates an impairment in inter-sarcomeric dynamics, likely due to the altered load conditions[53]. Comparable passive properties of 10M wt and Tg indicated that late diastolic dysfunction is due to impaired ventricular relaxation (lusitropy), not impaired passive stiffness (Figure 8D). Additional possible contributors to

cardiomyocyte dysfunction, such as altered intracellular Ca^{2+} dynamics and impaired energetic costs[54,55] most likely contribute to the diastolic impairment.

The mechanistic links between ANKRD1 overexpression and cardiac disease progression can only partially be elucidated. However, transgene nucleo-sarcomeric sublocalization during postnatal life indicates that ANKRD1 can sense the altered cardiomyocyte status and, once a certain threshold is reached, can respond by modulating its interacting partners.

ANKRD1 gain of function mutations have been identified in HCM and DCM patients[18,19]. DCM-associated features are ventricular dilatation, wall thinning and reduced systolic function, whereas HCM presents with normal or increased systolic function and strong variability: a subset of patients develop HF, a minority further progresses to end stage HF, which resembles DCM[56]. At the organ level, ANKRD1 Tg hearts present typical features of HCM, *ie* diastolic dysfunction with preserved systolic functionality and phenotypic variability associated to disease progression[57]. Hypertrophic response, the hallmark of human HCM disease, was not present in *ANKRD1* Tg mice, however this is a shared characteristic of Tg mouse models of sarcomere-associated HCM mutations[58,59].

Contractile dysfunction plays a central role in cardiomyopathies onset and progression. Increased contraction is associated to HCM onset, whereas disruption of sarcomeric function and/or structure has been suggested as early landmark of DCM[56]. ANKRD1 Tg neonatal hearts presented both features, *ie* increased myofibrils maximal force and an initial sarcomeric loss (Figure 8C,D). Cardiac disease progression is characterized by increased cardiomyocyte compliance, which is generally higher in DCM and end-stage HF, compared to early-stage patients[60,61]. In this line, the dynamic alteration of contractile properties in Tg myofibrils parallels functional changes observed in human disease.

5. Conclusions and perspectives

Our study defines for the first time a unifying picture for ANKRD1 role in heart development, CHD and adult cardiomyopathy occurrence. The complexity and multifactorial components of human disease suggests a note of caution for any direct extrapolation from animal models to humans. Phenotypic variability of our Tg mice allows to speculate that fine modulation of interacting partners and signalling

pathways could results in different disease outcome in humans, as previously proposed[62]. Our results open the perspective that gain of function mutations of *ANKRD1* gene could be a prognostic early genetic marker for adult cardiomyopathy, in addition to congenital malformations, such as SV defects and TAPVR.

Funding

This work was supported by European Union's Horizon 2020 research and innovation program under grant agreement no. 777204 (SILICOFCM) to C.P, University of Insubria (FAR 2016-2018) and Federico Ghidoni Memorial Fund to F.A., Italian Ministry of Education, University and Research (DOR 2018) to SA.

Acknowledgements

We thank Cinzia Parolini for help and support in animal handling and tissue harvesting, Walter Giuriati for histological analysis, Sandra Furlan and Marco Sandri for help in data analysis, Marta Murgia for critical reading of the manuscript and for discussion.

Conflict of interests

None declared.

References

1. Lun AS, Chen J, Lange S. Probing muscle ankyrin-repeat protein (MARP) structure and function. *Anat Rec (Hoboken)* 2014;**297**:1615–1629.
2. Miller MK, Bang M-L, Witt CC, Labeit D, Trombitas C, Watanabe K, Granzier H, McElhinny AS, Gregorio CC, Labeit S. The muscle ankyrin repeat proteins: CARP, ankrd2/Arpp and DARP as a family of titin filament-based stress response molecules. *J Mol Biol* 2003;**333**:951–964.
3. Ling SSM, Chen Y-T, Wang J, Richards AM, Liew OW. Ankyrin Repeat Domain 1 Protein: A Functionally Pleiotropic Protein with Cardiac Biomarker Potential. *Int J Mol Sci* 2017;**18**:1362.
4. Badi I, Cinquetti R, Frascoli M, Parolini C, Chiesa G, Taramelli R, Acquati F. Intracellular ANKRD1 protein levels are regulated by 26S proteasome-mediated degradation. *FEBS Lett* 2009;**583**:2486–2492.

5. Zou Y, Evans S, Chen J, Kuo HC, Harvey RP, Chien KR. CARP, a cardiac ankyrin repeat protein, is downstream in the Nkx2-5 homeobox gene pathway. *Development* 1997;**124**:793–804.
6. Kuo H, Chen J, Ruiz-Lozano P, Zou Y, Nemer M, Chien KR. Control of segmental expression of the cardiac-restricted ankyrin repeat protein gene by distinct regulatory pathways in murine cardiogenesis. *Development* 1999;**126**:4223–4234.
7. Jeyaseelan R, Poizat C, Baker RK, Abdishoo S, Isterabadi LB, Lyons GE, Kedes L. A novel cardiac-restricted target for doxorubicin. CARP, a nuclear modulator of gene expression in cardiac progenitor cells and cardiomyocytes. *J Biol Chem* 1997;**272**:22800–22808.
8. Bang ML, Mudry RE, McElhinny AS, Trombitás K, Geach AJ, Yamasaki R, Sorimachi H, Granzier H, Gregorio CC, Labeit S. Myopalladin, a novel 145-kilodalton sarcomeric protein with multiple roles in Z-disc and I-band protein assemblies. *J Cell Biol* 2001;**153**:413–427.
9. Chen B, Zhong L, Roush SF, Pentassuglia L, Peng X, Samaras S, Davidson JM, Sawyer DB, Lim CC. Disruption of a GATA4/Ankrd1 Signaling Axis in Cardiomyocytes Leads to Sarcomere Disarray: Implications for Anthracycline Cardiomyopathy. Capogrossi MC, ed. *PLoS One* 2012;**7**:e35743.
10. Zhong L, Chiusa M, Cadar AG, Lin A, Samaras S, Davidson JM, Lim CC. Targeted inhibition of ANKRD1 disrupts sarcomeric ERK-GATA4 signal transduction and abrogates phenylephrine-induced cardiomyocyte hypertrophy. *Cardiovasc Res* 2015;**106**:261–271.
11. Aihara Y, Kurabayashi M, Saito Y, Ohyama Y, Tanaka T, Takeda S, Tomaru K, Sekiguchi K, Arai M, Nakamura T, Nagai R. Cardiac ankyrin repeat protein is a novel marker of cardiac hypertrophy: role of M-CAT element within the promoter. *Hypertens (Dallas, Tex 1979)* 2000;**36**:48–53.
12. Wei Y-J, Cui C-J, Huang Y-X, Zhang X-L, Zhang H, Hu S-S. Upregulated expression of cardiac ankyrin repeat protein in human failing hearts due to arrhythmogenic right ventricular cardiomyopathy. *Eur J Heart Fail* 2009;**11**:559–566.
13. Kempton A, Cefalu M, Justice C, Baich T, Derbala M, Canan B, Janssen PML, Mohler PJ, Smith SA. Altered regulation of cardiac ankyrin repeat protein in

heart failure. *Heliyon* 2018;**4**:e00514.

14. Bang M-L, Gu Y, Dalton ND, Peterson KL, Chien KR, Chen J. The muscle ankyrin repeat proteins CARP, Ankrd2, and DARP are not essential for normal cardiac development and function at basal conditions and in response to pressure overload. Xu X, ed. *PLoS One* 2014;**9**:e93638.
15. Shen L, Chen C, Wei X, Li X, Luo G, Zhang J, Bin J, Huang X, Cao S, Li G, Liao Y. Overexpression of ankyrin repeat domain 1 enhances cardiomyocyte apoptosis by promoting p53 activation and mitochondrial dysfunction in rodents. *Clin Sci* 2015;**128**:665–678.
16. Song Y, Xu J, Li Y, Jia C, Ma X, Zhang L, Xie X, Zhang Y, Gao X, Zhang Y, Zhu D. Cardiac Ankyrin Repeat Protein Attenuates Cardiac Hypertrophy by Inhibition of ERK1/2 and TGF-β Signaling Pathways. Hirsch E, ed. *PLoS One* 2012;**7**:e50436.
17. Arimura T, Bos JM, Sato A, Kubo T, Okamoto H, Nishi H, Harada H, Koga Y, Moulik M, Doi YL, Towbin JA, Ackerman MJ, Kimura A. Cardiac Ankyrin Repeat Protein Gene (ANKRD1) Mutations in Hypertrophic Cardiomyopathy. *J Am Coll Cardiol* 2009;**54**:334–342.
18. Duboscq-Bidot L, Charron P, Ruppert V, Fauchier L, Richter A, Tavazzi L, Arbustini E, Wichter T, Maisch B, Komajda M, Isnard R, Villard E, EUROGENE Heart Failure Network. Mutations in the ANKRD1 gene encoding CARP are responsible for human dilated cardiomyopathy. *Eur Heart J* 2009;**30**:2128–2136.
19. Moulik M, Vatta M, Witt SH, Arola AM, Murphy RT, McKenna WJ, Boriek AM, Oka K, Labeit S, Bowles NE, Arimura T, Kimura A, Towbin JA. ANKRD1, the gene encoding cardiac ankyrin repeat protein, is a novel dilated cardiomyopathy gene. *J Am Coll Cardiol* 2009;**54**:325–333.
20. Acquati F, Russo A, Taramelli R, Tibiletti MG, Taborelli M, Camesasca C, Papa M. Nonsyndromic total anomalous venous return associated with a de novo translocation inolving chromosomes 10 and 21 t(10;21)(q23.1;q11.2). *Am J Med Genet* 2000;**95**:285–286.
21. Cinquetti R, Badi I, Campione M, Bortoletto E, Chiesa G, Parolini C, Camesasca C, Russo A, Taramelli R, Acquati F. Transcriptional deregulation and a missense mutation define ANKRD1 as a candidate gene for total

anomalous pulmonary venous return. *Hum Mutat* 2008;**29**:468–474.

22. Correa-Villaseñor A, Ferencz C, Boughman JA, Neill CA. Total anomalous pulmonary venous return: familial and environmental factors. The Baltimore-Washington Infant Study Group. *Teratology* 1991;**44**:415–428.

23. Cinquetti R, Badi I, Campione M, Bortoletto E, Chiesa G, Parolini C, Camesasca C, Russo A, Taramelli R, Acquati F. Transcriptional deregulation and a missense mutation define ANKRD1 as a candidate gene for total anomalous pulmonary venous return. *Hum Mutat* 2008;**29**.

24. Subramaniam A, Jones WK, Gulick J, Wert S, Neumann J, Robbins J. Tissue-specific regulation of the alpha-myosin heavy chain gene promoter in transgenic mice. *J Biol Chem* 1991;**266**:24613–24620.

25. Piroddi N, Belus A, Eiras S, Tesi C, Velden J van der, Poggesi C, Stienen GJM. No direct effect of creatine phosphate on the cross-bridge cycle in cardiac myofibrils. *Pflügers Arch* 2006;**452**:3–6.

26. Colomo F, Piroddi N, Poggesi C, Kronnie G te, Tesi C. Active and passive forces of isolated myofibrils from cardiac and fast skeletal muscle of the frog. *J Physiol* 1997;**500 (Pt 2)**:535–548.

27. Scellini B, Piroddi N, Flint G V., Regnier M, Poggesi C, Tesi C. Impact of tropomyosin isoform composition on fast skeletal muscle thin filament regulation and force development. *J Muscle Res Cell Motil* 2015;**36**:11–23.

28. Lange FJ de, Moorman AFM, Anderson RH, Männer J, Soufan AT, Gier-de Vries C de, Schneider MD, Webb S, Hoff MJB van den, Christoffels VM. Lineage and morphogenetic analysis of the cardiac valves. *Circ Res* 2004;**95**:645–654.

29. Christoffels VM, Mommersteeg MTM, Trowe M-O, Prall OWJ, Gier-de Vries C de, Soufan AT, Bussen M, Schuster-Gossler K, Harvey RP, Moorman AFM, Kispert A. Formation of the Venous Pole of the Heart From an *Nkx2–5* – Negative Precursor Population Requires *Tbx18*. *Circ Res* 2006;**98**:1555–1563.

30. Tretter JT, Chikkabyrappa S, Spicer DE, Backer CL, Mosca RS, Anderson RH, Bhatla P. Understanding the spectrum of sinus venosus interatrial communications. *Cardiol Young* 2017;**27**:418–426.

31. Berg G van den, Moorman AFM. Development of the pulmonary vein and the systemic venous sinus: An interactive 3D overview. *PLoS One* 2011;**6**.

32. Campione M, Ros MA, Icardo JM, Piedra E, Christoffels VM, Schweickert A, Blum M, Franco D, Moorman AFM. Pitx2 expression defines a left cardiac lineage of cells: Evidence for atrial and ventricular molecular isomerism in the iv/iv mice. *Dev Biol* Academic Press Inc.; 2001;**231**:252–264.
33. Hoogaars WMH, Tessari A, Moorman AFM, Boer PAJ de, Hagoort J, Soufan AT, Campione M, Christoffels VM. The transcriptional repressor Tbx3 delineates the developing central conduction system of the heart. *Cardiovasc Res* 2004;**62**:489–499.
34. Christoffels VM, Habets PE, Franco D, Campione M, Jong F de, Lamers WH, Bao ZZ, Palmer S, Biben C, Harvey RP, Moorman AF. Chamber formation and morphogenesis in the developing mammalian heart. *Dev Biol* 2000;**223**:266–278.
35. Chen H, Shi S, Acosta L, Li W, Lu J, Bao S, Chen Z, Yang Z, Schneider MD, Chien KR, Conway SJ, Yoder MC, Haneline LS, Franco D, Shou W. BMP10 is essential for maintaining cardiac growth during murine cardiogenesis. *Development* 2004;**131**:2219–2231.
36. Heldin C-H, Moustakas A. Signaling Receptors for TGF-β Family Members. *Cold Spring Harb Perspect Biol* 2016;**8**.
37. Broberg CS, Pantely GA, Barber BJ, Mack GK, Lee K, Thigpen T, Davis LE, Sahn D, Hohimer AR. Validation of the myocardial performance index by echocardiography in mice: a noninvasive measure of left ventricular function. *J Am Soc Echocardiogr* 2003;**16**:814–823.
38. Faggiano P, Vizzardi E, Pulcini E, Maffeo D, Fracassi F, Nodari S, Dei Cas L. The study of left ventricular diastolic function by Doppler echocardiography: the essential for the clinician. *Heart Int* 2007;**3**:42.
39. Rigatelli G, Zuin M, Dell'Avvocata F. Atrial fibrillation and patent foramen potentially share same atrial flow dynamic profile and thrombotic mechanism. *Eur J Intern Med* 2017;**44**:e20–e21.
40. LINKE W. Sense and stretchability: The role of titin and titin-associated proteins in myocardial stress-sensing and mechanical dysfunction. *Cardiovasc Res* Oxford University Press; 2008;**77**:637–648.
41. Granzier HL, Labeit S. The Giant Protein Titin. *Circ Res* 2004;**94**:284–295.
42. Linke WA, Hamdani N. Gigantic Business. *Circ Res* 2014;**114**:1052–1068.

43. Gui Y-H, Linask KK, Khowsathit P, Huhta JC. Doppler Echocardiography of Normal and Abnormal Embryonic Mouse Heart. *Pediatr Res* 1996;**40**:633–642.

44. Brewer AC, Alexandrovich A, Mjaatvedt CH, Shah AM, Patient RK, Pizzey JA. GATA Factors Lie Upstream of Nkx 2.5 in the Transcriptional Regulatory Cascade That Effects Cardiogenesis. *Stem Cells Dev* 2005;**14**:425–439.

45. McCulley DJ, Black BL. Transcription Factor Pathways and Congenital Heart Disease. *Current Topics in Developmental Biology* Academic Press Inc.; 2012. p. 253–277.

46. Butts RJ, Crean AM, Hlavacek AM, Spicer DE, Cook AC, Oechslin EN, Anderson RH. Veno-venous bridges: the forerunners of the sinus venosus defect. *Cardiol Young* 2011;**21**:623–630.

47. Elhamine F, Radke MH, Pfitzer G, Granzier H, Gotthardt M, Stehle R. Deletion of the titin N2B region accelerates myofibrillar force development but does not alter relaxation kinetics. *J Cell Sci* 2014;**127**:3666–3674.

48. Sequeira V, Velden J van der. The Frank–Starling Law: a jigsaw of titin proportions. *Biophys Rev* 2017;**9**:259–267.

49. Zhou T, Fleming JR, Franke B, Bogomolovas J, Barsukov I, Rigden DJ, Labeit S, Mayans O. CARP interacts with titin at a unique helical N2A sequence and at the domain Ig81 to form a structured complex. *FEBS Lett* 2016;**590**:3098–3110.

50. Anderson BR, Granzier HL. Titin-based tension in the cardiac sarcomere: molecular origin and physiological adaptations. *Prog Biophys Mol Biol* 2012;**110**:204–217.

51. Walker JS, Tombe PP de. Titin and the Developing Heart. *Circ Res* 2004;**94**:860–862.

52. Opitz CA, Leake MC, Makarenko I, Benes V, Linke WA. Developmentally Regulated Switching of Titin Size Alters Myofibrillar Stiffness in the Perinatal Heart. *Circ Res* 2004;**94**:967–975.

53. Poggesi C, Tesi C, Stehle R. Sarcomeric determinants of striated muscle relaxation kinetics. *Pflugers Arch* 2005;**449**:505–517.

54. Borlaug BA, Kass DA. Mechanisms of Diastolic Dysfunction in Heart Failure. *Trends Cardiovasc Med* 2006;**16**:273–279.

55. Lopes LR, Elliott PM. A straightforward guide to the sarcomeric basis of cardiomyopathies. *Heart* 2014;**100**:1916–1923.
56. Garfinkel AC, Seidman JG, Seidman CE. Genetic Pathogenesis of Hypertrophic and Dilated Cardiomyopathy. *Heart Fail Clin* 2018;**14**:139–146.
57. Velden J van der, Ho CY, Tardiff JC, Olivotto I, Knollmann BC, Carrier L. Research priorities in sarcomeric cardiomyopathies. *Cardiovasc Res* 2015;**105**:449–456.
58. Moore RK, Grinspan LT, Jimenez J, Guinto PJ, Ertz-Berger B, Tardiff JC. HCM-linked Δ160E cardiac troponin T mutation causes unique progressive structural and molecular ventricular remodeling in transgenic mice. *J Mol Cell Cardiol* 2013;**58**:188–198.
59. Michele DE, Gomez CA, Hong KE, Westfall M V, Metzger JM. Cardiac dysfunction in hypertrophic cardiomyopathy mutant tropomyosin mice is transgene-dependent, hypertrophy-independent, and improved by beta-blockade. *Circ Res* 2002;**91**:255–262.
60. Heerebeek L van, Borbély A, Niessen HWM, Bronzwaer JGF, Velden J van der, Stienen GJM, Linke WA, Laarman GJ, Paulus WJ. Myocardial Structure and Function Differ in Systolic and Diastolic Heart Failure. *Circulation* 2006;**113**:1966–1973.
61. Vikhorev P, Vikhoreva N. Cardiomyopathies and Related Changes in Contractility of Human Heart Muscle. *Int J Mol Sci* 2018;**19**:2234.
62. Lange S, Gehmlich K, Lun AS, Blondelle J, Hooper C, Dalton ND, Alvarez EA, Zhang X, Bang M-L, Abassi YA, Remedios CG Dos, Peterson KL, Chen J, Ehler E. MLP and CARP are linked to chronic PKCα signalling in dilated cardiomyopathy. *Nat Commun* 2016;**7**:12120.

Figure legends

Figure 1: *Ankrd1* mRNA and protein expression in cardiac development. A-C: *Ankrd1* mRNA expression in E8.5-E14.5 hearts, ISH analysis. Myocardium is identified by *Mhc* transcripts. A: E8.5(a,b), E10.5(c), E12.5(d), E14.5(h) hearts, global view. Dotted areas in e are magnified below. B: *Ankrd1* expression at venous pole of E10(a,b), E10.5(c,d), E12.5(e,f), E14.5(g,h) embryos. C: *Ankrd1* expression in atrial and ventricular chambers of E10.5(a-d) and E14.5(e,f) embryos. D-E: Ankrd1

protein expression and sub-cellular localization in E10.5 and E14.5 hearts, double immunofluorescence and confocal analysis. D: E10.5(a,b) and E14.5(c,d) hearts, overview pictures. Note heterogeneous reaction of α-Ankrd1(a,c) *vs* α-actinin(b,d) antibody. E: at E10.5(a,b) Ankrd1 presents sarcomeric and nuclear (arrows) co-localization; at E14.5(c,d) Ankrd1 is exclusively sarcomeric. Note strong (yellow star) or low (white star) α-Ankrd1 antibody reaction in neighboring cardiomyocytes. ca: common atrium; v: primitive ventricle; avc: atrioventricular canal; oft: outflow tract; rv: right ventricle; lv: left ventricle; r,l-pr: right,left pulmonary ridge; rsh,lsh: righ,left sinus horn; sp: septum primum; ivs: interventricular septum; vv: venous valves; icv: inferior caval vein; pv: pulmonary vein; lscv, rscv: left, right superior caval vein. Scale bar: A-C=100 μm; D=100 μm, E=10μm.

Figure 2: ANKRD1 overexpression affects fine rotation and remodeling in the early myocardium. A: abnormal rotation and remodeling in E10.5 Tg compared to wt embryos, ISH whole mount (a,e) and on sections (b-d, f-h,) analysis. Dotted lines in a,e show LA-LV angle in wt (white) and Tg (red); double-headed arrow shows cranio-caudal extension of the heart from the LV base to the outflow tract. b,f: abnormal shape and position of cardiac chambers, atrioventricular canal (asterisk) and septum primum (dotted box) in Tg. Red dotted lines in c,d,g,h indicate the myocardium of the pulmonary ridges. Black arrow indicates the pulmonary pit, misplaced in Tg embryos. Yellow arrowheads indicate $Tbx18^{+}$ cells within the dorsal mesocardium (dm). B: Venous pole organization in E10.5 Tg (a-d) and E9.5 wt (e-g) embryos, ISH on sections (a-d,f,g) and whole mount (e). Red dotted lines delineate the sino-atrial myocardium. Yellow arrowheads indicate *Tbx18*$^{+}$ cells within the dm. Black dotted circle in f'-g highlights the base of the dm where some $Tbx18^{+}$ cells are visible, flanking the loosely arranged mesoderm (red asterisks). fg: foregut; pe: proepicardium. See Figure legend 1 for other abbreviations. Scale bar:A,B=100μm.

Figure 3: SV defects in mid-fetal and neonatal ANKRD1 Tg hearts. A: 3D reconstruction of the sino-atrial region and venous system lumen in E13.5 hearts, highlighting anomalous venous pole organization in Tg hearts. Note in d, the canalizations around PV and systemic veins and a compressed shape of the vestibular region; b,c,e,f: virtual sections at the venous pole. In Tg embryos, the

754 communications between PV and systemic veins around the vestibular regions define
755 the SV defects. Black lines delineate splanchnopleure. B: neonatal hearts, freshly
756 isolated (a,e) and H/E analysis (b-d, f-h). c: white arrow indicates atrial malrotation,
757 yellow arrow indicates rounded ventricular apex. g-h: SV defects in Tg hearts.
758 Confluence of RSCV and PV at the dorsal atrial wall (asterisk in g) and into the RA
759 (h) are clearly recognizable. Black arrowhead in g indicates the misshapen fossa
760 ovalis. See Figure legend 1 for abbreviations. Scale bar: Aa-f=100μm;
761 Ba,b,e,f=500μm; Bc,d,g,h=200 μm.
762
763 **Figure 4: Timed transcriptional modulation in ANKRD1 Tg embryos.** A: *GATA4*
764 and *Nkx2.5* mRNA expression levels in E10.5 (wt=5, Tg=4) and E14.5 (wt=4,Tg=5)
765 hearts, *p<0.05 , Student unpaired t-test; values are compared to the mean wt level at
766 each stage. B: ISH analysis shows that molecular patterning is not affected in E14.5
767 Tg hearts. san: sino-atrial node; avn: atrio-ventricular node; icv: inferior caval vein;
768 for other abbreviations see Figure legend 1. Scale bar: a–h:20 μm; i-r:10 μm.
769
770 **Figure 5: Adult ANKRD1 Tg hearts analysis**. A: Phenotypic variability in 10M Tg
771 hearts. a-d: freshly isolated hearts; e-n: histological analysis, sino-atrial (e-h) and
772 ventricular (i-n) regions; H/E (e-g, i-l) and Sirius red (h,m,n) staining. Black
773 arrowhead indicates the enlarged Tg LA, asterisk indicates thrombus. e-h: note in (f)
774 anomalous confluence of PV (red dotted arrow) and RSCV (black arrow) at the dorsal
775 atrial wall. g: dotted box indicates PFO, associated to thrombus formation. h: fibrotic
776 infiltration within LA thrombus. i-l: dilatation and altered geometry in Tg LV; m-n:
777 moderate fibrosis in Tg LV. o: Western blot analysis of BNP *vs* GADPH expression
778 in 10M wt (n=4) and Tg (n=5) hearts, representative results and box plot
779 quantification; *p<0.05 , Student unpaired t-test. Scale bar: a-d=1mm, e-g, i-l=
780 0.5mm, g-i=100μm. B: *In vivo* analysis. a,b: PV Doppler flow profile of a
781 representative 2M wt (a) and Tg (b) mouse. Red arrows indicate *d2* wave in Tg. c,d:
782 representation of mean PV Doppler flow curves in wt and Tg mice at 2 and 10M.
783 Mean *a*, *s* and *d* values are from Table 1. e,f: echocardiographic view of a 10M wt (e)
784 and Tg (f) heart. Note strongly enlarged LA in Tg (red line).
785

Figure 6: Modulation of contractile properties in ANKRD1 Tg hearts. A: functional analysis on isolated myofibrils. a-c: average sarcomere length-resting tension relation of myofibrils from E14.5 (a) newborn (b) and adult (c) hearts; wt, *black circle;* Tg, *red circle.* Vertical and horizontal bars are SEM. (d) Mechanical properties of myofibrils from newborn and adult hearts (myofibrils number in brackets). SL: sarcomere length, P_0: maximum isometric tension, k_{ACT} : rate constant of force development following maximal Ca^{2+}-activation, D_{slow}: duration of the slow linear phase of relaxation, Slow-Fast k_{REL} : rate constants of tension relaxation for slow and fast relaxation phases. $^{*}p < 0.001$, $^{\#}p < 0.02$, Student unpaired t-test. B**:** qPCR results of sarcomeric genes expression in E14.5 and newborn hearts. wt *vs* Tg: p>0.05 for each stage, Student unpaired t-test; values are compared to the mean wt level at each stage. C: titin splice variant analysis. Top: schematic representation of titin N2BA and N2B structure; arrows indicate position of primers used for N2BA combinatorial exon analysis, red arrows: regions with differential exon inclusion in newborn wt/Tg. Bottom left: N2B/N2BA isoform ratio analysis. $^{*}p < 0.05$, Student unpaired t-test; values are compared to the mean wt level at each stage. Bottom right: PCR amplification of exons 72-80 and exons 137-156 from wt and Tg hearts (n=5) results in multiple amplicons (square boxes) of different length. The longest amplicons are mostly detected in wt hearts. Y axis: amplicons length (bp); X axis: count of wt and Tg samples which present the specified amplicon (see Figure S5 for original data).

Figure 7: Impairment of cardiomyocyte organization and ultrastructure in ANKRD1 Tg hearts. A: Cardiomyocyte organization in embryonic wt and Tg hearts. H/E analysis at E10.5 (a,f) and confocal analysis of E14.5 RV wall (b,c,g,h), trabeculae (d,i) and atria (e,l);. b,g: bright field and nuclei, merged; c-e,h-l: actinin. b,c and g,h are adjacent sections. Scale bar: a,f=20μm; b-e,g-l=10μm B: TEM analysis of neonatal and adult ventricles and of adult atria, at low (a-c,f-h) and high magnification (d,e,i,l). Red asterisk: focal sarcomeric loss, red arrow: sarcomeric disorganization, double headed arrow: extensive sarcomeric loss, green asterisk: damaged mitocondria; yellow arrowheads: lipid droplets. Scale bar: a-c,f,h= 5μm; d,e,i,l= 1μm.

Figure 8: Working model linking ANKRD1 expression, overexpression and cardiac disease. A: Ankrd1 role in heart development. Heterogeneous Ankrd1 expression and its dynamic nucleo-sarcomeric sub-localization modulate developmental cardiac remodeling in response to hemodynamics by finely regulating cardiomyocyte transcription and mechanotransduction; the initially contiguous PV (yellow, dotted lines) and systemic veins (red, dotted lines) precursors become spatially separated by mid-fetal stage. B: temporally distinct transcriptional modulation scored in embryonic and neonatal Tg hearts (red arrows) and their proposed link with disease onset and early progression at the cellular and organ levels (black arrows). C,D: disease onset and progression in Tg hearts, with the underlying cardiomyocyte defects (C) and myofibrillar functional modifications (D). Embryos: impaired myocardial remodeling retains the contiguity of the regions where PV and systemic veins precursors are located, thereby causing SV defect. Postnatal life: neonatal Tg hearts present overt cardiomyocyte structural and functional impairment. Altered A-V hemodynamic cross talk (double headed arrow), due to SV defect and impaired functionality in Tg cardiomyocytes, initiates a vicious loop that progressively leads to diastolic dysfunction (dd), then heart failure (dHF). D: Tg myofibrillar functional properties (compliance, lusitropism and maximal force) present substantial modifications in prenatal and postnatal life, as shown by reduced and then increased compliance, progressive reduction of lusitropism and persistent higher maximal force. Color code: green, values in Tg myofibrils comparable to corresponding wt; red: values higher than wt.

Tables

Table 1: Ecocardiographic (top) and hemodynamic (botton) analysis of wt and ANKRD1 Tg mice at 2 and 10 months; n= number of animal analyzed (2M: wt=6 males, 4 females; Tg= 3 males, 5 females; 10M:wt=6 males, 3 females, Tg= 2 males, 5 females). Values are indicated as mean $\pm$ SE. *np*: not present; Legend: LV%EF: LV ejection fraction; LV%FS: LV fractional shortening; IVSd: interventricular septum diastolic thickness; IVSs: interventricular septum systolic thickness; LVIDd: LV internal diameter, diastolic; LVIDs: LV internal diameter, systolic; LVPWd: LV posterior wall, diastolic; LVPWs: LV posterior wall, systolic; MPI: myocardial

performance index. See text and supplementary methods for other abbreviations. Wt *vs* Tg data comparison at each stage (2M, 10M) was performed by Mann-Wilcoxon W test; 2M *vs* 10M data comparison for each experimental group (wt and Tg) was performed by Wilcoxon signed-rank test.

	Wt 2M (n=10)	Tg 2M (n=8)	Wt10M (n=9)	Tg 10M (n=7)	Wt *vs Tg* @2M (p)	Wt *vs* Tg @10M (p)	Wt: 2M *vs* 10M (p)	Tg: 2M *vs* 10M (p)
LV%EF	56,80 ±3,64	**63,75 ±4,87**	58,25 ±2,94	**63,29 ±4,03**	0,23	**0,22**	0,87	1
LV%FS	29,40 ±2,53	**34,50 ±3,39**	30,25 ±1,91	**34,43 ±2,90**	0,25	**0,20**	0,93	1
IVSd	-	-	1,05 ±0,05	**0,96 ±0,07**	-	**0,31**		-
IVSs	-	-	1,48 ±0,03	**1,43 ±0,05**	-	**0,56**	-	-
LVIDd	-	-	3,89 ±0,14	**3,81 ±0,15**	-	**1**	-	-
LVIDs	-	-	2,69 ±0,15	**2,50 ±0,19**	-	**0,30**	-	-
LVPWd	-	-	0,97 ±0,04	**0,94 ±0,06**	-	**0,90**	-	-
LVPWs	-	-	1,36 ±0,04	**1,15 ±0,10**	-	**0,05***	-	
E/A	2,13 ±0,21	**2,04 ±0,27**	2,06 ±0,23	**3,13 ± 0,57**	0,95	0,10	1	0,06
DT	19,05 ±2,12	**23,01 ±3,12**	14,90 ±1,66	**14,26 ±2,14**	0,41	0,79	0,23	0,06
MPI	0,79 ± 0,04	**0,80 ± 0,07**	0,71 ± 0,04	**0,86 ± 0,06**	0,89	0,06	0,55	0,45
d	363,20 ± 63,65	**507,25 ± 75,27**	587,13 ±121,23	**629,43 ±132,17**	0,14	0,86	0,91	0,19
d2	*np*	**298,5 ± 39,90**	*np*	***np***	-	-	-	-
a	-111,40 ± *13,18*	**-187,63 ± *30,36***	-191,13 ±*71,75*	**-132,57 ±*37,56***	0,03*	0,86	0,91	0,12
s	271,20 ± 13,18	**371,88 ± 30,36**	311,00 ±71,75	**203,86 ± 37,56**	0,17	0,02*	0,41	0,03*
s/d	1,01 ±0,22	**0,66 ±0,08**	0,80 ±0,22	**0,34 ±0,04**	0,45	0,01*	1	0,02*
a/d	-0,37 ±0,05	**-0,40 ±0,07**	-0,30 ±0,06	**-0,21 ±0,03**	0,82	0,22	1	0,08
a/s	-0,45 ±0,08	**-0,60 ±0,08**	-0,49 ±0,12	**-0,62 ±0,08**	0,12	0,32	0,32	0,67

884

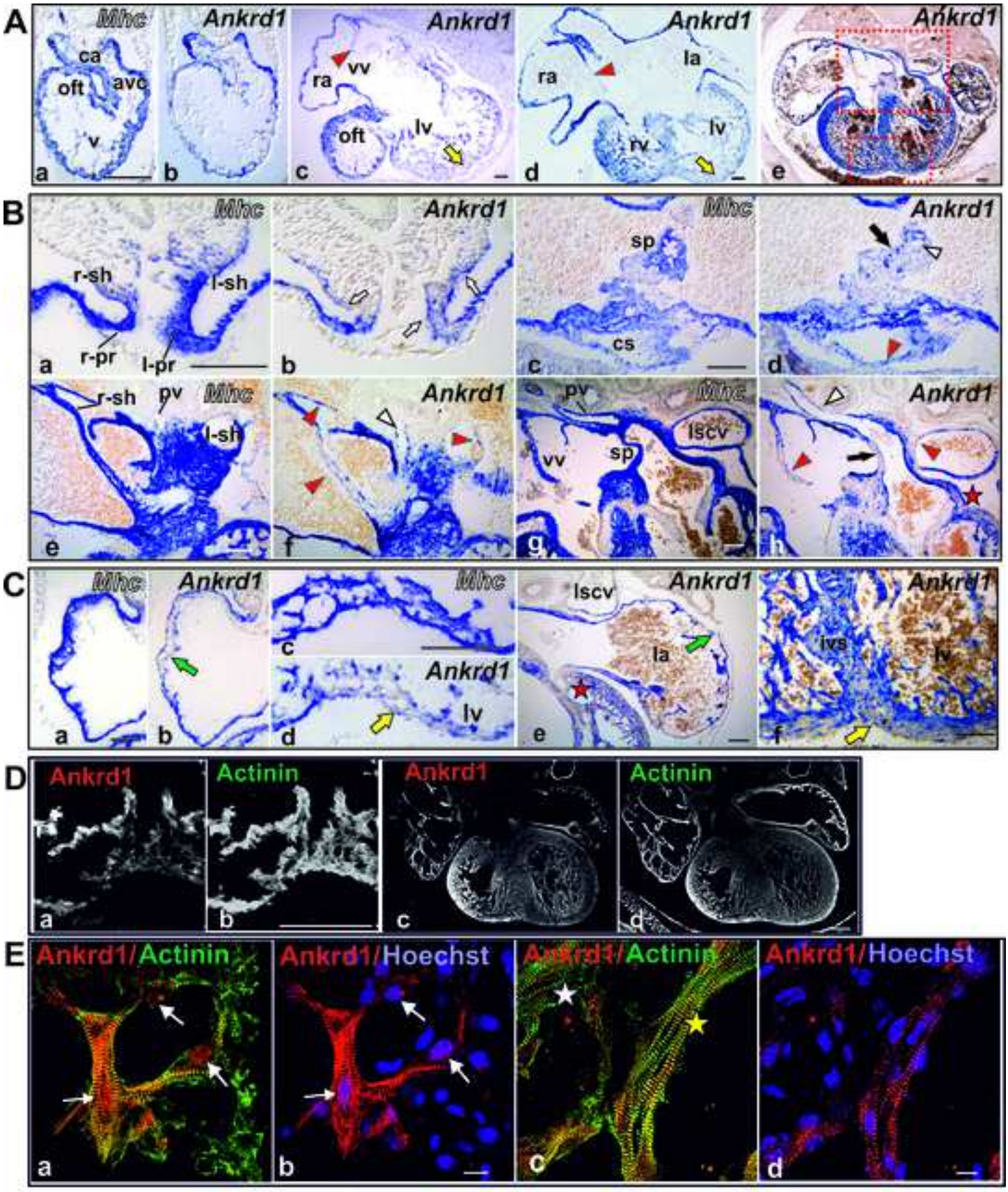

Figure 1

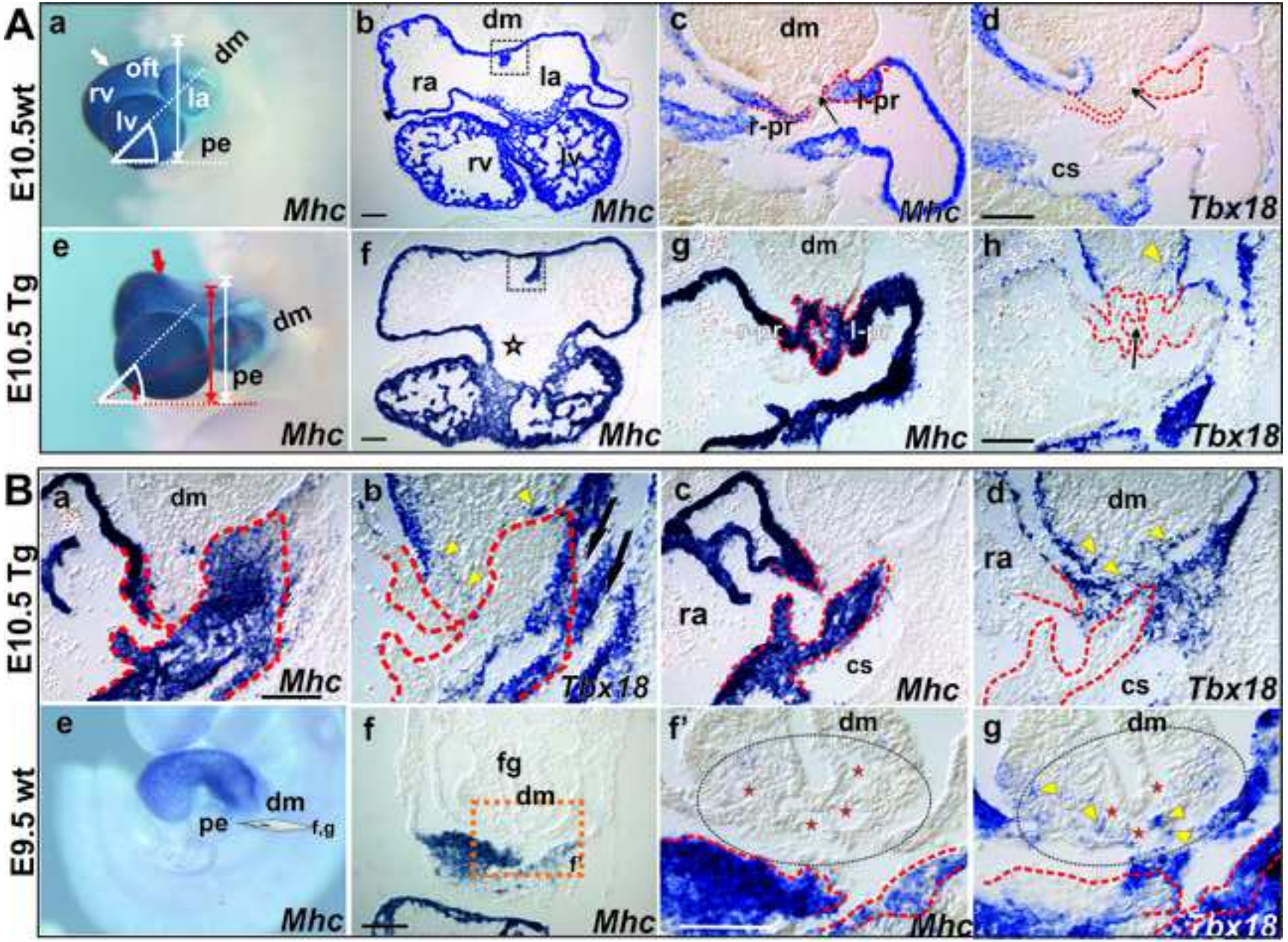

Figure 2

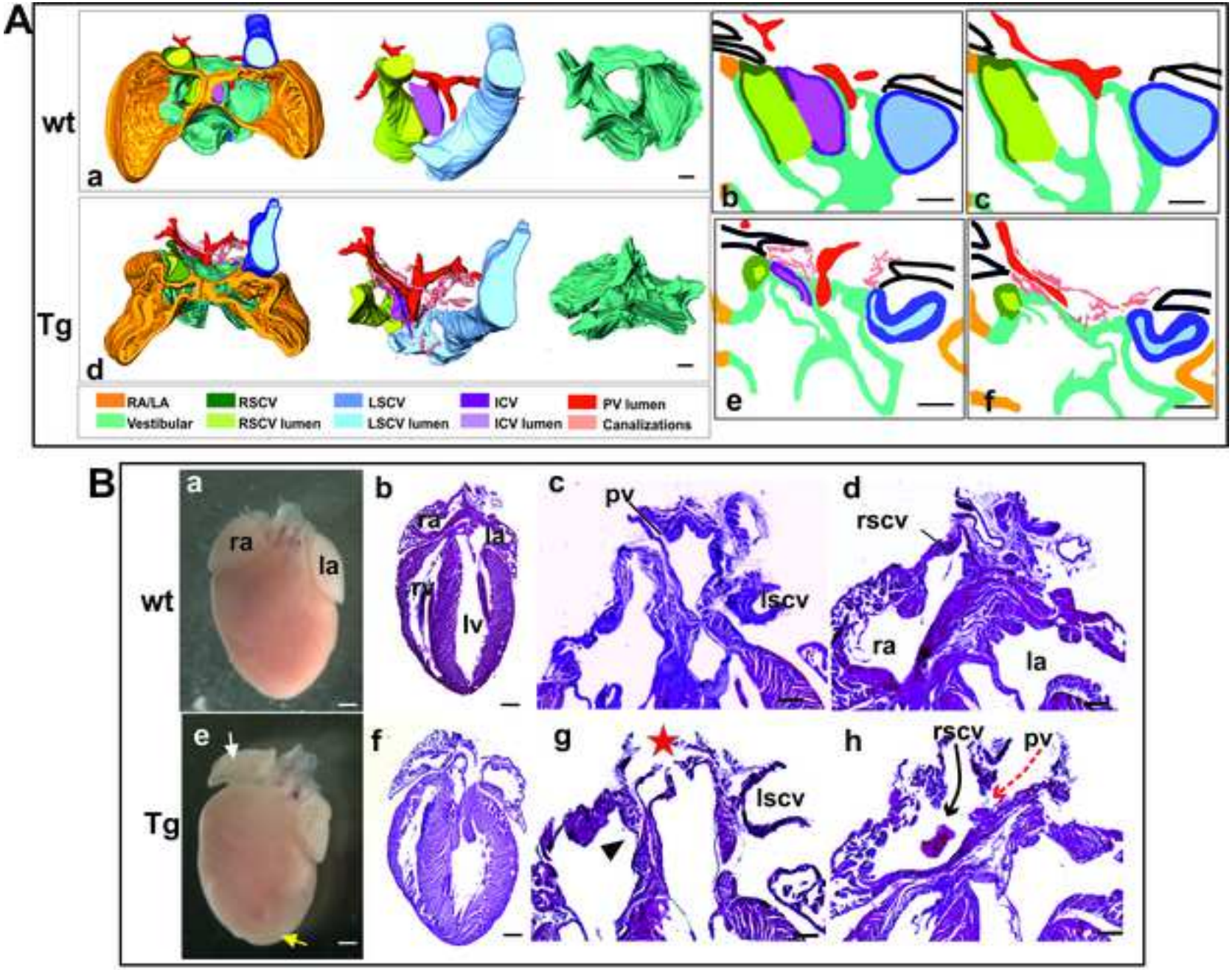

Figure 3

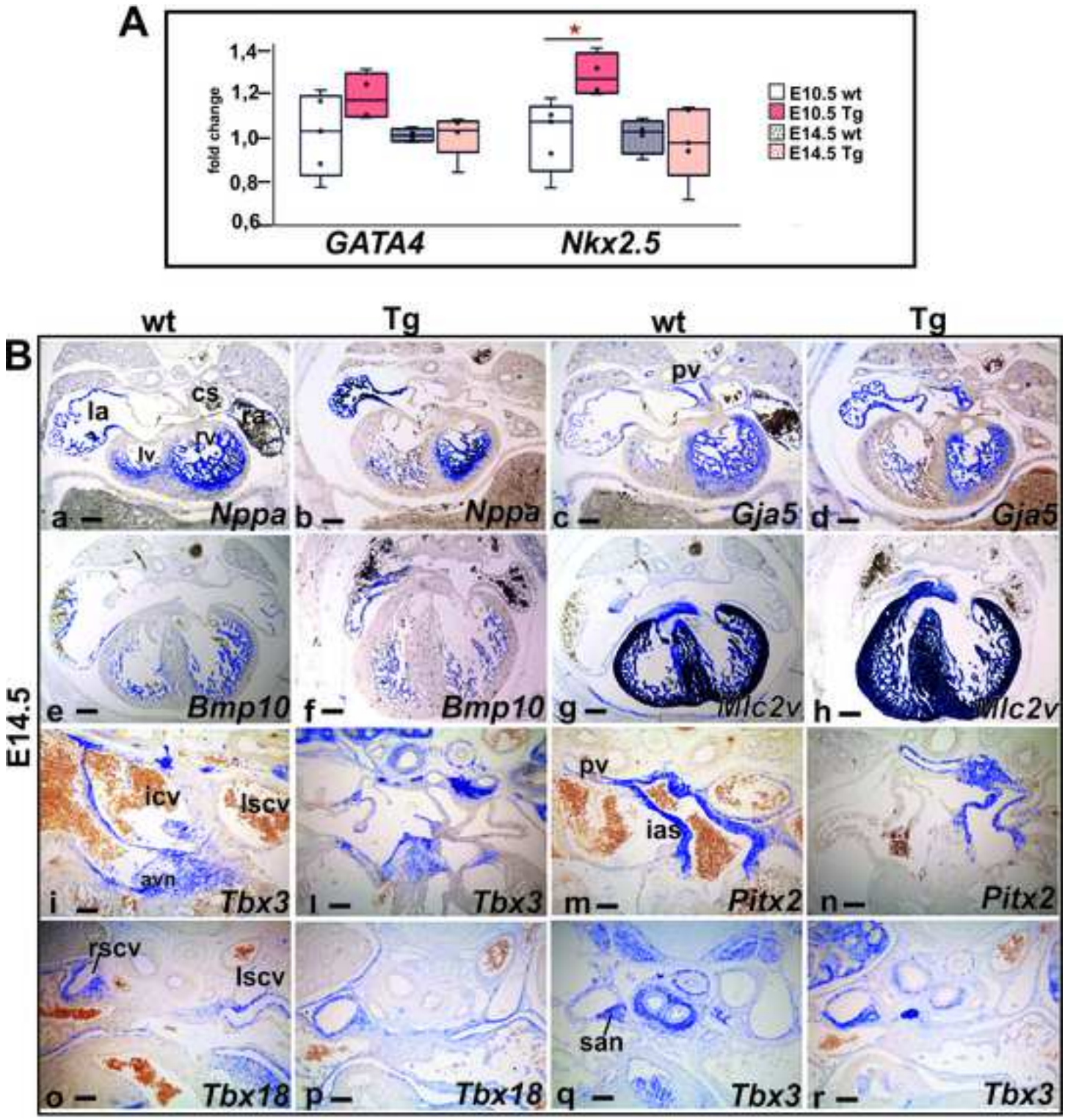

Figure 4

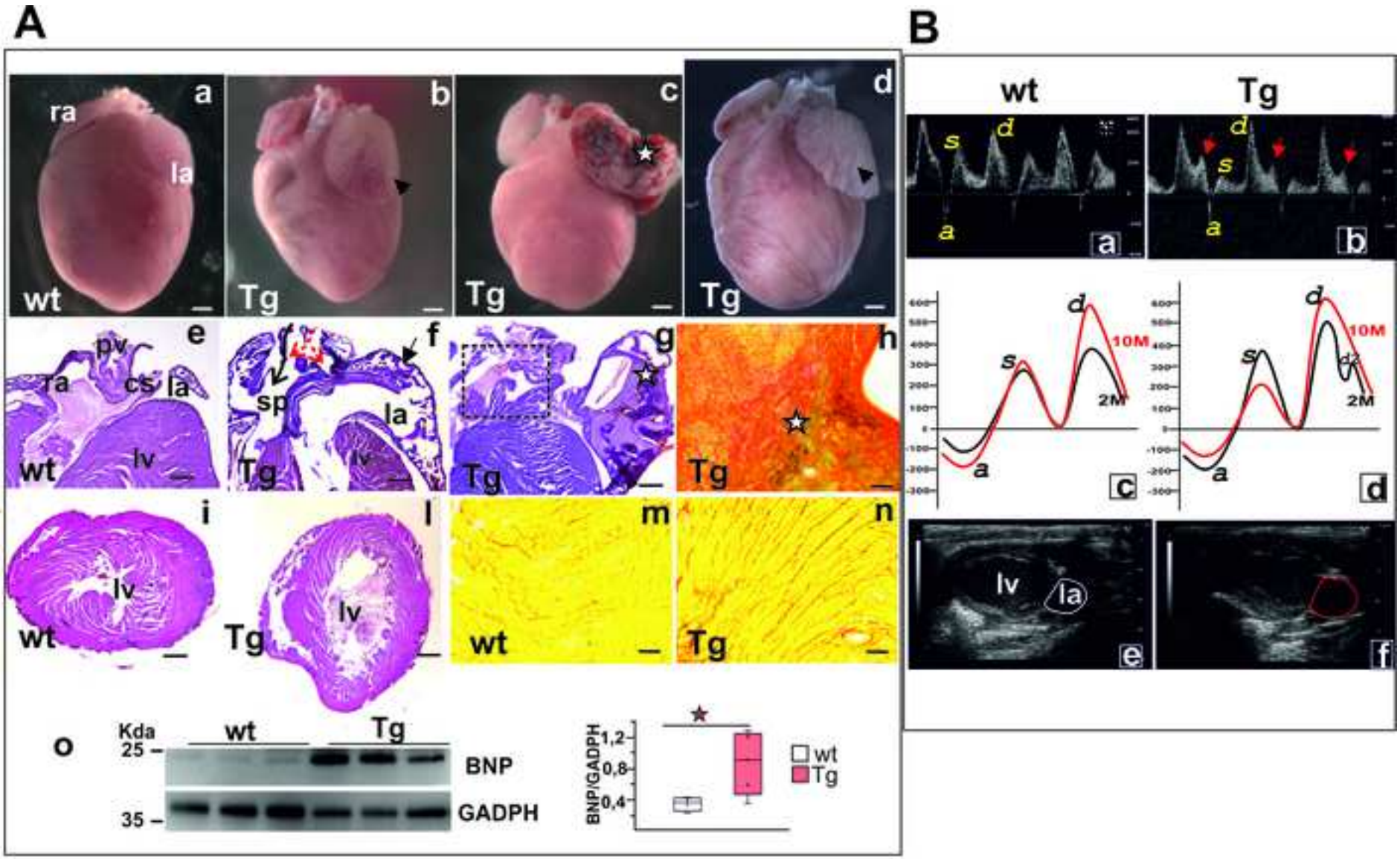

Figure 5

Figure 6

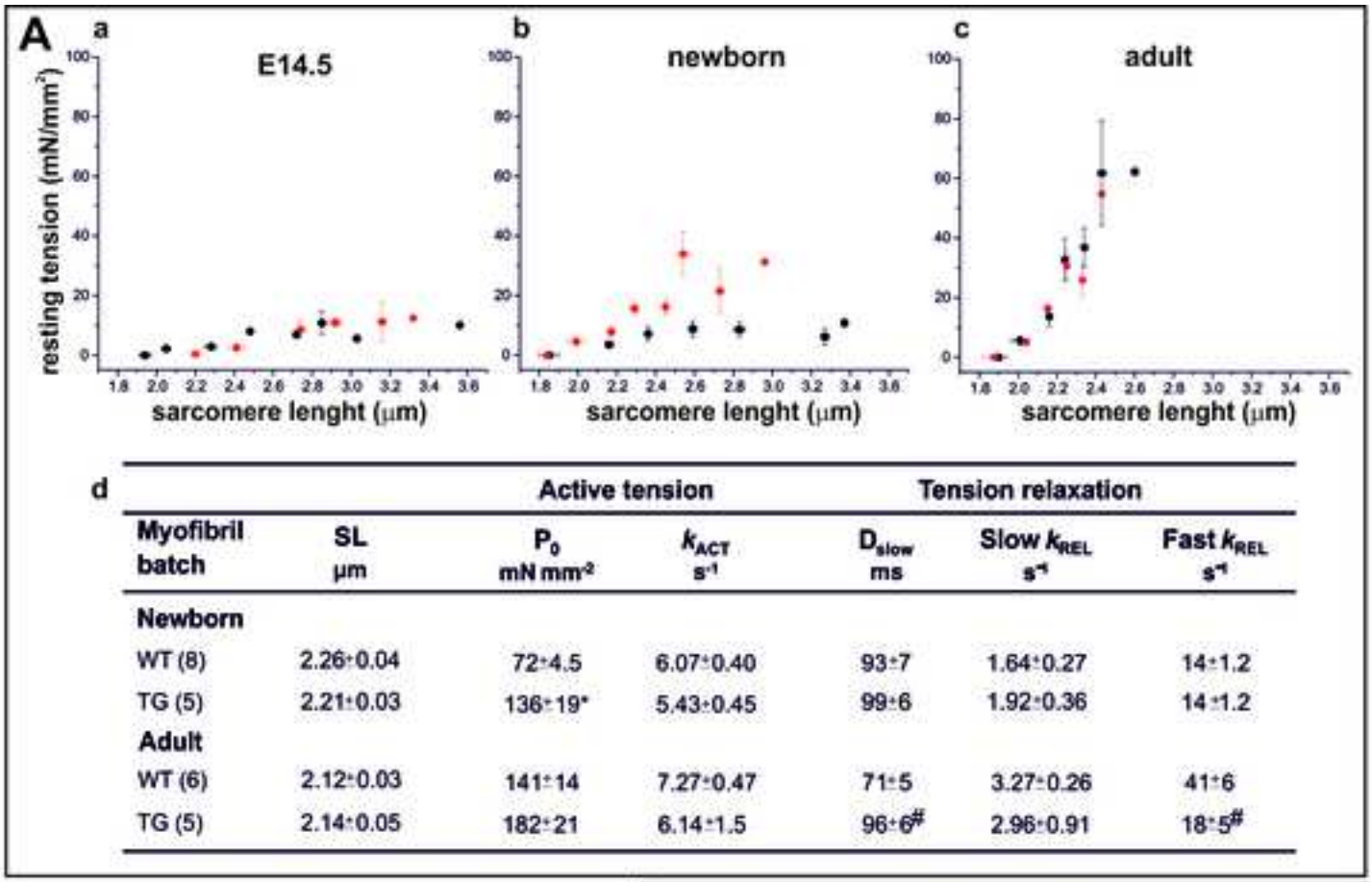

d

Myofibril batch	SL μm	Active tension P_0 mN mm^{-2}	Active tension k_{ACT} s^{-1}	Tension relaxation D_{slow} ms	Tension relaxation Slow k_{REL} s^{-1}	Tension relaxation Fast k_{REL} s^{-1}
Newborn						
WT (8)	2.26±0.04	72±4.5	6.07±0.40	93±7	1.64±0.27	14±1.2
TG (5)	2.21±0.03	136±19*	5.43±0.45	99±6	1.92±0.36	14±1.2
Adult						
WT (6)	2.12±0.03	141±14	7.27±0.47	71±5	3.27±0.26	41±6
TG (5)	2.14±0.05	182±21	6.14±1.5	96±6#	2.96±0.91	18±5#

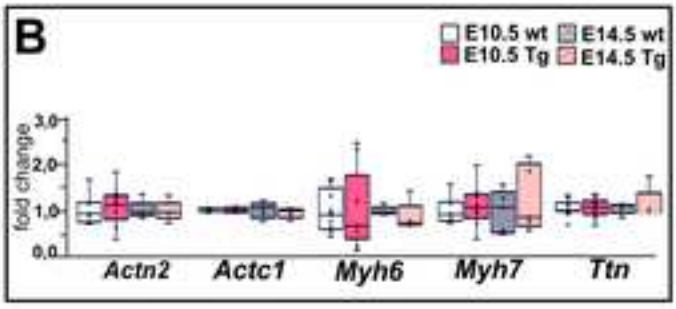

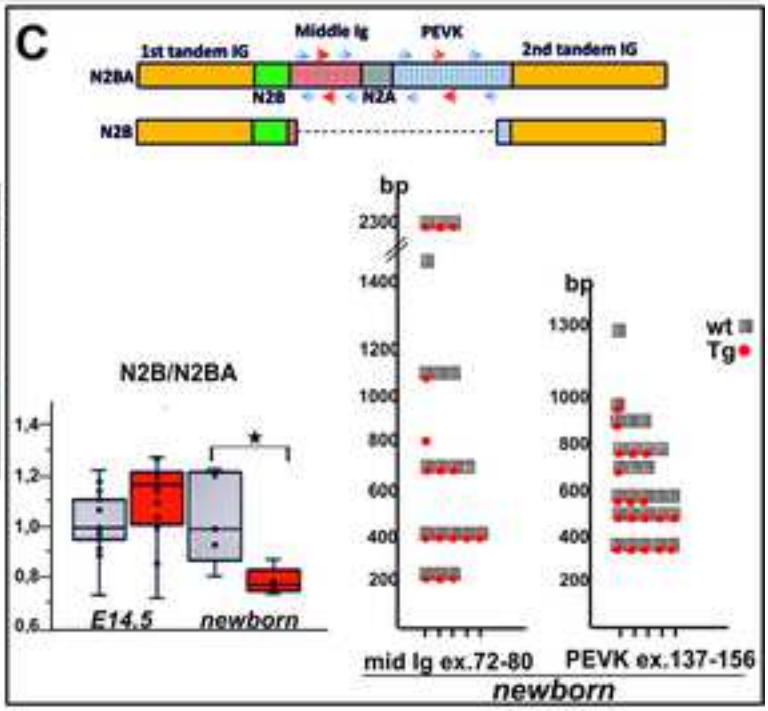

Figure 6

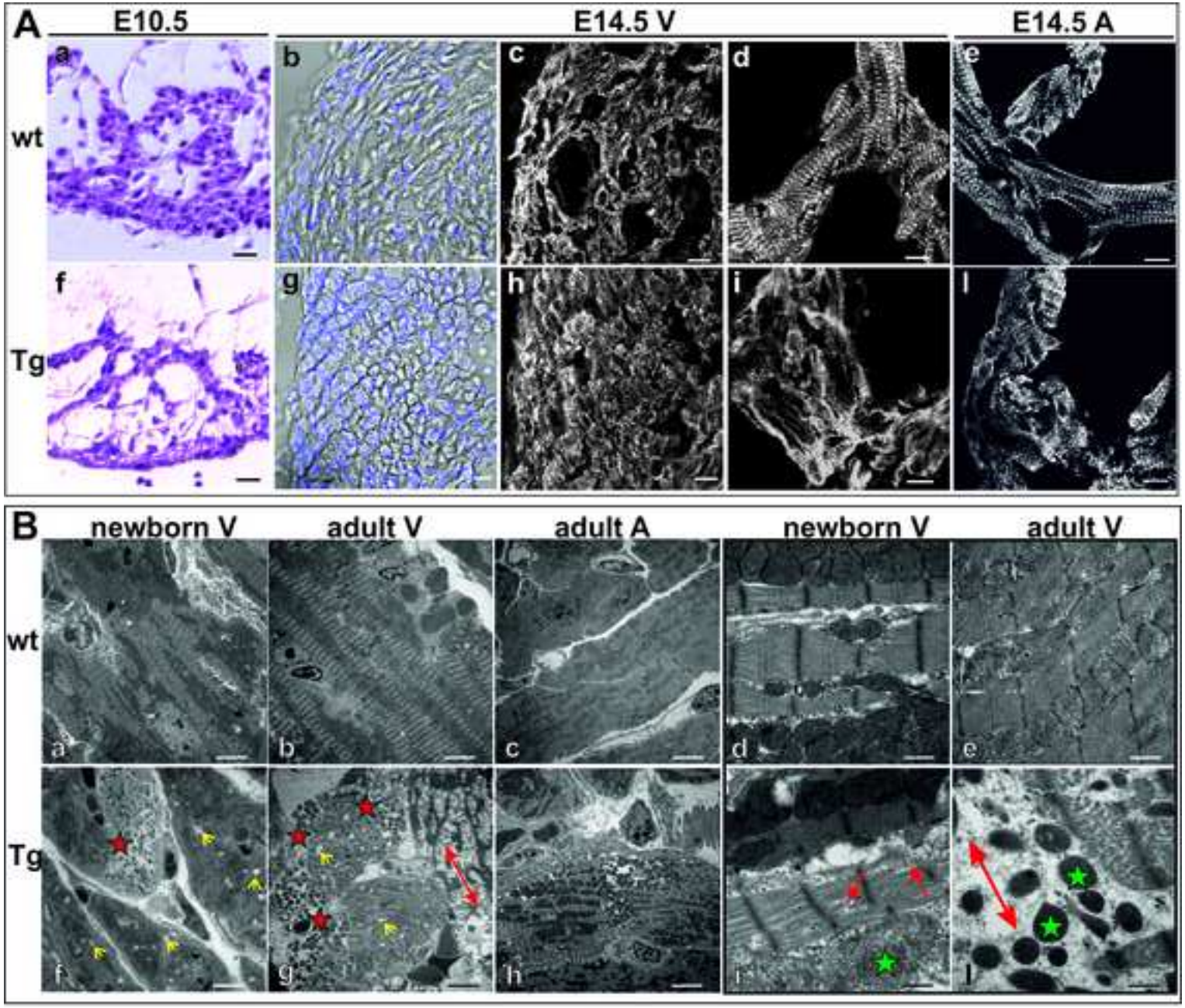

Figure 7

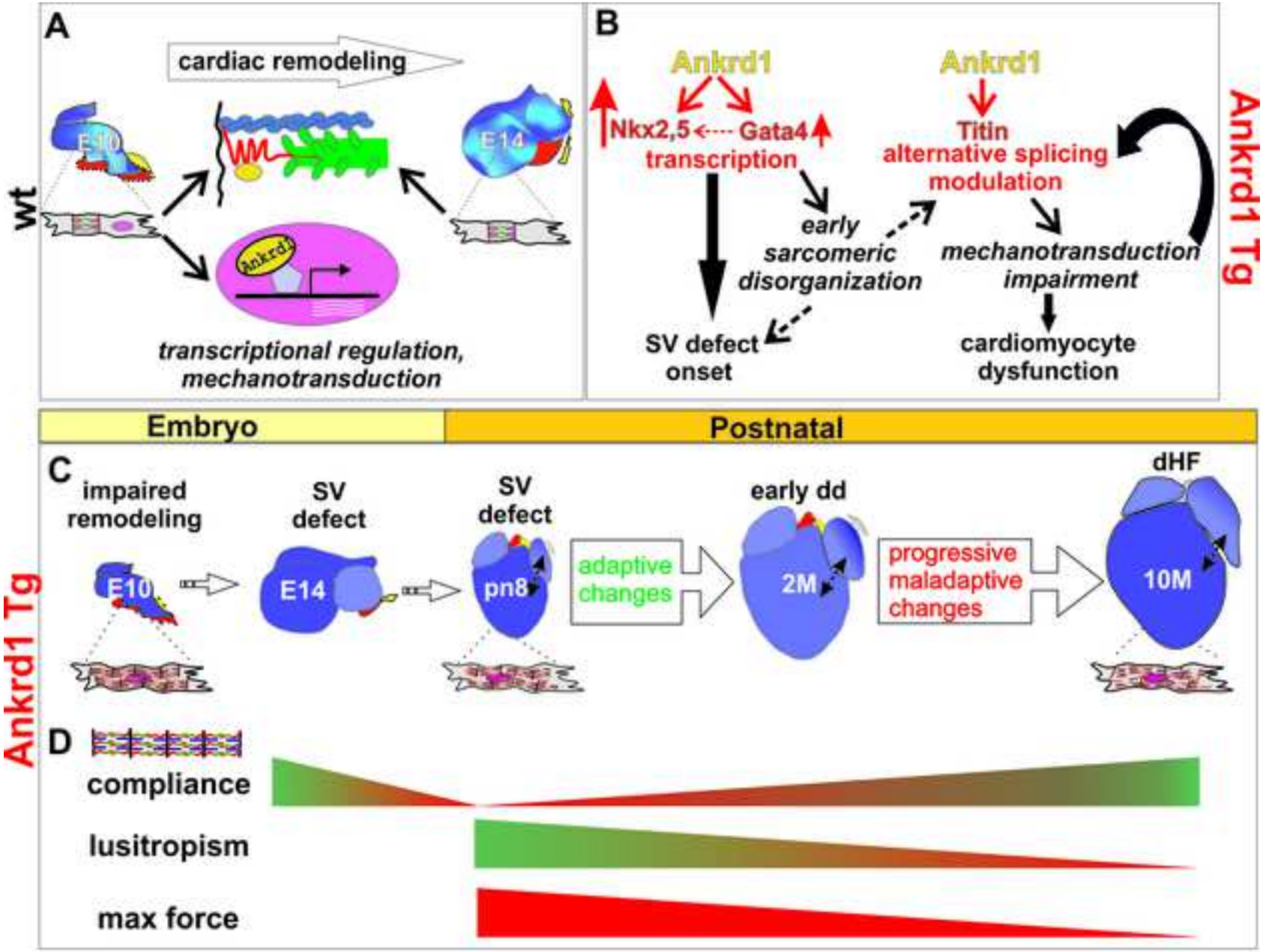

Figure 8

Graphical Abstract

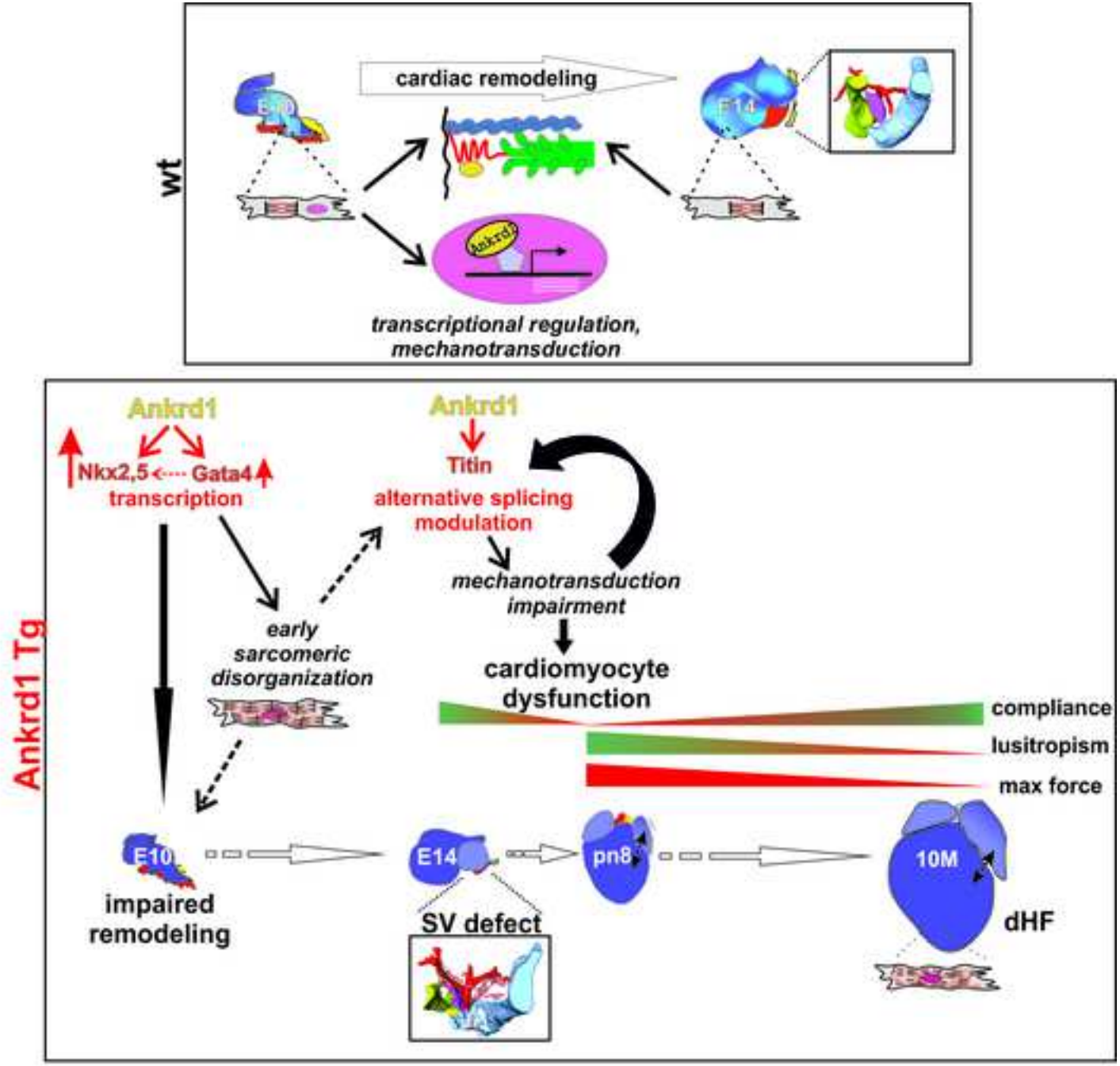

graphical abstract

CVR-2019-0215

Formatted: Italian (Italy)

Supplementary data

Myocardial overexpression of ANKRD1 causes sinus venosus defects and progressive diastolic dysfunction

Nicoletta Piroddi[1], Paola Pesce[2], Beatrice Scellini[1], Stefano Manzini[3], Giulia S. Ganzetti[3], Ileana Badi[4,5], Michela Menegollo[6], Virginia Cora[6], Simone Tiso[6], Raffaella Cinquetti[4], Laura Monti[4] , Giulia Chiesa[3], Steven B. Bleyl[7], Marco Busnelli[3], Federica Dellera[3], Daniele Bruno[4], Federico Caicci[8], Annalisa Grimaldi[4], Roberto Taramelli[4], Lucia Manni[8], David Sacerdoti[2], Chiara Tesi[1], Corrado Poggesi[1], Simonetta Ausoni[6*], Francesco Acquati[4*], Marina Campione[6,9*].

[1]Department of Experimental and Clinical Medicine, University of Florence, 50134 Florence, Italy; [2]Department of Medicine, University of Padua, 35121 Padua, Italy; [3]Dept. of Pharmacological and Biomolecular Sciences, University of Milan, 20133 Milan, Italy; [4]Dept. of Biotechnology and Life Sciences, University of Insubria, 21100 Varese, Italy; [6]Dept. of Biomedical Sciences, University of Padua, 35121 Padua, Italy; [7] Dept. of Pediatrics, University of Utah, Salt Lake City, 84132 Utah, USA; [8]Dep. of Biology, University of Padua, 35121 Padua, Italy; [9]CNR-Neuroscience Institute, 35121 Padua, Italy.

[5]**Present address:** Division of Cardiovascular Medicine, Radcliffe Department of Medicine, University of Oxford, John Radcliffe Hospital, Oxford OX3 9DU, UK.

***: corresponding Authors**

Marina Campione: fax: +39-049-8276040; tel: +39-049-8276031;

E-mail: campione@bio.unipd.it ;

Francesco Acquati: fax: +39-0332-421500; tel: +39-0332-421512;

E-mail: francesco.acquati@uninsubria.it

Simonetta Ausoni: fax +39-049-8276040; tel: +39-049-8276036;

E-mail: simonetta.ausoni@unipd.it

Running title: ANKRD1 role in heart development and disease

Formatted: Left

Supplementary methods

Mouse lines

Genomic DNA was PCR-genotyped from tails of anesthetized mice (Zoletil, 30mg/kg, i.p) or the amniotic sac of embryos isolated after sacrifice by cervical dislocation of the anesthetized mother. Animal experiments were approved by Italian Ministry of Health (n. 2012/4 and 42/2014). Animal procedures used conformed to the guidelines from Directive 2010/63/EU of the European Parliament on the protection of animals used for scientific purposes.

Histological analysis

Isolated embryos, neonatal (Pn8) and adult hearts were isolated, fixed overnight with 4% paraformaldehyde, dehydrated through graded ethanol series, and paraffin embedded. Alternatively, samples were fixed for 60 minutes in PFA 1%, dehydrated overnight in sucrose 30% / PBS and frozen in liquid nitrogen. Hematoxylin/Eosin staining or in situ hybridization were performed on paraffin embedded sections. Histochemical analysis of cardiac fibrosis was performed on cryosections using Sirius Red staining[1].

Field Code Changed

In situ hybridization

Whole mount and section ISH was performed as previously described[2]. RNA probes were generated using standard protocols.

Field Code Changed

Amira 3D reconstruction

For 3D reconstruction, digital images were aligned using Adobe Photoshop, then loaded into Amira 5.3.3 software. Segmentation into binary labels was generated by anatomically-based subdivision of cardiac regions. 3D models and virtual sections were generated using Resample and Surfaceview module. Images snapshots were taken with Amira, then annotated with Corel-draw. To add the outline of organs and internal structures, virtual sections were manually edited by side-by-side comparison with lower magnification pictures of corresponding histological sections.

Immunofluorescence and confocal analysis

Staged embryos, neonatal (Pn8) and adult hearts were fixed for 60 minutes in PFA 1%, dehydrated overnight in sucrose 30% / PBS and frozen in liquid nitrogen. Embryos were sectioned 7 μm thick

and individual sections were immunostained overnight at +4°C with one or a combination of the following antibodies: monoclonal anti-actinin (A7811, Sigma), ~~policlonal~~polyclonal anti-ANKRD1 (sc-3081, Santa Cruz), polyclonal anti-Flag (2368, Cell signalling). The following day, sections were washed in PBS 1x, then incubated 1 hour at room temperature with secondary antibodies anti-rabbit-cy2(111225144, Jackson lab) or anti-mouse-TRITC (R0270, Dako). Afterwards, sections were washed in PBS 1x, then incubated 5 minutes with Hoechst to visualize nuclei. Immunofluorescence imaging system consisted of a Leica inverted microscope DM I6000 and a Leica true confocal scanner TCS SP5II equipped with 405 Diode, Ar, He/Ne 543 and He/Ne 633 lasers. Images were recorded using a Leica HCX PL APO Lambda blu 63/1.40 oil immersion objective. Rotation movies were obtained with Fiji software through automatic processing of z-stack of analysed regions.

Electron microscopy

TEM sample preparation and analysis has been provided by the Electron Microscopy service of Department of Biology-University of Padua. Samples were fixed with 2.5% glutaraldehyde in 0.1M sodium cacodylate buffer pH 7.4 for 1 hour at 4°C, postfixed with 1% osmium tetroxide in 0.1M sodium cacodylate buffer for 1 hour at 4°. After three water washes, samples were dehydrated in a graded ethanol series and embedded in an epoxy resin (Sigma-Aldrich). Ultrathin sections (60-70 nm) were obtained with an Ultrotome V (LKB) ultramicrotome, counterstained with uranyl acetate and lead citrate and viewed with a Tecnai G^2 (FEI) transmission electron microscope operating at 100 kV. Images were captured with a Veleta (Olympus Soft Imaging System) digital camera.

Western blotting

Total proteins were extracted from ~~hearts of transgenic~~ embryonic, neonatal (Pn8) and adult hearts of transgenic and wild-type~~mice~~ ~~and wild-type~~ mice~~littermates~~, as previously reported[3]. Protein concentration was determined with BCA Protein Assay kit (Pierce.) Total proteins (30 to 80 µg) were resolved by SDS-PAGE, transferred to a polyvinylidene difluoride membrane (Millipore) and probed with antibodies. Antibodies used in this study were: ~~Flag expression was detected with polyclonal~~ anti-Flag (2368, Cell signalling), anti-ANKRD1 (Santa Cruz, sc-3081), anti-TGFβ□GFi-ANKRD1 (Santa Cruz, sc-3-total ERK1/2 (Cell signalling 9107), anti-phospho ERK1/2 (Cell signalling 9101S), ~~antibody. Loading control was assessed with~~ anti-GADPH (Santa Cruz sc-2578), anti-α-tubulin ~~mAb~~ (Sigma T9026~~, Sigma~~), anti-actinin (A7811, Sigma). Membranes were then incubated with secondary goat anti-rabbit or goat anti mouse antibodies conjugated to horseradish peroxidase (Biorads). ~~Antibody complexes~~ Reactivity ~~were~~ was

Formatted: Not Highlight

Field Code Changed

Formatted: Not Highlight

Formatted: Strikethrough

Formatted: Font: Times New Roman

Formatted: Font: Symbol

Formatted: Font: Times New Roman

Formatted: Font: Times New Roman

visualized with Pierce ECL Western Blotting Substrate (Thermo Scientific) and quantified by densitometry (ImageJ).

PCR analysis

Isolated hearts from genotyped E14,5 embryos and newborn (Pn8) mice were processed for RNA extraction. For RNA extraction from E10.5 embryos, two hearts were pooled on each tube. RNA extraction and cDNA synthesis was performed as described previously[4]. Real time amplification was performed on iQ5 Real-time machine (Bio-Rad). Gene expression values were normalized with housekeeping gene Ppia. Primers for titin PCR amplification were designed from Genebank nucleotide sequence BN001114.1, corresponding to mouse titin gene. Primers were selected to avoid regions with repetitive nucleotide sequences and potential incorrect priming. Real time titin PCR oligos were designed to selectively amplify N2B or N2AB isoforms, or a common amplicon present in N2B and N2BA isoforms[5]. Oligos for PCR scanning analysis of N2BA MidIg and PEVK regions were designed according to published strategy[6]. Soleus muscle cDNA, characterized by reduced alternative spicing, was used as a control to assess the specificity of PCR amplification. PCR products were run on a 1% agarose gel. All primers sequences are listed in Table S1.

Isolated myofibril analysis

Atria and ventricles were dissected from isolated embryonic, neonatal (Pn8) and adult hearts, washed in PBS and rapidly frozen at -80°C. Myofibrils were prepared by homogenization of permeabilized strips of frozen ventricular tissue in relaxing solution on ice, as previously described[7] and used for up to 4 days. Mechanical measurements from myofibrils in isometric conditions were performed during activation-relaxation cycles achieved by fast solution switching as previously described[8]. For force recording, a small volume of myofibril suspension was transferred to a thermostatically controlled observation chamber mounted on an inverted microscope (15°C). Myofibrils in relaxing solution (pCa 9.0) were mounted horizontally between two glass microtools: one connected to a length-control motor and the other acting as a calibrated cantilever force probe. After mounting, the initial length of selected preparations (single myofibrils or bundles of a few myofibrils, 25–80 µm long, 2-4 µm wide) was set just 5–10% above the slack length and the initial sarcomere length (SL) was measured. Mounted myofibrils were then continuously perfused by one of two streams of relaxing (pCa 9.0) or activating (pCa 3.5) solution flowing by gravity from a double-barreled glass pipette placed within a 1 mm distance. The solution change, achieved by displacing the perfusion pipette with a stepped-motor-controlled system,

Field Code Changed

Field Code Changed

Field Code Changed

Formatted: Font: (Default) Times New Roman, Not Bold, English (United Kingdom), Not Highlight

Field Code Changed

Field Code Changed

occurred with a time constant of 2–4 ms and was complete in <10 ms. The maximal force developed (P_0) was optically measured from the deflection of the force probe and normalized by the cross sectional area of the preparation. The rate of force development (k_{ACT}) was estimated from the time required to reach 50% of the maximal isometric force. The rate constant of the early slow force decline (slow k_{REL}) was estimated from the slope of the regression line fitted to the tension trace normalized to tension measured just before relaxation. The duration of the slow relaxation phase was estimated from the start of the solution change. The rate constant for the final fast phase of tension decline (fast k_{REL}) was estimated from a monoexponential fit. Resting tension (RT) at pCa 9.0 was measured by imposing up to 30% releases of initial length to myofibrils mounted for force recording. The quasi-steady-state SL-resting tension relations were determined several seconds after the imposition of ramp elongations of different extents (10–30% of the initial myofibril length)[9] when most of the stress relaxation was over. The diameter, average SL, and length of mounted myofibrils were measured by calibrated visualization of video images. Force and length signals were collected and analyzed by commercial software (National Instruments®, LabVIEW®). Activating and relaxing solutions were calculated as previously described[7].

Data from myofibrils are expressed as mean±SEM (number of samples and animals as indicated in legends). All sets of variables were checked for normality (Shapiro-Wilk test) and for homogeneity of variances among groups (Levene's Test). Unpaired T-test was used to calculate P-values for each data set.

Doppler analysis of PV flow

Doppler analysis of PV flow was performed from a corrected long axis B-mode image placing the sample volume just before the entry of the PV in the left aria. PV Doppler flow is characterized by two anterograde waves, the systolic (*s*) and the diastolic (*d*), and a retrograde wave (*a*) during atrial systole[10] (Figure S2). The *a* wave is the reverse flow wave directed from LA to PV and is caused by atrial contraction; *s* wave is the flow wave directed from PV to LA caused by LV shortening, with closed mitral valve, during ventricular systole; *d* wave is a flow wave directed from PV to LA caused by diastolic flow from LA to LV during ventricular diastole (after mitral valve opening). The maximal velocity of PV atrial (a), systolic (s) and diastolic (d) flow waves were measured.

Supplementary Tables

Table S1: Oligo list. A: list of oligos used for real time PCR analysis, with the exception of titin oligos. B: top box shows a schematic representation of titin isoforms and the oligos used for titin

PCR analysis. Arrows indicate the position of the oligos, flanked by the corresponing exon number; black closed arrow: oligos for real time PCR; blue open arrows: oligos for N2BA exon scanning. Detailed oligos sequence is indicated in the lower part of the table. Exon indicates the number of the exon where the primers are located. Bp position indicates the position of the oligos within mouse titin gene.

A

gene	5'-3' Forward	5'-3' Reverse
Ppia	agcactggggagaaaggatt	agccactcagtcttggcagt
ANKRD1 transgene	tcgttccagctgtggtccacat	cttcttccagtgaccagttcctct
GATA4	ctgtcatctcactatgggcac	ccaagtccgagcaggaatttg
Nkx2.5	agaccctcgggcggataaaa	ctgtcgcttgcacttgtagc
Ankrd1	ctgtggatgtgccgaggtttctgaa	ccgtccgtttatactcatcgcagac
~~*Actc1*~~	~~gtcaacactcccaaacccga~~	~~ctccaacagctcactcgcta~~
~~*Rpia1*~~	~~agcctcaggaagcaaggatt~~	~~agccagtcagtcttggcagt~~
~~*ANKRD1* transgene~~	~~tcgttccagctgtggtccacat~~	~~cttcttccagtgaccagttcctct~~
~~*Myh7*~~	~~ctgtcatctcactatgggcac~~	~~ccaagtccgagcaggaatttg~~
~~*Myh6*~~	~~agaccctcgggcggataaaa~~	~~ctgtcgcttgcacttgtagc~~
~~*Ankrd1*~~	~~ctgtggatgtgccgaggtttctgaa~~	~~ccgtccgtttatactcatcgcagac~~
~~*Actn2*~~	~~gtcaacactcccaaacccga~~	~~ctccaacagctcactcgcta~~
~~*Actc1*~~	~~cgcctacagaacccaccaaa~~	~~gtcaggatacctcgcttgct~~
~~*Myh7*~~	~~ctccagaagagaagaactcc~~	~~ccacctgctggacattctgc~~
~~*Myh6*~~	~~gagatgagaggctgagccgt~~	~~cactggataaccagcagggca~~

Formatted Table

Formatted Table

Formatted: Line spacing: single

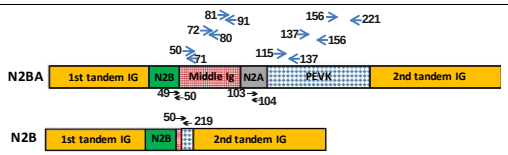

	Amplicon subtype	Forward 5'-3'	Reverse 5'-3'	Exon	bp position in BN001114.1
Real time PCR	total titin	aaagagctgcccctgtgatc	ctttgaaccactggaaccgg	49/50-50	89299- 90203
	N2B isoform	tgagtatggcagtgtcagct	tcagcaccacctcttccttt	50-219	90325-177776
	N2BA isoform	gcctttaacaagcacggtga	tcttgagggctggagtcttt	103-103/104	123732-124664
N2BA exon scanning	Mid_Ig region	agcctccaatgagtatggcagtg	ccgcttgtctttgtaccacacc	50-71	90315-10439
		tgcaagcatccatagaaggtgc	agtgtcctcagcactggcttc	72-80	103794-108640
		ggaagcaagtgcgaagcag	acgttcaggatgtggatgctc	81-91	109248-115366
	PEVK	cttctgagattattgacgtgtcctc	gctccacctcacgctctg	115-137	132843-145919
		gcgtgaggtggagcactatg	cagcctctaggaactcaatgacc	137-156	145905-156239
		cattgagttcctagaggctgaag	ttcctttggtgtaggctctgg	156-221	156220-187742

Supplementary figures and videos legend:

Figure S1: ANKRD1 Tg mouse model characterization. A: a-c, WB analysis of transgene expression. a: five adults hearts from transgenic lines A and B; top: α-flag antibody, bottom: loading control α-tubulin.~~**myocardial overexpression of human ANKRD1 in transgenic mice.** A: human ANKRD1 protein expression in transgenic lines. Western blotting analysis of adult heart lysates from ANKRD1 transgenic lines A and B. M: molecular weight marker; 1-5: four Tg^{+ve} hearts from line A (2, 3) and B (1,4), and one Tg^{-ve} heart from line B (5). Arrow indicates the signal of α flag antibody. Bottom: loading control: α tubulin.~~ b: top, immunobotting detection of ANKRD1 protein in isolated hearts from E14.5, newborn and 10M wt and Tg mice, representative results. Note that in Tg mice ANKRD1 signal detects endogenous plus human transgene expression. Bottom, loading control actinin. c: quantification of ANKRD1 protein expression levels in wt *vs* Tg newborn (n=4wt, 5Tg) and adult (n=5wt, 5Tg) hearts; values are compared to the mean wt level at each stage. *p<0.01 , Student unpaired t-test. d: ~~real time PCR analysis of~~ mRNA expression levels of endogenous Ankrd1 and human transgene in E14.5 and newborn ~~neonatal (P8)~~ wt and ~~transgenic~~Tg hearts (n=5 wt, 5Tg). Values are compared to E14.5 mouse Ankrd1 mRNA expression. In newborn Tg hearts, note the differences between very high transgene mRNA (d), and ANKRD1 protein levels (c). This indicates some post-transcriptional compensation. B,C: Flag expression and sub-localization from early development to adult stage. B: Immunofluorescence ~~detection~~ analysis of Flag *vs.* actinin expression in ~~in E17.5 embryonic hearts~~E10.5 and E14.5 wt and Tg hearts, overview pictures. In E10.5 Tg hearts Flag Ab reaction is higher at the sino-atrial region (closed arrow), gradually decreases in the ventricles (open arrow) and is not detectable at the outflow tract (asterisk). Flag Ab reaction is stronger in E14.5 Tg hearts. ra, la: right, left atrium; rv: right ventricle; oft: outflow tract; scale bar: 100µm. C: confocal images of E14.5, newborn and adult Tg hearts. Flag expression is sarcomeric; nuclear and perinuclear sublocalization can be additionally observed in adult Tg hearts (arrows); scale bar: 10µm~~ from line A. a: ANKRD1 Transgenic; b: non transgenic littermate. C: real time PCR analysis of mRNA expression levels of endogenous Ankrd1 and human transgene in E14.5 and neonatal (P8) wt and transgenic hearts (n=5). Values are compared to E14.5 mouse Ankrd1 mRNA expression.~~

Figure S2: PV Doppler flow analysis of a 2M wt mouse. Top: long axis visualization of PV blood inflow (red) into the LA. Yellow horizontal lines indicate sample volume placement. Bottom: PV

Formatted: Font: Not Bold
Formatted: Font: Not Bold
Formatted: Font: Not Bold
Formatted: Font: Not Bold
Formatted: Not Highlight
Formatted: Font: Italic
Formatted: Not Highlight
Formatted: Not Highlight
Formatted: Font color: Red
Formatted: Not Highlight
Formatted: Highlight
Formatted: Font: Not Bold, Font color: Auto
Formatted: Font color: Auto
Formatted: Font: Not Bold, Font color: Auto
Formatted: Not Highlight
Formatted: Font: Not Bold, Font color: Auto
Formatted: Not Highlight
Formatted: Font: Not Bold, Font color: Auto
Formatted: Font: Not Bold
Formatted: Font: Italic
Formatted: Not Highlight
Formatted: Not Highlight
Formatted: Not Highlight
Formatted: Not Highlight
Formatted: Not Highlight
Formatted: Not Highlight
Formatted: Not Highlight
Formatted: Font: Not Bold, Not Highlight
Formatted: Not Highlight
Formatted: Font: Symbol, Not Highlight
Formatted: Not Highlight
Formatted: English (United States)
Formatted: Font: Symbol
Formatted: Not Highlight

Doppler flow. Note the presence of two anterograde waves, systolic (s) and diastolic wave (d), and one retrograde wave (a) during atrial systole.

Figure S3: Venous pole histological analysis in E13.5 wt and Tg hearts, H/E ~~analysis~~staining. A: ~~4-~~heart overview ~~chamber view~~at different levels. Note in Tg heart the irregular venous pole organization, altered morphology of atrial chambers and ventricular malrotatation (black arrowheads in d,f) ~~Black arrowhead indicates ventricular malrotation in the transgenic heart.~~ B: venous pole analysis of ~~-~~wt (a,c) and transgenic hearts (d-i); g-i are magnifications of the regions within red dotted box in the neighboring picture. Red asterisks show the microcanalizations around the vestibular region; yellow arrows show the fenestrations at the vestibular region; red curved arrows indicate ectopic communications between systemic and pulmonary veins generated by the canalizations. Abbreviations: rv: right ventricle; lv: left ventricle; lscv, rscv: left, right superior caval vein; icv: inferior caval vein; pv: pulmonary vein; ias: interatrial septum; vv: venous valves; daw: dorsal atrial wall. Scale bar: A=200µm; Ba-f= 100µm; g-i= 50 µm.

Figure S4:. adult ANKRD1 Tg hearts present moderate fibrosis. A: Representative immunoblotting showing increased TGFβ expression and increased phosphorylated ERK1/2 (pERK1/2) over total ERK (tERK1/2) in 10M Tg heart. B: Quantification of TGFβ/GADPH (n=4 wt, 5Tg), and pERK/tERK protein levels (n=5 wt, 5Tg); p>0.05, Student unpaired t-test.

Formatted: Font: Not Bold
Formatted: Font: Symbol, Not Bold
Formatted: Font: Not Bold
Formatted: Font: Symbol
Formatted: Font: Not Bold
Formatted: Not Highlight
Formatted: Not Highlight
Formatted: Font: Not Bold

Figure S5~~4~~: Different combinatorial exon usage within the middle Ig and PEVK region of titin N2BA in 5 neonatal wt and Tg hearts. Representative 1% agarose gel of RT-PCR products obtained from 5 neonatal wt and Tg hearts using primers spanning titin exons 72-80 (middle Ig region) and exons 137-156 (PEVK region), indicated with red arrows in the scheme. M1: Lambda phage DNA, BstEII digested; M2: Sharp mass 50 (Euroclone); bp: molecular weights; S: soleus muscle. Asterisk indicates the full length amplicon in soleus muscle, which presents a reduced rate of alternative splicing[6]. PCR experiments have been repeated at least 3 times.

Suppplementary Movie 1:

E14.5 wt heart, ventricular trabecolae stained with α-actinin Ab. 3D rotation from z-stack of confocal images.

Supplementary Movie 2:

E14.5 Tg heart, ventricular trabecolae stained with α-actinin Ab. 3D rotation from z-stack of confocal images.

Supplementary bibliography

1. Hadi AM, Mouchaers KTB, Schalij I, Grunberg K, Meijer GA, Vonk-Noordegraaf A, Laarse WJ van der, Beliën JAM. Rapid quantification of myocardial fibrosis: a new macro-based automated analysis. *Cell Oncol (Dordr)* 2011;**34**:343–354.
2. Tessari A, Pietrobon M, Notte A, Cifelli G, Gage PJ, Schneider MD, Lembo G, Campione M. Myocardial Pitx2 Differentially Regulates the Left Atrial Identity and Ventricular Asymmetric Remodeling Programs. *Circ Res* 2008;**102**:813–822.
3. Badi I, Cinquetti R, Frascoli M, Parolini C, Chiesa G, Taramelli R, Acquati F. Intracellular ANKRD1 protein levels are regulated by 26S proteasome-mediated degradation. *FEBS Lett* 2009;**583**:2486–2492.
4. Ammirabile G, Tessari A, Pignataro V, Szumska D, Sutera Sardo F, Benes J, Balistreri M, Bhattacharya S, Sedmera D, Campione M. Pitx2 confers left morphological, molecular, and functional identity to the sinus venosus myocardium. *Cardiovasc Res* 2012;**93**.
5. Opitz CA, Leake MC, Makarenko I, Benes V, Linke WA. Developmentally Regulated Switching of Titin Size Alters Myofibrillar Stiffness in the Perinatal Heart. *Circ Res* 2004;**94**:967–975.
6. Warren CM, Krzesinski PR, Campbell KS, Moss RL, Greaser ML. Titin isoform changes in rat myocardium during development. *Mech Dev* 2004;**121**:1301–1312.
7. Piroddi N, Belus A, Eiras S, Tesi C, Velden J van der, Poggesi C, Stienen GJM. No direct effect of creatine phosphate on the cross-bridge cycle in cardiac myofibrils. *Pflügers Arch* 2006;**452**:3–6.
8. Colomo F, Piroddi N, Poggesi C, Kronnie G te, Tesi C. Active and passive forces of isolated myofibrils from cardiac and fast skeletal muscle of the frog. *J Physiol* 1997;**500 (Pt 2)**:535–548.
9. Scellini B, Piroddi N, Flint G V., Regnier M, Poggesi C, Tesi C. Impact of tropomyosin isoform composition on fast skeletal muscle thin filament regulation and force development. *J Muscle Res Cell Motil* 2015;**36**:11–23.
10. Tabata T, Thomas JD, Klein AL. Pulmonary venous flow by doppler echocardiography: revisited 12 years later. *J Am Coll Cardiol* 2003;**41**:1243–1250.

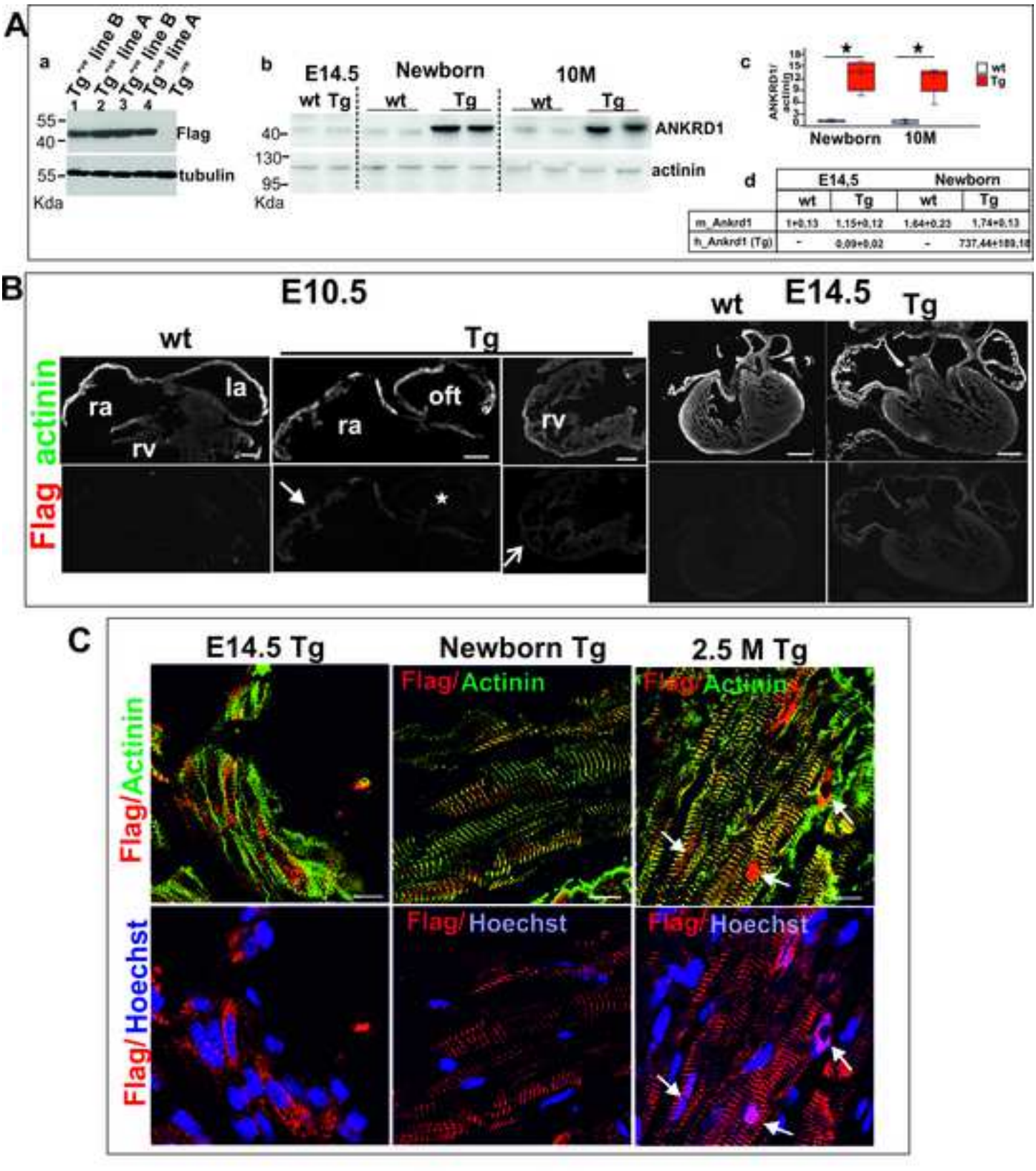

Figure S1

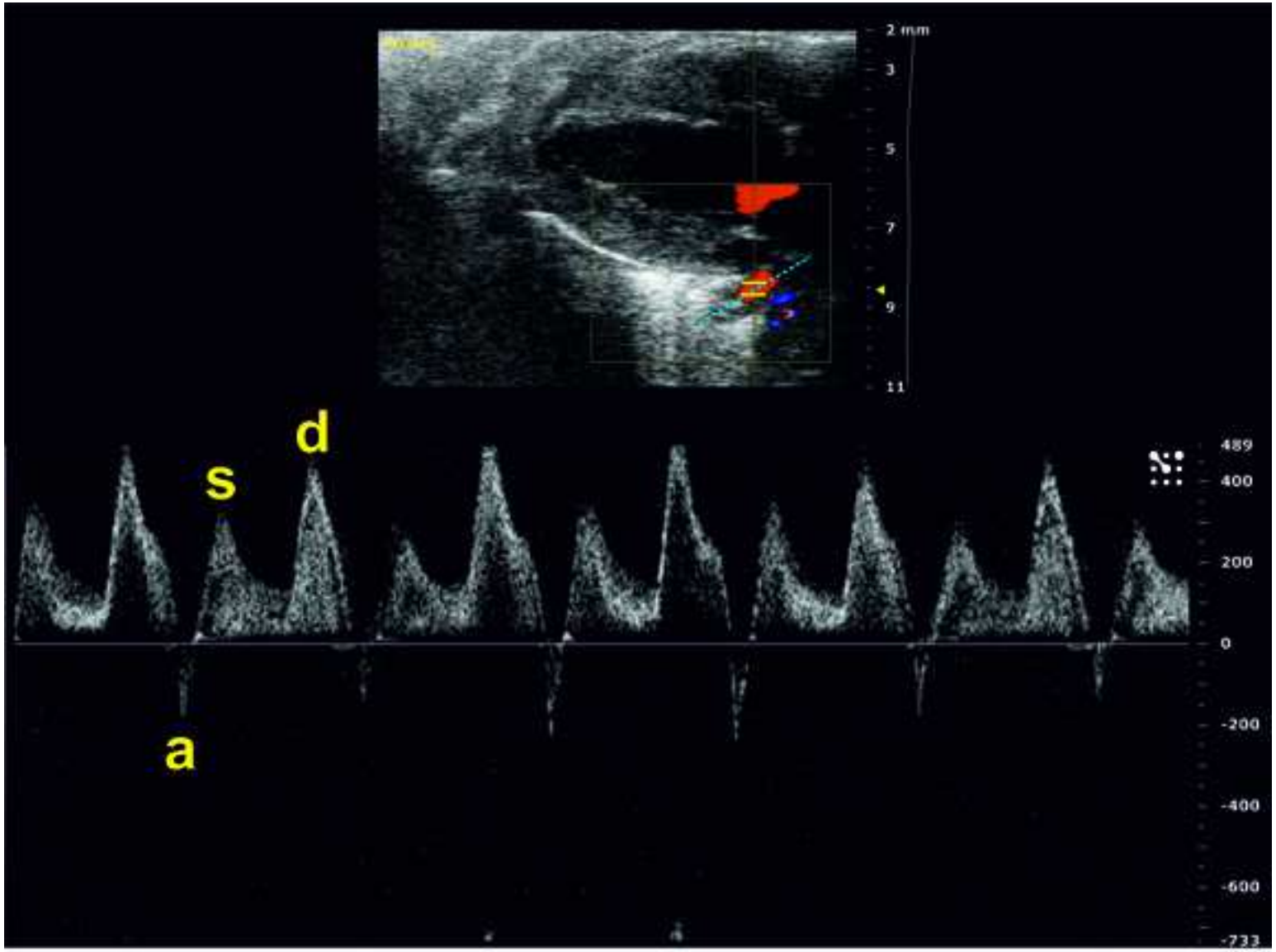

Figure S2

Supplementary Figure 3

Click here to access/download;Supplementary Material - Other;figure S3 rev final.tif

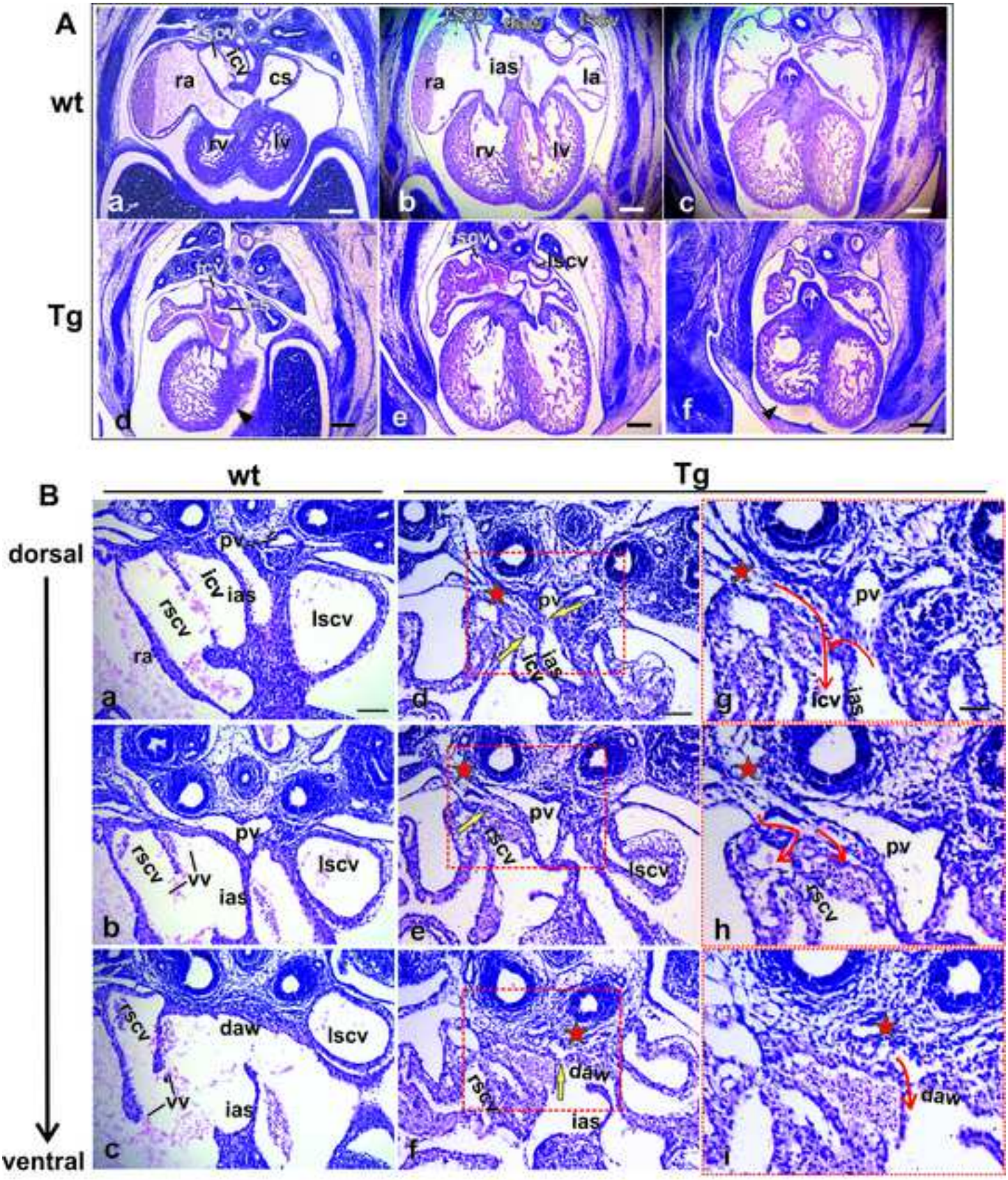

Figure S3

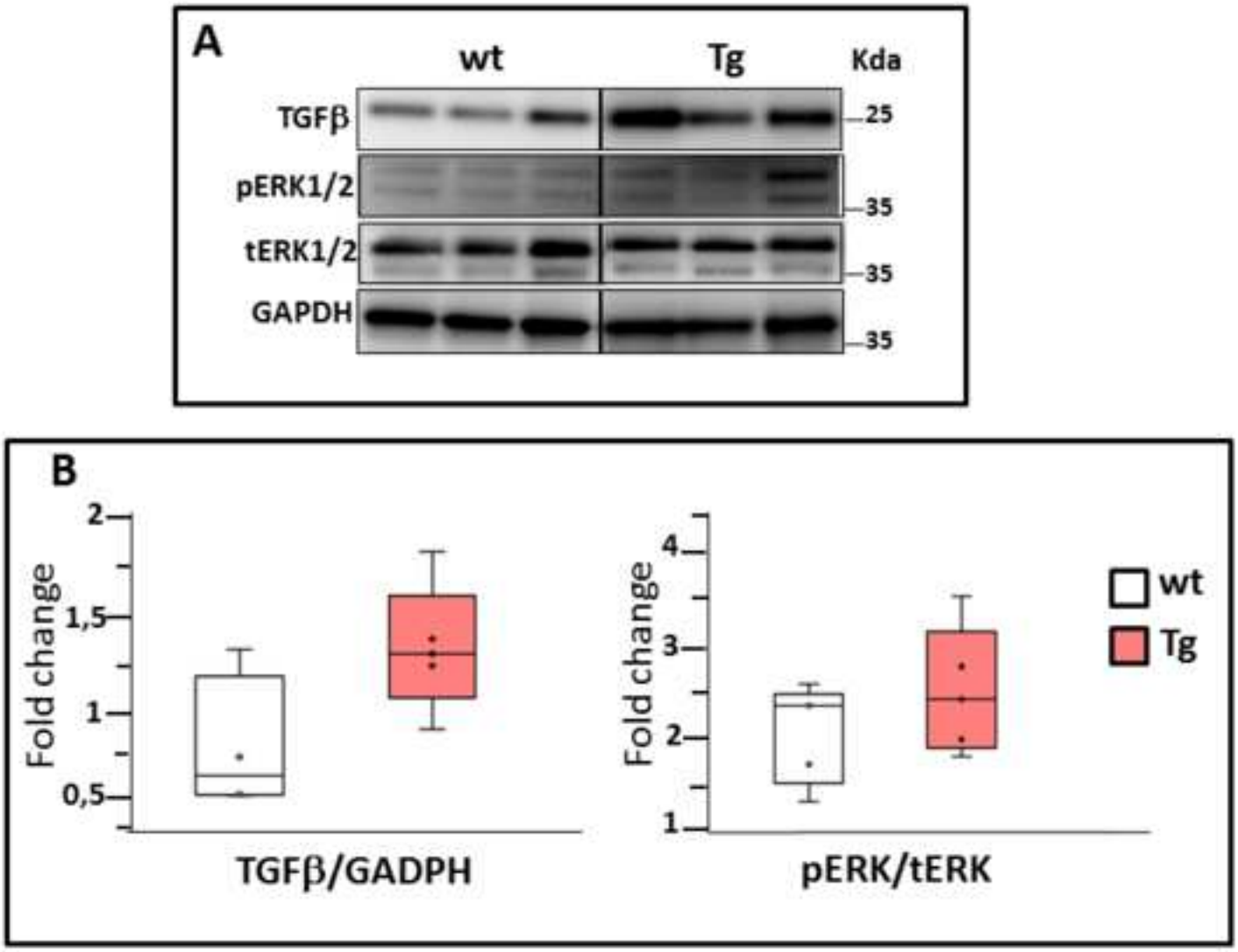

Figure S4

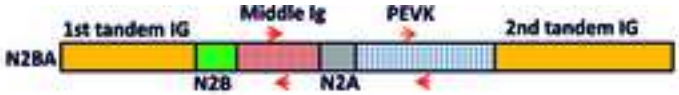

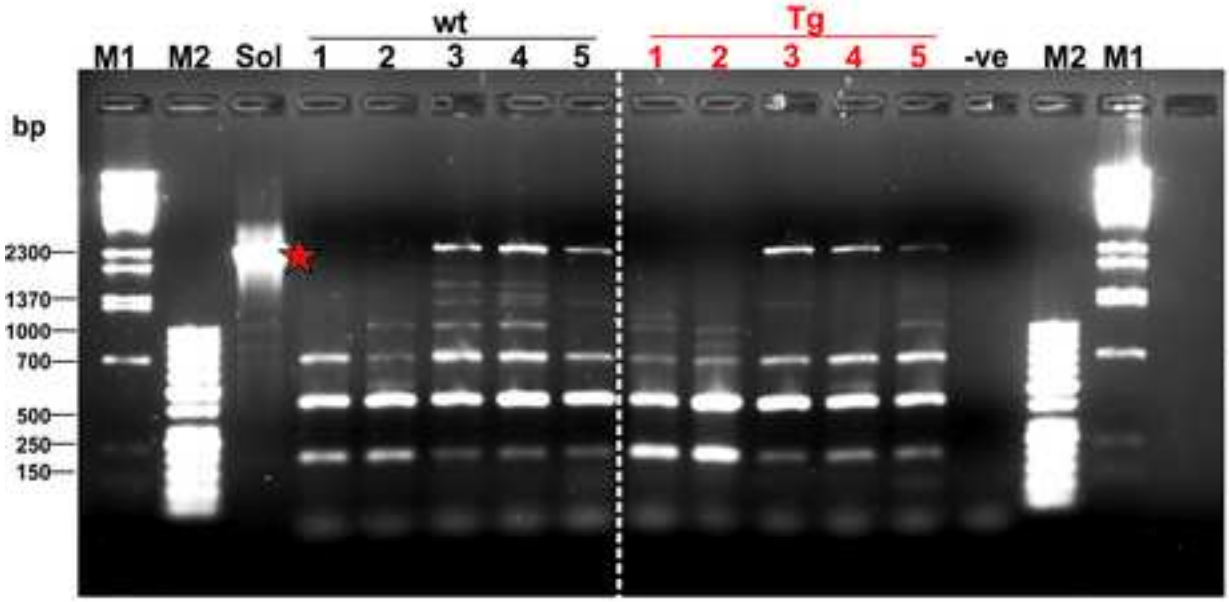

Middle Ig
ex. 72-80

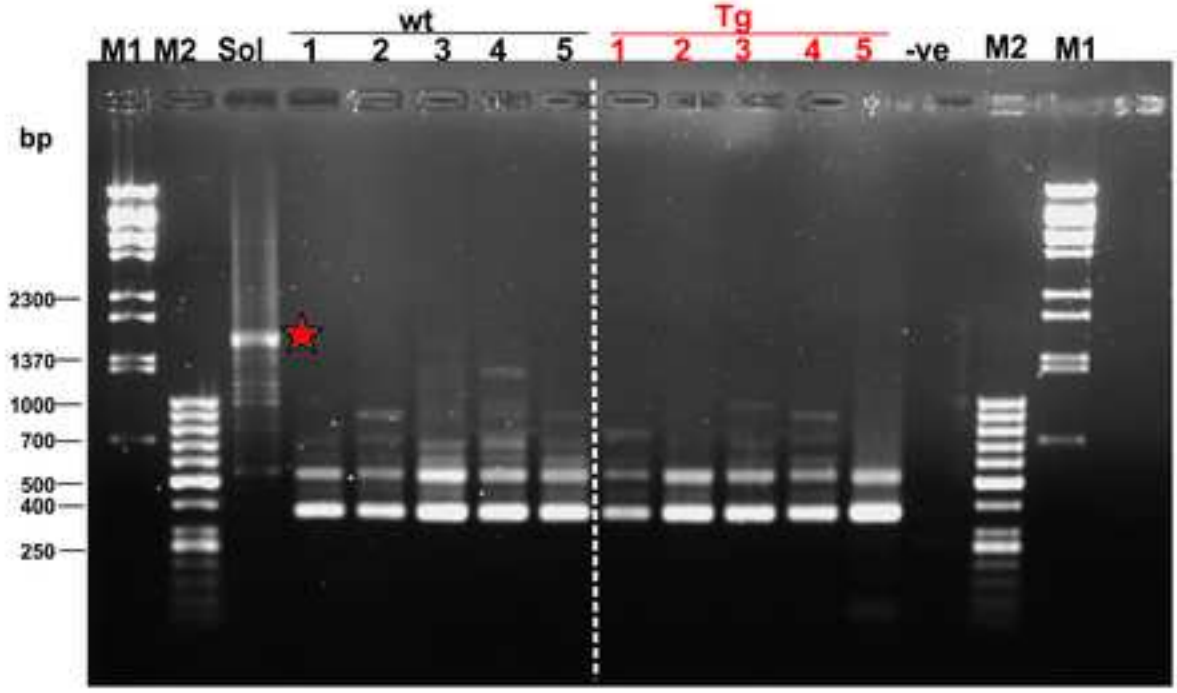

PEVK
ex. 137-156

Figure S5

Supplementary video 1

Click here to access/download

Supplementary Material - Video, Audio

video wt.mp4

Supplementary video 2

Click here to access/download

Supplementary Material - Video, Audio

video tg.mp4